1971

Components of interelectrode resistance in an electrofluid bed reactor

Ted Merrill Knowlton
Iowa State University

Components of interelectrode resistance in an electrofluid bed reactor

by

Ted Merrill Knowlton

A Dissertation Submitted to the
Graduate Faculty in Partial Fulfillment of
The Requirements for the Degree of
DOCTOR OF PHILOSOPHY

Major Subject: Chemical Engineering

Approved:

Signature was redacted for privacy.

In Charge of Major Work

Signature was redacted for privacy.

Head of Major Department

Signature was redacted for privacy.

Dean of Graduate College

Iowa State University
Ames, Iowa

1971

Components of interelectrode resistance in an electrofluid bed reactor

by

Ted Merrill Knowlton

An Abstract of
A Dissertation Submitted to the
Graduate Faculty in Partial Fulfillment of
The Requirements for the Degree of
DOCTOR OF PHILOSOPHY

Approved:

Signature was redacted for privacy.
In Charge of Major Work

Signature was redacted for privacy.
Head of Major Department

Signature was redacted for privacy.
Dean of Graduate College

Iowa State University
Ames, Iowa

1971

Components of interelectrode resistance in an electrofluid bed reactor

Ted Merrill Knowlton

Under the supervision of Thomas D. Wheelock
From the Department of Chemical Engineering
Iowa State University

The purpose of this investigation was to determine the nature of the interelectrode resistance of an electrofluid bed system. To this end, experiments were carried out to determine what system parameters affected interelectrode resistance and bed resistivity. Several models concerning the interelectrode resistance and its constituent parts were forwarded and tested as to their validity. All of these experiments were carried out at room temperature in a 6 in. diameter Plexiglas fluidization column containing a bed of conducting calcined coke particles. Low amperage current (0 to 150 ma.) was passed through the bed between a brass-screen wall electrode and a cylindrical center electrode concentric with the column wall.

Interelectrode resistance was determined as a function of current density at several relative gas velocities and with different center electrode areas available for current flow. Different electrode diameters and materials were used. In fluidized beds interelectrode resistance was found to decrease with increasing current density (over a 0 to 12 amps/sq. in. range) and relative gas velocity. No dependence of inter-

electrode resistance on current density was observed in unfluidized beds. Changing the direction of direct current flow through the bed had no effect upon interelectrode resistance. Similarly, no noticeable effect on interelectrode resistance was observed when alternating current was used. Interelectrode resistance was not affected by different electrode materials.

Bed resistivity was determined as a function of current density, column diameter and gas velocity. A four-point probe method was used to measure the bed resistivity independently of interelectrode resistance components. No effect of current density on bed restivity was noted. Bed resistivity was also found to decrease with increasing relative velocity and column diameter in the fluidized bed.

Interelectrode resistance was hypothesized to be the sum of two components--bed resistance and the contact resistance at the center electrode. Some support for this hypothesis was obtained, but it was not proven conclusively.

A Laplacian field model of the bed was hypothesized in order to calculate bed resistance independently of inter-electrode resistance. This model assumes that the distribution of electrical potential throughout the bed can be predicted using Laplace's equation. It was also necessary to assume that the bed material was homogeneous and that the contact resistance at the bed electrodes was uniform over their surface.

The bed was probed to verify the Laplacian field model. Experimental voltage profiles obtained by bed probing were compared to the profiles predicted by the model. Good agreement between measured and predicted values was obtained except in the region of the bed immediately below the center electrode. It was concluded from this that the Laplacian field model of the bed was a satisfactory mathematical analog.

Contact resistance at the center electrode was hypothesized to be inversely proportional to the center electrode area available for current flow. Strong support for this model was found. Contact resistance was calculated by subtracting values of bed resistance obtained from the Laplacian field theory method from interelectrode resistance values.

A statistically designed study of the effect of several system parameters on contact resistance was also conducted. An analysis of variance technique was used to analyze the laboratory data. Contact resistance was found to be a function of current density, relative velocity, and the interactions of current density and relative velocity, longitudinal position of exposed center electrode area and relative velocity, and longitudinal position of exposed center electrode area and current density. Contact resistance did not appear to vary significantly with electrode shape.

TABLE OF CONTENTS

INTRODUCTION

An electrofluid bed is a fluidized bed of conducting particles heated directly by passing a current (either AC or DC) between electrodes immersed in the bed. A chemical reactor operating on this principle is called an electrofluid bed reactor. This type of reactor combines the inherent advantages of a fluidized bed (high heat and mass transfer rates and uniformity of bed temperature) with the efficiency of direct electrical heating. Because the reaction zone is heated directly, no heat transfer surfaces are needed, and the reactor can be constructed of refractory materials to accommodate corrosive reactants which attack metals. Also, energy conversion efficiency does not decline with increasing temperature, and heating rates are rapid compared to those of conventional furnaces. Perhaps the principal advantage of the electrofluid bed reactor is its versatility since it can be operated over a wide range of temperature and pressure.

Because of dwindling oil and natural gas reserves, much effort has been spent towards developing processes for the production of gaseous and liquid fuels from coal, which is relatively plentiful. In nearly all of these processes large amounts of hydrogen are needed to hydrogenate the coal. Recognizing the advantages of the electrofluid bed reactor and the need for hydrogen, the Office of Coal Research (OCR) has sponsored research on the gasification of coal char with steam

in an electrofluid bed reactor to produce hydrogen. Carried out at Iowa State University, this research has been directed toward gathering information which will prove useful for the design and operation of commercial electrofluid bed reactors.

In order to accurately design and control large-scale commercial electrofluid bed reactors, it is necessary to relate the electrical power requirements of the electrofluid bed system to the design parameters which can be selected by the design engineer. Since the design of the reactor power supply depends upon the interelectrode resistance of the system, a method of predicting this resistance is needed. Some studies of the resistance have been made (6, 7, 10, 12, 32, 38, 42). However, until more information is obtained about the resistance, the design of an electrofluid bed reactor will be crude at best.

The overall purpose of this investigation was to determine the nature of the interelectrode resistance of an electrofluid bed system. The first part of the investigation was devoted to a parameter study of the interelectrode resistance and the bed resistivity. Later work was directed toward studying individual components of interelectrode resistance and different electrofluid bed electrode configurations. Nearly all experiments were made at room temperature in a 6 in. diameter Plexiglas column containing a bed of conducting calcined coke particles fluidized with nitrogen. Low amperage current was passed through the bed between a brass-screen electrode

cemented to the inside wall of the column and a cylindrical center electrode concentric with the column wall.

In the interelectrode resistance parameter study, interelectrode resistance measurements were made over a range of current densities at several relative gas velocities (2, 3, and 4 times incipient fluidization velocity) and with different center electrode areas available for current flow. Both high (12 amps/sq. in. maximum) and low (0.15 amps/sq. in. maximum) current density studies were undertaken. The high current density study was undertaken to determine the effect of current density on interelectrode resistance at current densities at or exceeding those in industrial scale electrofluid bed reactors. This study utilized small diameter electrodes (1/16 and 1/25 in.) compared to the 1 in. diameter center electrode used in the low current density study. Also, the effect of alternating versus direct bed current on interelectrode resistance and the effect of the direction of direct current flow through the bed were studied.

Bed resistivity was measured as a function of current density, gas velocity and column diameter in the second parameter study. The effect of current on bed resistivity was determined using a four-point probe measuring technique which enabled the determination of bed resistivity independently of other interelectrode resistance components. The effect of velocity and column diameter on bed resistivity was also

investigated using this technique.

Because of the results of previous related work (38) and a theoretical study of electrical contacts (17), the inter-electrode resistance, R_i, was hypothesized to be the sum of the bed particle resistance, R_b, the contact resistance between the screen wall electrode and the bed, R_w, and the contact resistance between the center electrode and the bed, R_c, or:

$$R_i = R_b + R_w + R_c \quad . \tag{1}$$

The concept of contact resistance arises from noting that when two conductors make electrical contact, their surfaces are sub-microscopically rough. Therefore, the conductors make contact through their surface projections and the actual contact surface is less than the apparent contact surface. This results in a constriction of the current flow at the reduced area of contact and, therefore, an increase in the resistance to current flow. This constriction resistance is what is commonly termed a contact resistance.

Viewing the contact resistance in this manner a model was proposed that the contact resistance is inversely proportional to the electrode area available for current flow, or

$$R_c \propto \frac{1}{A} \quad . \tag{2}$$

This model was tested by comparing contact resistances at different electrode areas. It was further assumed that the

contact resistance of the brass-screen wall electrode was negligible compared to the contact resistance of the center electrode by insuring that the area of the center electrode available for current flow was much less than that of the brass-screen wall electrode area. Using this assumption, Equation 1 became:

$$R_i = R_c + R_b \quad . \tag{3}$$

This model was indirectly tested by calculating the bed resistance and comparing it to values of the interelectrode resistance obtained from the parameter study.

Two methods of calculating the bed resistance were used. The first method was used by previous investigators (14, 24). This technique was to apply the following equation:

$$R_b = \frac{\rho l}{A} \tag{4}$$

where ρ is the bed resistivity, l is the length of current path, and A is the cross-sectional area available for current flow, to a differential volume element in the bed and integrate to obtain a value for the bed resistance. However, this method is restrictive as it does not take into account the distortion of the electrical field in the bed. Therefore, a Laplacian field model of the bed was hypothesized to analytically determine the magnitude of the bed resistance independently of the contact resistance at the center electrode. Physically,

this meant that the bed was assumed to be homogeneous with respect to its resistivity. Mathematically, Laplace's equation was applied to the actual physical system used. This was solved numerically to obtain the voltage and current flux distributions throughout the bed. By means of these solutions the capacitance of the system was obtained and related to the bed resistance by the equation:

$$R_b = \frac{\rho\varepsilon}{C} \tag{5}$$

where R_b is the bed resistance, ρ is the bed resistivity, ε is the dielectric constant of the bed material, and C is the capacitance of the system.

An experiment was then conducted to test the field theory model by comparing how well the field theory model voltage distribution approximated the voltage distribution in an actual bed. In this study brass voltage probes were inserted through the column wall at five longitudinal positions. The probe positions were varied radially and the voltage drop between the center electrode and the bed and the total voltage profile was then compared to the voltage profile predicted using the Laplacian field model.

Obtaining values of bed resistivity from the parameter study, the bed resistance could be calculated by both of the methods described above. The bed resistance was then subtracted from the interelectrode resistance to obtain the

contact resistance. Being able to calculate the contact resistance, a statistically designed experiment utilizing both laboratory experiment and Laplacian field theory was conducted to determine the effect of current density, relative gas velocity, electrode shape, and longitudinal position of the center electrode area available for current flow on contact resistance.

The field model was also used to analyze different electrode geometries. Concentric and end-to-end electrode configurations were analyzed in regard to bed voltage gradients, electrode current density, and bed heat generation.

LITERATURE REVIEW

There are numerous excellent literature surveys available describing the salient characteristics of fluidized beds in general (7, 33, 36, 46). However, the electrothermal fluidized bed, being a relatively recent concept, has not been so extensively reviewed. Therefore, the following literature review will concern itself with only the electrical properties of electrofluid beds and a related topic--the electrofluid reactor.

The Electrofluid Bed Reactor

Most references to the electrofluid reactor appear in the patent literature. The first literature reference describing an electrofluid device appeared in a patent granted to Wickenden and Okell (44) for a process to make decolorizing carbon in 1927. F. Winkler, a chemist for I. G. Farbenindustrie, proposed a more feasible electrothermal process in his German patent for the production of water gas in 1928 (45). Winkler suggested heating a bed of coke, fluidized with steam, by passing an electric current through the bed via two electrodes submerged in the bed. However, the commercial potential of the process was never exploited.

The development of the electrofluid reactor remained dormant until the late 1950's when a Canadian research group under H. S. Johnson began exploring potential applications of

the electrofluid bed reactor. This research led to patents for the manufacture of hydrocyanic acid (21, 27, 28), carbon monoxide (20), carbon disulfide (19, 23), titanium tetrachloride (20), a process for the desulfurization of coke (19), and heating beds of solid particles (30). As far as is presently known, only hydrocyanic acid is being produced commercially in an electrofluid reactor. In this process, a mixture of ammonia and a hydrocarbon (usually propane or methane) is passed through a bed of coke at 1400°F to 1600°F, producing hydrocyanic acid.

Others followed the Canadians into the electrofluid bed reactor field. Schenck and Wenzel (41) obtained a patent for reducing iron ore in an electrothermal fluidized bed, while Miles and Stephens (34) patented an electrothermal process for producing phosphorous from finely ground phosphate shales. Paquet and Foulkes (37) studied the calcination of coke in an electrothermal fluidized bed. High pressure, high temperature research involving the electrofluid reactor is being conducted by the Institute of Gas Technology in Chicago (32). Also, two Polish research groups are also investigating the properties and applications of the electrofluid reactor (3, 4, 5, 6, 25, 26).

Johnson (18), in an article summarizing much of his research with the electrothermal fluidized bed, commented upon some of the above processes and listed other reactions which

were studied. He concluded that the main applications of the electrofluid reactor would most likely be in the following areas:

(1) reactions favored by rapid heating

(2) reactions favored by temperature levels of 1800°F or above

(3) reactions which have large energy requirements.

Goldberger et al. (10) studied the electrofluid reactor on a broad scale, and stated that the major applications of this type of reactor should lie in three areas:

(1) in the metallurgical field

(2) in the chemical industry

(3) in environmental use as a high temperature gas heater.

Several types of processes which would seem to lend themselves readily to the electrofluid reactor were suggested by them in each area. They operated an electrofluid reactor at temperatures up to 5000°F, and reported that a maximum temperature of 8000°F appears possible. The maximum temperature obtainable depends upon the temperature limitations of the reactor material and the softening or volitilization of the bed particles.

One of the advantages of the electrothermal fluidized bed is the excellent temperature control obtainable. Goldberger et al. (10) explained that temperature control is a matter of power loading, and this can be adjusted by three means:

(1) variation of the velocity of the fluidizing gas

(2) variation of the effective area of the electrodes in the bed

(3) conventional variation of power supplied to the bed.

It was suggested that the first two methods of control would be used for fine adjustments of temperature because of their limited effectiveness, while the third method would be used for coarse temperature control.

Properties of the Electrothermal Bed

Mechanism of current transfer through the bed

One of the primary areas of interest to researchers has been the mechanism of current flow through an electrofluid bed. Goldschmidt and Le Goff (12) suggested the following mechanisms for the passage of current through the bed:

(1) flow by conduction along continuous chains of touching particles

(2) flow by "diffusion"--where a charge is shared between colliding particles

(3) current flow by arcs between particles.

Calculations showed that method (2) was not possible. Also, operating conditions were such that current flow by method (3) was negligible. Therefore, they concluded that mechanism (1) was the primary mode of current transfer through the bed. Graham and Harvey (15) as well as Reed and Goldberger (38)

also reported current flow through fluidized beds by conduction along particle chains.

At higher temperatures and especially at higher voltages and current densities, current transfer may occur jointly by mechanisms (3) and (1). Johnson (18) observed arcing occurring at high voltage gradients (200 volts/in.) and reported that it was objectionable because of the difficulty of controlling the current through the bed. Reed and Goldberger (39) also observed small arcs within their fluidized bed at current densities above 2 amps/sq. in., but concluded that gas-phase ionization appeared minor at current densities below this. This result was supported by Graham and Harvey (15) who reported that current flow by arcing was negligible in their low-voltage studies. However, Goldschmidt and Le Goff (11) observed sparking near the wall of their apparatus at current densities and at voltages much lower than were expected to produce arcing.

Lee et al. (32) in their high-temperature, high-pressure work (up to 1000 lb./sq. in.) felt that the mechanism for current flow at these conditions is through spark discharge between bed particles and across gas gaps. They reported that this mechanism followed a modified Paschen's Law and was analogous to sparking discharge between sperical electrodes in a gaseous atmosphere.

Agreement with Ohm's Law

Several researchers have tried to verify whether the electrofluid bed follows Ohm's Law. Johnson (18) reported that in normal operation the electrofluid bed approximately obeyed Ohm's Law. However, at high voltage gradients he noted a deviation from Ohm's Law and attributed the amount of deviation to the degree of arcing present in the bed. He reported the observation of three distinct regions resulting from different operating conditions of the electrofluid bed:

(1) the Ohm's Law region

(2) an arcing region

(3) a region intermediate between the arcing and Ohm's Law region.

Graham and Harvey (15) also observed that at high voltages (40 to 250 volts across a 2 in. electrode gap) Ohm's Law was not obeyed and suggested the reason as being caused by heating at particle to particle contacts. Ballain (1) operating his reactor at approximately 200 volts noted a reproducible non-ohmic current jump upon an increase in voltage. And, Lee et al. (32) concluded that their operation was in the "intermediate" region between the Ohm's Law and the arcing region.

Components of Interelectrode Resistance

There is indication in the literature (17, 39) that the interelectrode resistance is the sum of a contact resistance between the electrodes and the bed particles and the resistance of the particles themselves. However, more literature has been published concerning parameters which affect the particle resistance of the bed than the contact resistance.

Factors affecting bed resistance

The mechanism of current transfer is closely related to the resistance of the bed particles in that factors which inhibit the transfer of current through the bed would be expected to increase the resistance of the bed. Since most researchers (10, 12, 15) feel that at normal electrical operating levels the flow of current through the bed is by particle to particle linkages, then factors which would cause the breaking of these linkages would be expected to increase the resistivity of the bed. Conversely, factors which assist in the formation of these conductive chains would be expected to decrease the bed resistivity.

Velocity of fluidizing gas Jones (24) measured the effect of velocity on the resistivity of fluidized beds of coke and graphite at room temperatures. As the fluidizing gas velocity was increased in the fixed bed the resistivity rose gradually until the incipient fluidization velocity was

reached. Then the resistivity increased sharply up to a maximum which occurred just beyond the incipient fluidization velocity. Upon further increase of velocity, the resistivity decreased to a minimum value and then increased again. Graham and Harvey (15) reported similar findings, but Goldschmidt and Le Goff (12) reported no peak resistivity occurring after the incipient fluidization velocity was exceeded. Instead, they observed a continuous increase in bed resistivity with increasing gas velocity. At the incipient fluidization velocity, the maximum rate of change of resistivity with velocity occurred.

Temperature In their comprehensive study of the factors influencing bed resistivity, Graham and Harvey (15), observed the effect of temperature on the resistivity of beds of graphite and coke particles fluidized with nitrogen. By increasing the temperature of the bed at a fixed gas flow rate, they reported an increase of bed resistance with temperature up to 600°C. Above this temperature the resistance of both bed materials started to decrease. The graphite bed resistance continued to decrease with increasing temperature, while the resistance of the coke bed passed through a minimum and then increased.

Bed composition The nature of the electrofluid bed material appears to be limited to granular materials capable of conducting an electric current, or non-conductors which have

a surface layer of conducting material. Kalinowski et al. (25) reported that uranium and thorium powders may have potential as coating agents. However, in most of the other investigations as well as in the present study, carbonaceous materials (coke, graphite, or coal char) have been used as the bed material.

Studies of the electrical resistivity of fluidized beds of mixtures of conducting and non-conducting particles were carried out at Iowa State University (7, 40). The results of this research show that addition of non-conducting coke or sand to conducting beds of graphite does not increase the resistance of the bed significantly until at least 50% of the bed is composed of the non-conducting material. Above the 50% range, however, the addition of sand or non-conducting coke strongly affects bed resistivity. Small amounts of Cab-O-Sil, a super-fine silica, amounting to 2 to 3% of the bed material added to a graphite bed had a marked effect on the resistivity of the bed. Evidently, the graphite particles are surrounded by the non-conducting Cab-O-Sil, which insulates the particles to current flow.

Particle size The effect of particle size on bed resistance has been investigated by several researchers (15, 24, 38). There is general agreement among all of them that the bed resistance increases as the average particle size of the bed decreases. This may be due to the fact that the conductive chain linkages in the bed are more easily broken in beds of

finer particle sizes.

Bubbles and particle shape Graham and Harvey (15) investigated the effect of bubbles on bed resistivity and determined that the net effect of bubbles was to decrease bed resistivity. They hypothesized that the increase in the density of the dense phase in a fluid bed would cause the bed particles to become more concentrated and would thus facilitate the transfer of current by particle to particle linkages. Graham and Harvey also stated that the probable difference between the resistance of beds of spherical and angular particles was due to the fact that bubbles can be formed more easily in the angular particles.

Current density Reed and Goldberger (38) were the first to report on the variation of resistivity with current density. At room temperature and at current densities of 2.5 to 100 ma./sq. in. they found the resistance of the bed to be constant with current densities ranging from 0.3 to 2.5 amps/sq. in., they reported a decrease in bed resistivity with an increase in current density.

Contact resistance

Carbon surfaces are submicroscopically rough and, therefore, the apparent contact area between two contacts is not the actual contact area (17). Usually the actual contact area is less than the apparent contact area because the two surfaces make actual contact only through their surface projections.

And, the number of surface projections in intimate contact between the two surfaces constitutes only a very small fraction of the apparent contact area. Actually, the contact resistance can be more accurately termed a constriction resistance since the current flow is constricted to flowing through the surface projections in contact at the two surfaces (17).

Contact resistance in fixed beds Because of interest in the conductivity of packed beds of carbon used in carbon microphones , there is some work reported in the literature concerning contact resistance between particles in fixed beds.

The resistance of a fixed bed of carbon granules is the sum of the resistance of the inter-particle contacts and the resistance of the particle bodies themselves. Grisdale (16) found that for pyrolytic carbon the contact resistance is large compared to the body resistance for carbon thicknesses exceeding 0.00003 cm. Also, he noted that the orientation of carbon crystals has an effect upon the resistivity of carbon particles and, that the resistance to current flowing perpendicular to the basal plane of a graphite crystal is 100 to 10,000 times greater than the resistance to current flowing parallel to the basal plane. Therefore, the contact resistance is dependent upon the degree of orientation of graphitic crystal at the surface.

Fluid bed contact resistance Graham (14), using a voltage probing technique, first reported the presence of an

"electrode" or contact resistance in an electrofluid bed. He inserted a probe into a bed between two concentric electrodes and obtained a voltage profile by varying the radial position of the probe. The resulting experimental profile agreed with the theoretical profile expected for a homogeneous conducting material except near the center electrode. At the center electrode a significant deviation from the theoretical curve was found. However, his results were somewhat inconclusive because of the inaccuracies associated with probe measurements near the center electrode. This was due to the fact that the probe length was large with respect to the voltage gradient near the center electrode.

Reed and Goldberger (38) reported that interelectrode resistance in an electrofluid bed was the sum of the resistance through the bed and the contact resistance at the electrodes, and they attempted to isolate the two components of the inter-electrode resistance. They inserted copper screens into a rectangular bed between two electrodes. The voltage drop between the screens was measured at zero current flow in the measuring circuit. Knowing the bed current flow, the bed resistance was calculated by Ohm's Law. The overall voltage drop between the bed electrodes was also measured and the voltage drop due to the bed resistance subtracted from it to give the voltage drop due to the contact resistance. They also reported a deviation in the voltage profile near the electrode

and concluded that it was due to the effect of contact resistance between the bed particles and the electrode.

Reed and Goldberger noted that the contact resistance decreased with increasing current density and was sensitive to the condition of the electrode surface. Glidden (9) concluded in his room temperature studies that the contact resistance was a function of particle diameter, relative gas velocity, and the interaction between the particle diameter and the electrode diameter squared. Moreover, he reported that contact resistivity was only 1 or 2% of bed resistivity. Shine (43), however, reported that the contact resistance between the electrode and the bed constituted the greater part of the effective electrical resistance in an industrial-scale electrofluid bed reactor. He also stated that the bed resistance was so small relative to the contact resistance that the bed resistance could be neglected in most circumstances.

EXPERIMENTAL INVESTIGATION

Equipment and Procedure

The equipment used in the investigation consisted of a gas recycle system, columns used to contain a fluidized bed of conducting particles, and electrical measurement apparatus used to determine the electrical characteristics of the fluidized bed.

Gas recycle system

The purpose of the gas recycle system was to provide fluidizing gas for the bed, and to efficiently reuse this gas to minimize the cost of operation. The gas recycle system flowsheet is shown in Figure 1.

Nitrogen gas was used as the fluidizing medium and was obtained from nitrogen shipping cylinders. A positive displacement Gast model 2065 rotary compressor which compressed the gas to approximately 10 lb./sq. in. gauge was used to pump the nitrogen through the system. Following the compressor, the nitrogen passed through a felt oil filter element and then through an air-cooled, finned-tube heat exchanger with the 142 sq. ft. of surface area which removed the heat of compression. A silica gel dryer was installed after the heat exchanger to remove any moisture in the gas stream.

Figure 1. Gas recycle system flowsheet

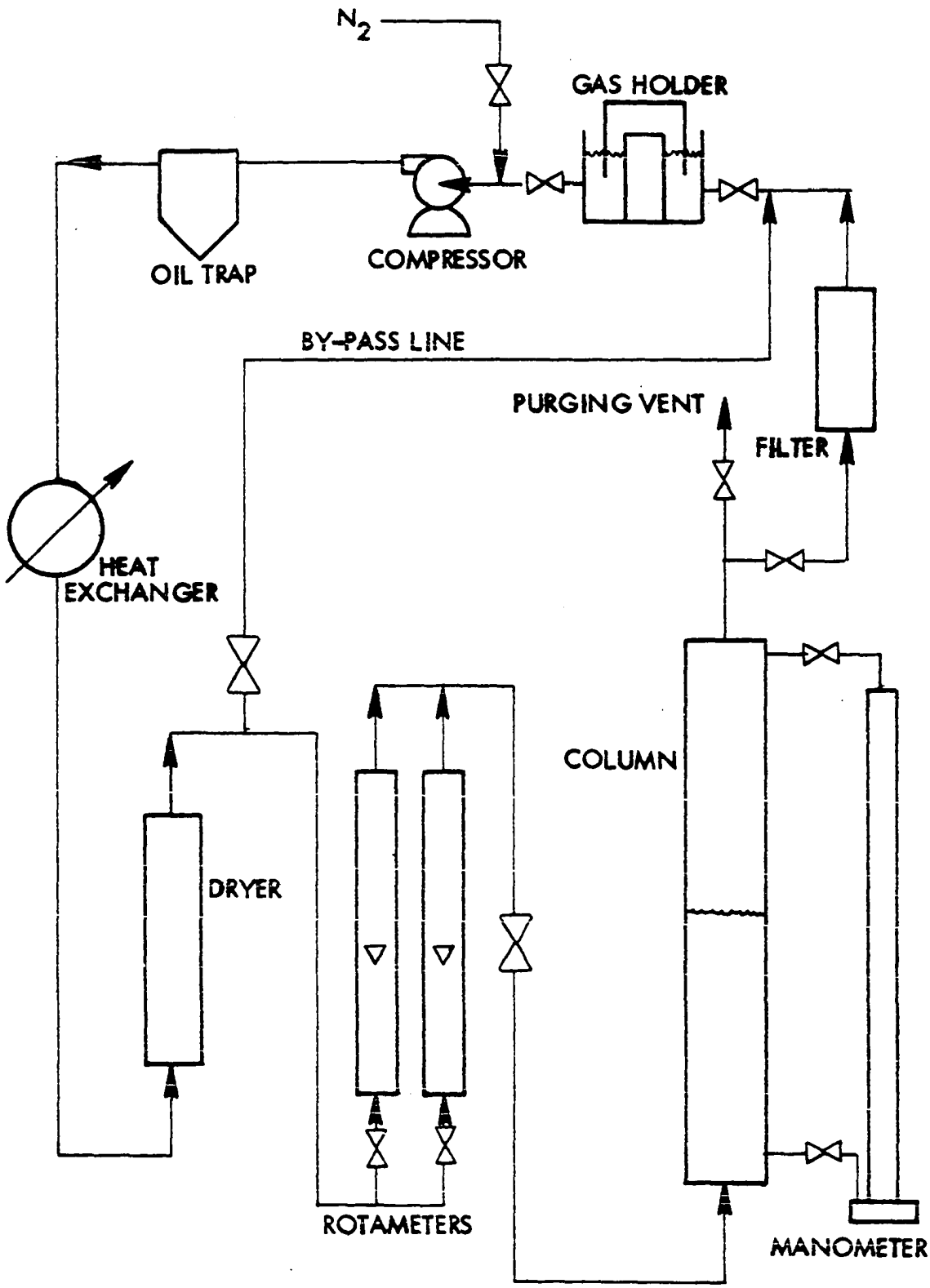
N_2
GAS HOLDER
OIL TRAP
COMPRESSOR
BY-PASS LINE
PURGING VENT
FILTER
HEAT EXCHANGER
COLUMN
DRYER
ROTAMETERS
MANOMETER

Following the dryer a by-pass line was used to reroute the gas in excess of that needed to fluidize the bed to a gas holder. The gas holder was a double-drum, annular, oil-sealed tank which was counterweighted. Limit switches actuated by the counterweight shut off the compressor when the holder was empty and activated a buzzer-alarm when the holder was full.

The nitrogen which passed through the column was metered by two rotameters. The smaller rotameter had a flow rate range of 0 to 1.76 std. cu. ft./min. and the larger rotameter flow rate range was from 0 to 12.9 std. cu. ft./min. The gas flow through the rotameters was controlled by adjusting the by-pass valve. Taps in the gas line after the rotameters enabled the gas pressure to be measured at that point for flow rate corrections.

From the rotameters the nitrogen entered the bottom of the column and passed through a porous plate gas distributor. The distributor was a Norton Alundum P-2120 plate 1 in. thick. A 4 in. diameter plate was used with the 4 in. column and a 6 in. diameter plate with the 6 in. column. The plates were seated in a steel support spacer and Devcon Flexane 85, a flexible urethane casting material, was poured into the space between the plates and the spacers to prevent gas leakage around the circumference of the Alundum plates. Rubber gaskets were placed on both sides of the Alundum plate to seal against gas leakage between the bottom section of the column and the

support spacer.

After leaving the column, the nitrogen passed through a filter to remove dust and elutriated bed particles from the gas. The nitrogen was then routed to the gas holder, and at this point was ready to be recycled through the system again.

Columns

Column sizes of 4 in. and 6 in. inside diameter were used in the investigation. Both sizes were constructed of Plexiglas tubing with a 1/4 in. wall thickness. Both columns basically consisted of two sections. The bottom section of each column contained the fluidized bed and was used as the test section. Four different types of test sections were used, depending on the type of measurements to be made. In both the 4 in. and 6 in. columns, a 4-1/2 ft. section was placed atop the test section so as to minimize the elutriation of fine particles from the bed.

The 6 in. diameter test section shown in Figure 2 was used in measuring the interelectrode resistance of the bed. A brass screen was cemented to the inside of the column wall and served as one electrode of the test cell. The other electrode was a 1 in. diameter graphite rod, 24 in. in length, which was positioned in the center of the column by means of a brass electrode holder. A brass cup 3/4 in. deep, into which the center electrode fit, firmly anchored the center electrode to the electrode holder. The holder itself rested upon the top

Figure 2. Detailed drawing of the 6 in. diameter fluidized bed test cell used to measure interelectrode resistance

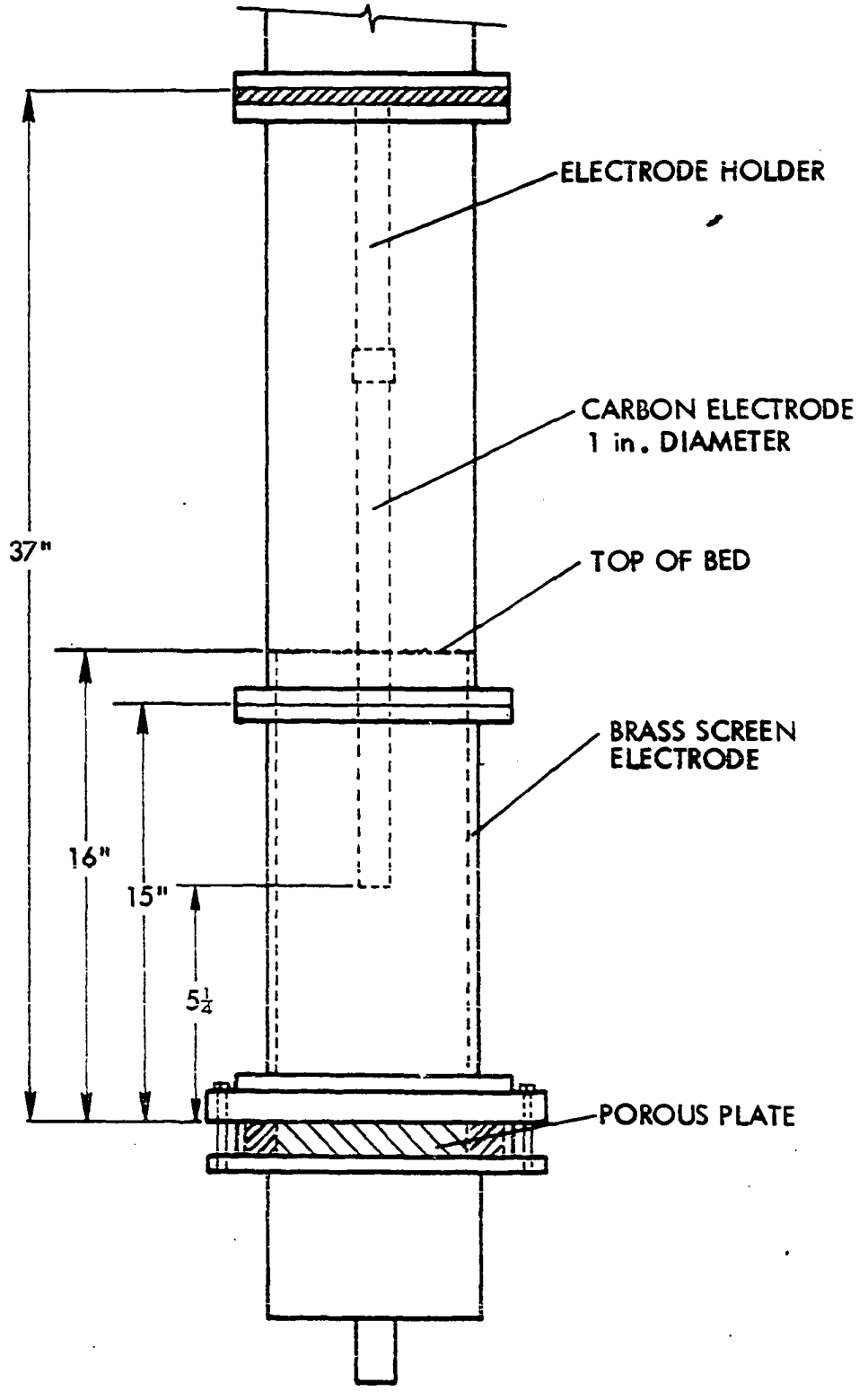
ELECTRODE HOLDER
CARBON ELECTRODE
1 in. DIAMETER
37"
TOP OF BED
BRASS SCREEN
ELECTRODE
16"
15"
5¼
POROUS PLATE

flange of the test section. Cork gaskets were glued to both sides of the electrode holder to prevent gas leakage.

The test sections shown in Figures 3 and 4 were used in measuring the bed resistance and differed from each other only in dimension. In the 6 in. diameter test section two copper-foil electrodes, 1/2 in. in width and 12 in. apart, were cemented to the wall of the column by an epoxy glue. Copper wires were connected to the electrodes through holes drilled in the column wall. The end of each wire was flattened by a hammer and the wires electrically connected to the copper strips by Silver Circuit Print--a silver emulsion used in repairing printed circuits in the electronics industry.

Holes, vertically aligned and 1/2 in. apart, were drilled perpendicular to the axis of the bed in both the 4 in. and 6 in. diameter test sections to accommodate the voltage probes. The probes were two steel bead needles 0.017 in. in diameter and 2-1/4 in. in length, and were located 1-1/2 in. apart in the midsection of the column between the copper-foil electrodes.

The test section shown in Figure 5 was used to visually detect arcing in the bed. A small steel rod (1/16 in. in diameter and flat on the end) was inserted through the side of a 6 in. diameter test section and approximately 1/16 of an inch into the bed. The rod served as the outer wall electrode and its small size concentrated the voltage gradient near its tip.

Figure 3. Detailed drawing of 6 in. diameter test section used to measure bed resistance

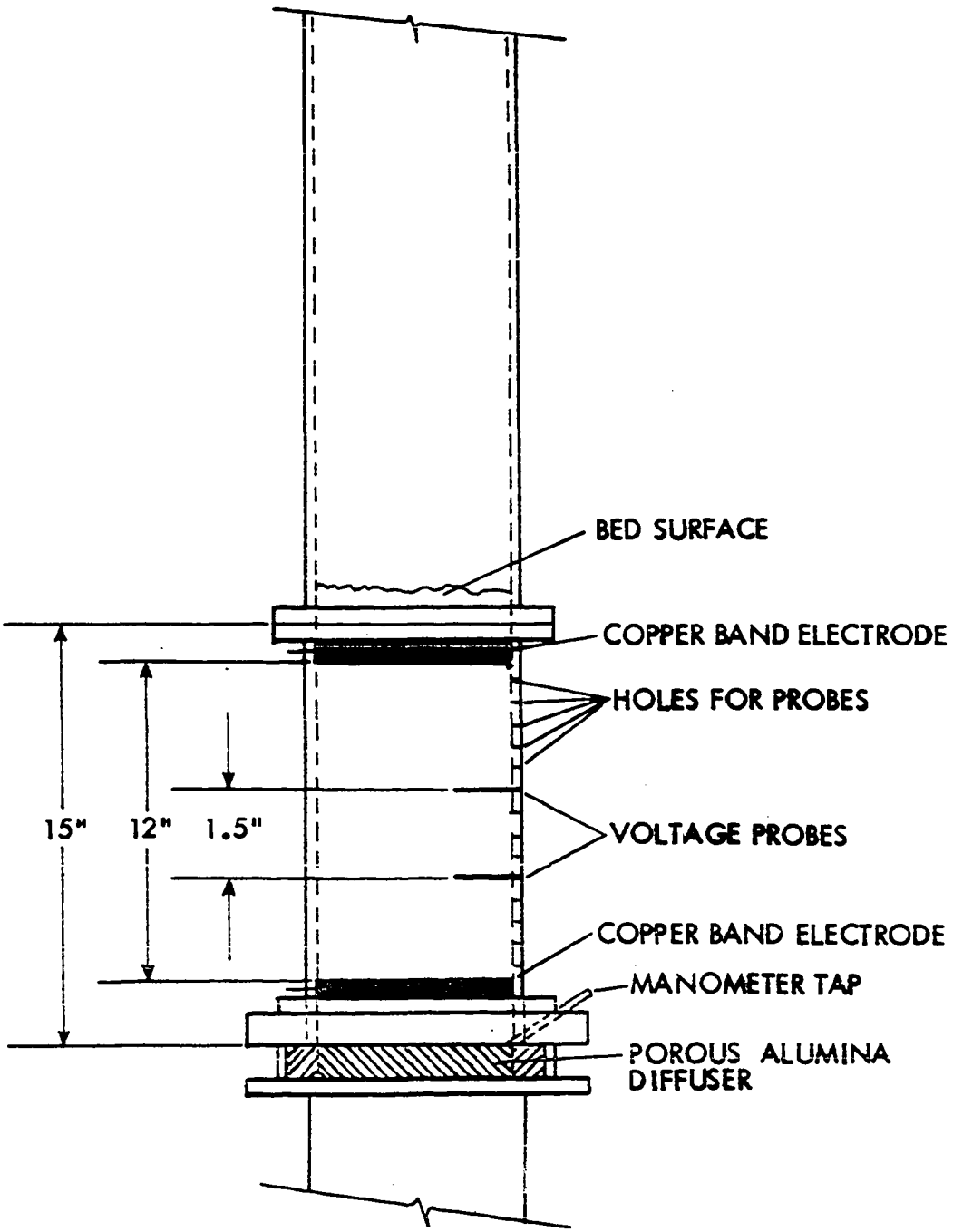
BED SURFACE
COPPER BAND ELECTRODE
HOLES FOR PROBES
15"
12"
1.5"
VOLTAGE PROBES
COPPER BAND ELECTRODE
MANOMETER TAP
POROUS ALUMINA DIFFUSER

Figure 4. Detailed drawing of 4 in. diameter test section used to measure bed resistance

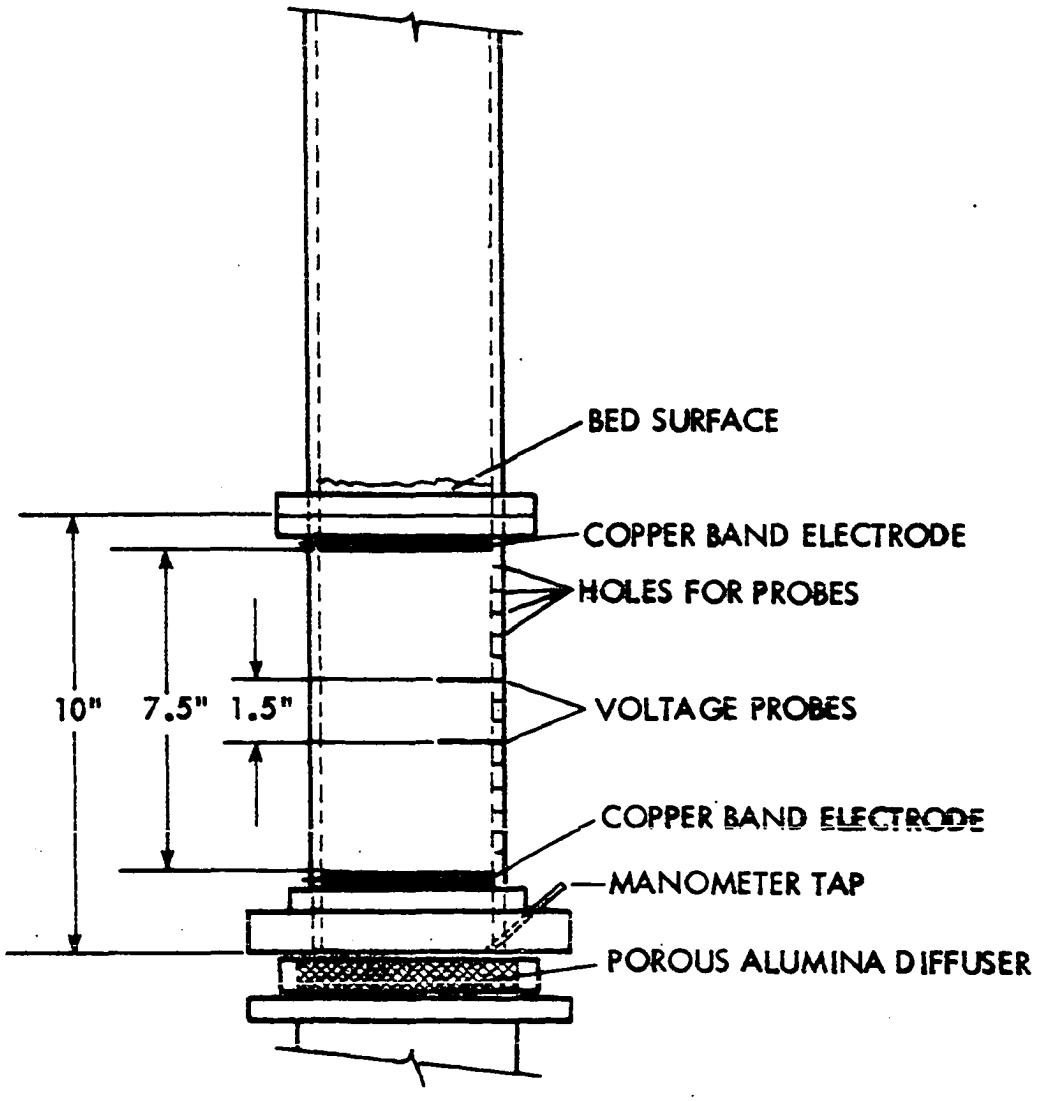
BED SURFACE
COPPER BAND ELECTRODE
HOLES FOR PROBES
10"
7.5"
1.5"
VOLTAGE PROBES
COPPER BAND ELECTRODE
MANOMETER TAP
POROUS ALUMINA DIFFUSER

Figure 5. Drawing of test section used to detect arcing in the bed

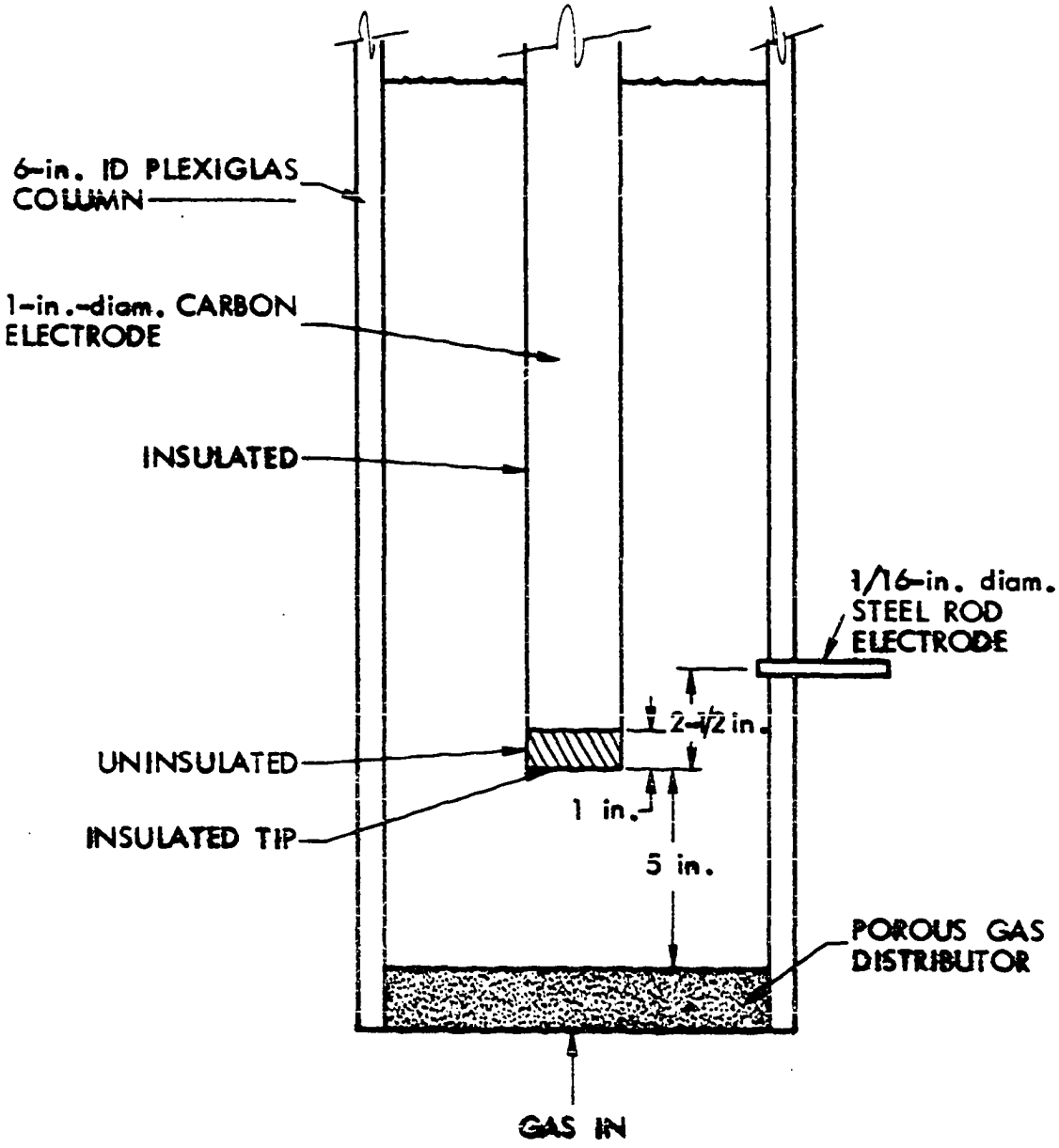
6-in. ID PLEXIGLAS COLUMN
1-in.-diam. CARBON ELECTRODE
INSULATED
1/16-in. diam. STEEL ROD ELECTRODE
2-1/2 in.
UNINSULATED
INSULATED TIP
1 in.
5 in.
POROUS GAS DISTRIBUTOR
GAS IN

The shallow bed insertion of the rod made it possible to visually detect arcing occurring near the tip of the rod.

The rod was positioned 2 in. above the tip of the 1 in. diameter graphite center electrode which was insulated everywhere except for a 1 in. length at its tip.

The test section shown in Figure 6 was used to measure the potential field between a center graphite electrode 1 in. in diameter and a brass-screen wall electrode 14 in. in length. A Plexiglas slab was cemented to the test section of Figure 6. Five holes 1/2 in. in diameter were drilled in the slab at points 3.33, 5.67, 8.00, 10.33, and 12.67 in. above the gas distributor to accommodate the voltage probes.

The voltage probes were made of a 3-1/4 in. length of 1/16 in. diameter brass rod soldered to a 9 in. length of 1/2 in. diameter brass rod. The larger diameter portion of the voltage probes fitted snugly in the holes in the slab. These holes acted as guides to minimize probe tip movements perpendicular to the direction of probe travel. The smaller diameter part of the probes (which was the portion of the probes which actually probed the bed) was insulated electrically from the bed except at the very tip of the probes, so that point voltages could be measured. Brass fittings, 1/2 in. in diameter in conjunction with O-rings held the probes in the desired radial position, and also provided a gas-tight seal. A dial micrometer (accurate to .001 in.) attached to an

Figure 6. Detailed drawing of 6 in. diameter test cell used to determine the bed potential field

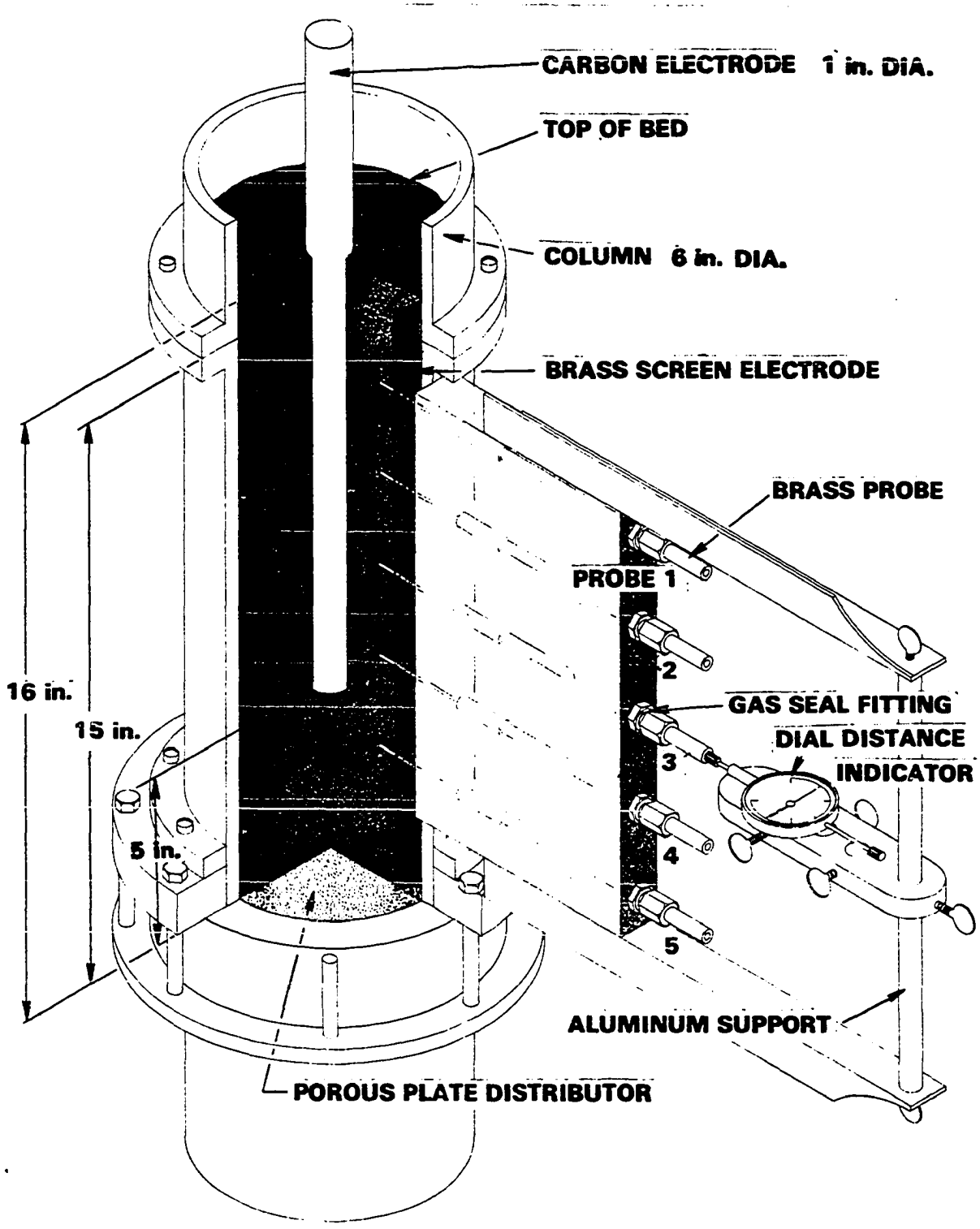
CARBON ELECTRODE 1 in. DIA.
TOP OF BED
COLUMN 6 in. DIA.
BRASS SCREEN ELECTRODE
BRASS PROBE
PROBE 1
2
GAS SEAL FITTING
DIAL DISTANCE INDICATOR
3
4
5
16 in.
15 in.
5 in.
ALUMINUM SUPPORT
POROUS PLATE DISTRIBUTOR

aluminum support was used to measure the distance of the probe tip from the center of the column or the center electrode.

The bottom of the brass-screen wall electrode did not touch the distributor plate as in the other test sections of this type. Since the fluidization immediately above a distributor is characteristically atypical compared to that in the rest of the bed, it was felt that this could cause an uncharacteristic distortion of the potential field in the bed region immediately above the distributor. Therefore, the bottom of the screen electrode was raised to a point 2 in. above the distributor plate.

Electrical instrumentation

Several different electrical circuits were used in the investigation. In most cases the electrical instrumentation consisted of two basic circuits--a current circuit and a measuring circuit. The current circuit was used to supply and control the type and amount of current (or voltage) to the bed. The measuring circuit was used to measure the characteristic voltage drop between two points in the bed.

Interelectrode resistance Three different electrical setups were used in the measurement of the interelectrode resistance. The electrical instrumentation used in nearly all the interelectrode resistance measurements is shown in Figure 7. In this arrangement a direct current power supply capable of supplying 0 to 30 volts was employed as the current source for

Figure 7. Schematic of electrical circuit used to measure interelectrode resistance (negative ground)

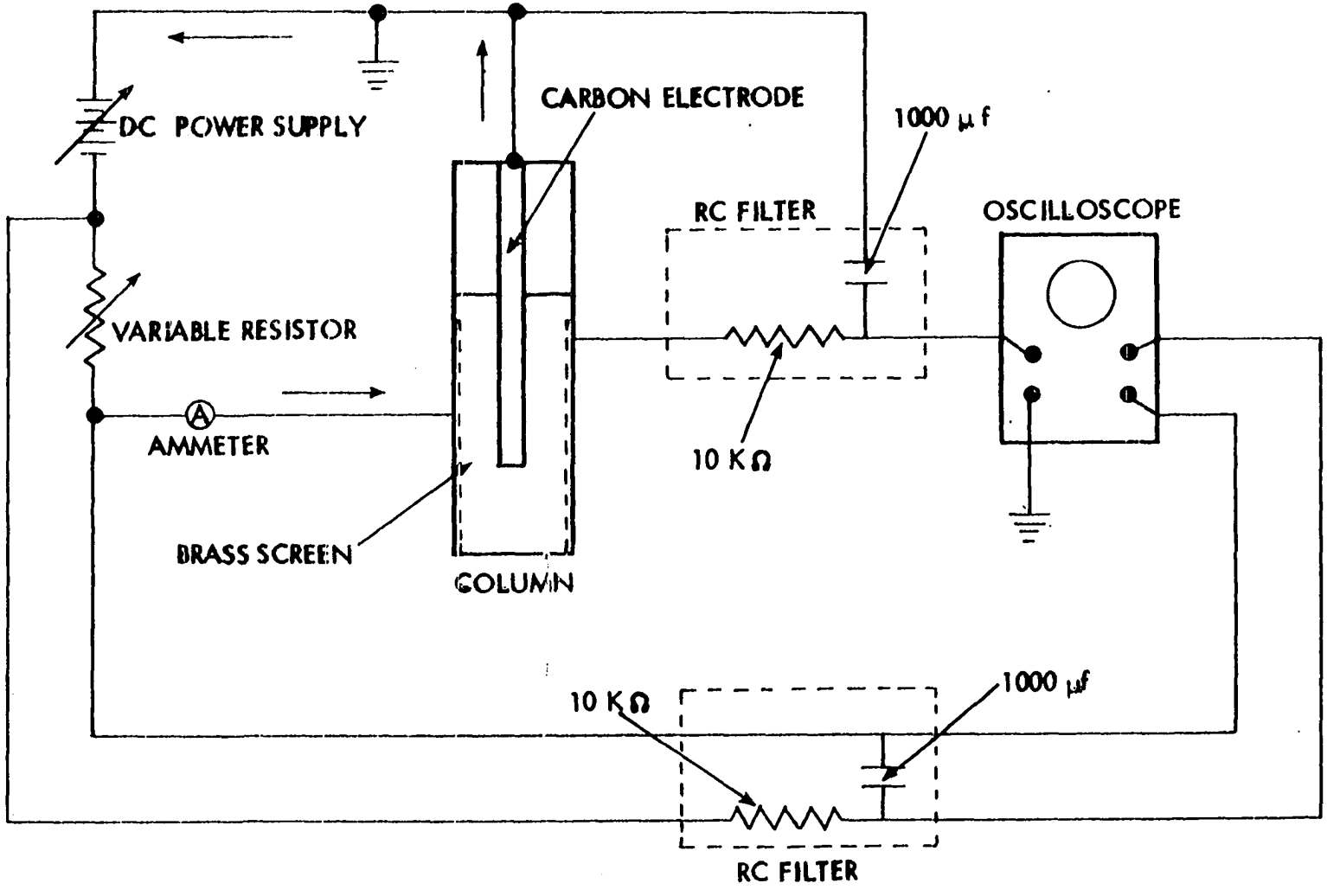
DC POWER SUPPLY
CARBON ELECTRODE
1000 μf
RC FILTER
OSCILLOSCOPE
VARIABLE RESISTOR
A
AMMETER
10 KΩ
BRASS SCREEN
COLUMN
10 KΩ
1000 μf
RC FILTER

the current circuit. The current flowed from the power supply to a model 1171 Eico decade resistance box with a range of 0 to 99,999 ohms which was used in conjunction with the power supply. By varying the resistance setting of the decade box at a constant voltage setting, the desired bed current level could be obtained. A Hewlett-Packard 410-C combination voltmeter and ammeter with a range of 0 to 150 ma. was placed in the circuit after the decade box to indicate the current flow in the current circuit. Following the ammeter, the current flowed through the test section of the column. It then passed on to the power supply, the negative terminal of which was grounded, completing the circuit.

Because of the violent movement of the fluidized bed particles, the current flow through the current circuit fluctuated, resulting in random oscillations of the ammeter needle. Thus, the ammeter was used only as a general indicator of the current level. Therefore, the voltage drop across the decade box was measured on one beam of a dual beam Tektronix 502A oscilloscope. Although this voltage drop fluctuated also, the fluctuations were smoothed by an RC filter located between the decade box and the oscilloscope. From the value of the voltage drop across the decade box and the resistance of the box, an average bed current could be calculated.

In the measuring circuit, two leads were connected across the center electrode (at ground potential) and the brass wall

electrode of the test cell (Figure 2) to obtain the voltage drop representative of the interelectrode resistance. The voltage signal from the bed was then sent through an RC filter which "averaged" the voltage fluctuations caused by the motion of the bed particles. This average interelectrode voltage drop was then measured on the second beam of the oscilloscope.

The second setup used in the study of the interelectrode resistance is shown in Figure 8. This setup was used to determine whether reversing the polarity of the direct current voltage in the current circuit would appreciably affect the interelectrode resistance. The difference between this setup and the setup described above was that in the above current circuit the direct current power supply was negatively grounded and in this setup the power supply was positively grounded.

In order to determine whether alternating current affected interelectrode resistance differently than direct current, the electrical setup shown in Figure 9 was employed. A Variac transformer was used to control the line voltage from 0 to 100% of its maximum value (104 volts) in the current circuit. The current passed from the Variac to the Eico decade resistance box used in the above current circuits, and from there to an AC ammeter having a range of 0 to 1 amp. Following the ammeter, the current passed through the test cell and then back to the Variac, completing the circuit.

Figure 8. Schematic of electrical circuit used to measure interelectrode resistance (positive ground)

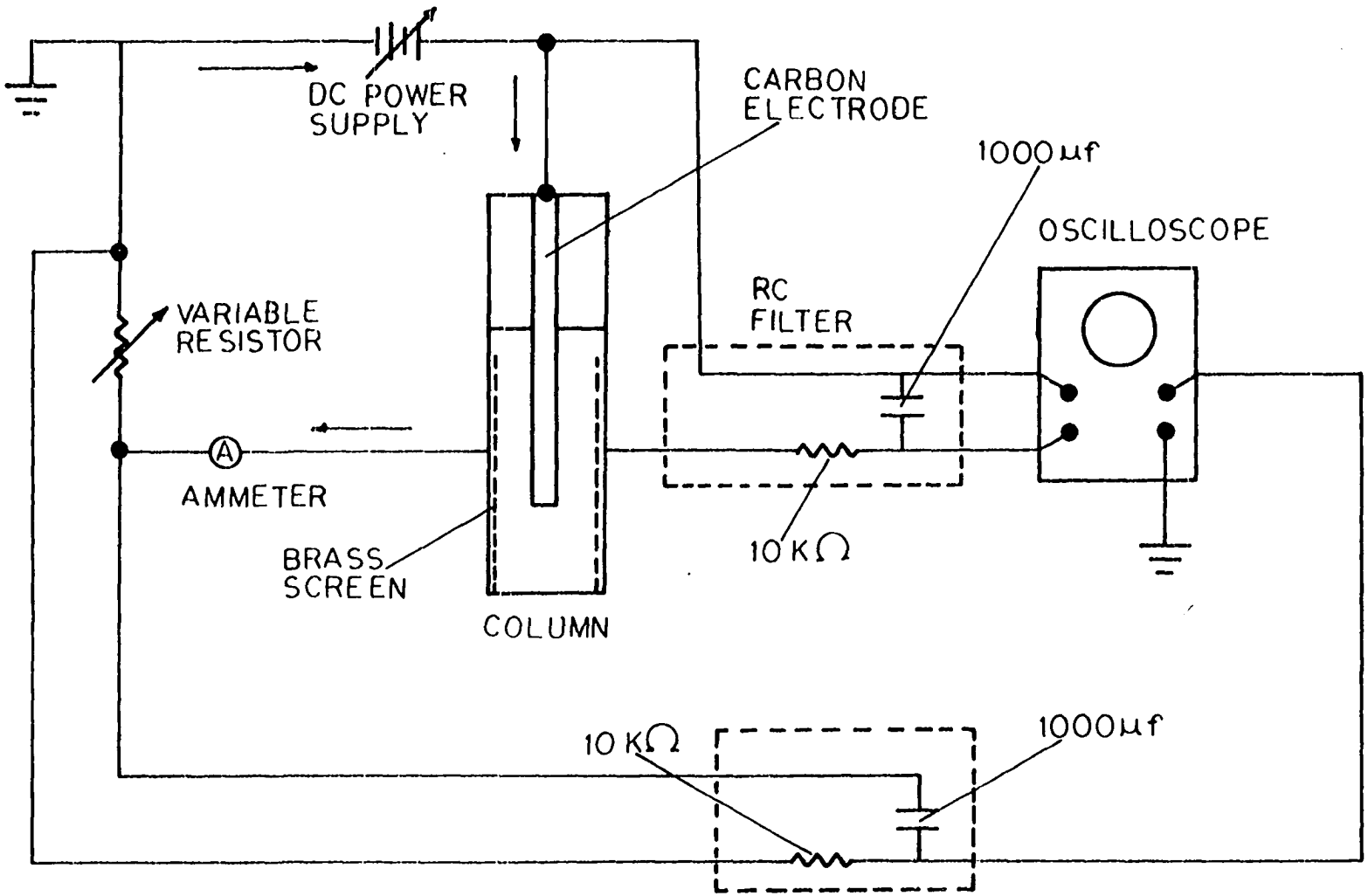
DC POWER SUPPLY
CARBON ELECTRODE
1000μf
OSCILLOSCOPE
RC FILTER
VARIABLE RESISTOR
A
AMMETER
BRASS SCREEN
COLUMN
10 KΩ
10 KΩ
1000μf

Figure 9. Schematic of electrical circuit used to measure interelectrode resistance (alternating current)

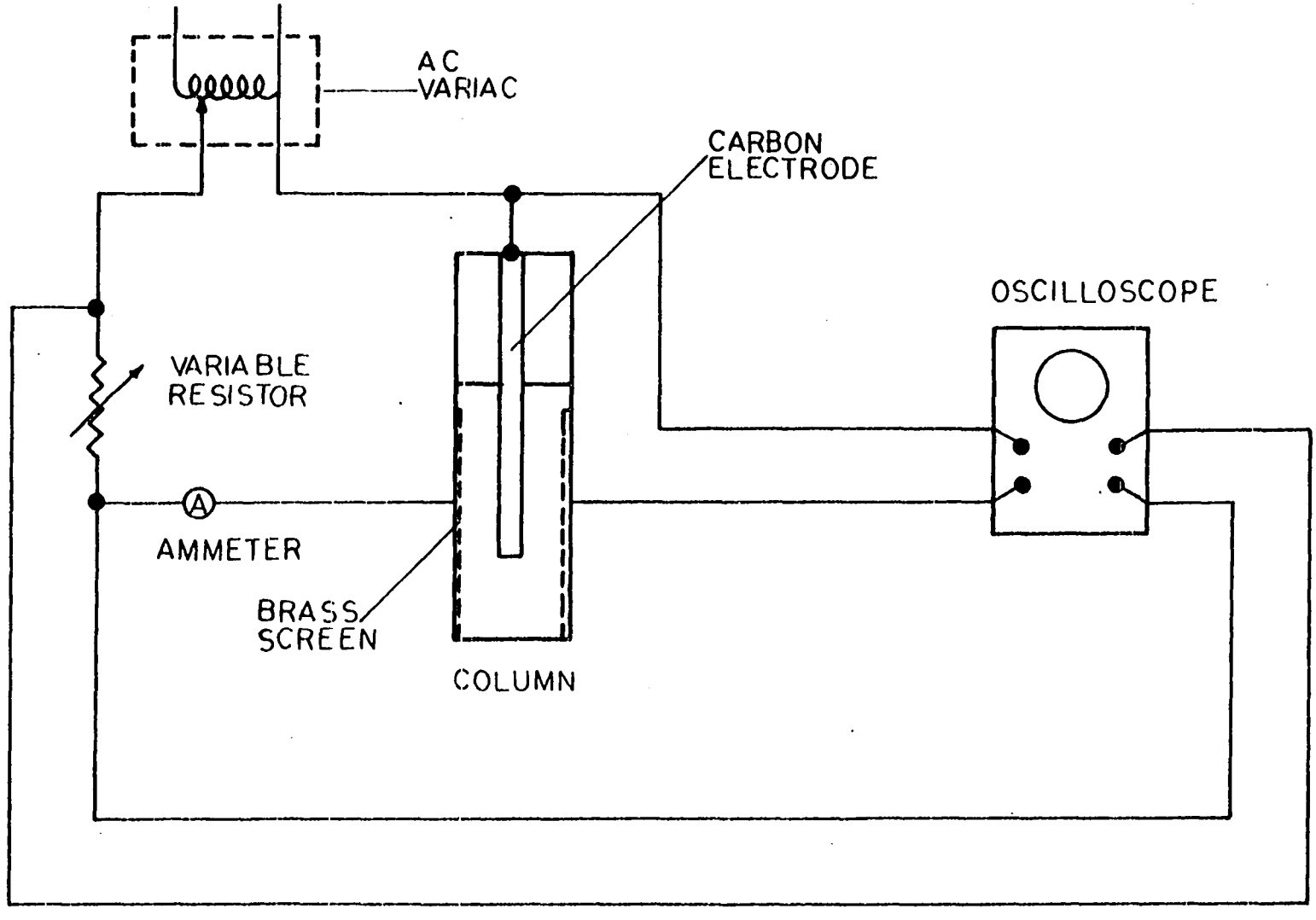
AC
VARIAC
CARBON
ELECTRODE
OSCILLOSCOPE
VARIABLE
RESISTOR
A
AMMETER
BRASS
SCREEN
COLUMN

The RC filters were not used to average the fluctuations of the bed and decade box voltage drops in the measuring circuit. This was because the filters acted as voltage attenuators to the alternating voltage signal and the fluctuations could not be averaged. Therefore, a Polaroid camera was mounted on the scope and photographs were taken of the bed and decade box voltage traces. Average values of the voltage measurements were taken from the photographs.

Bed resistivity Bed particle resistance was measured using the four-point probe method described by Jones (24). The circuitry used for this technique is shown in Figure 10. With the exception of the test section, the current circuit used was exactly the same as was used in the measurement of the inter-electrode resistance with the negative terminal of the power supply grounded (Figure 7).

In the measuring circuit, two leads were connected to the needle voltage probes of the test cell. This voltage drop was not averaged by an RC filter, but was sent directly to the oscilloscope. Because of the relatively large resistance of the oscilloscope (1 megohm input impedance) negligible current flowed through the probes. Theoretically then, no contact resistance was present at the probes and the voltage drop across the probes was due to the bed resistance alone.

The probe voltage drop was not smoothed by the use of an RC filter in order to prevent inducing a current in the

Figure 10. Schematic of electrical circuit used to measure bed resistance

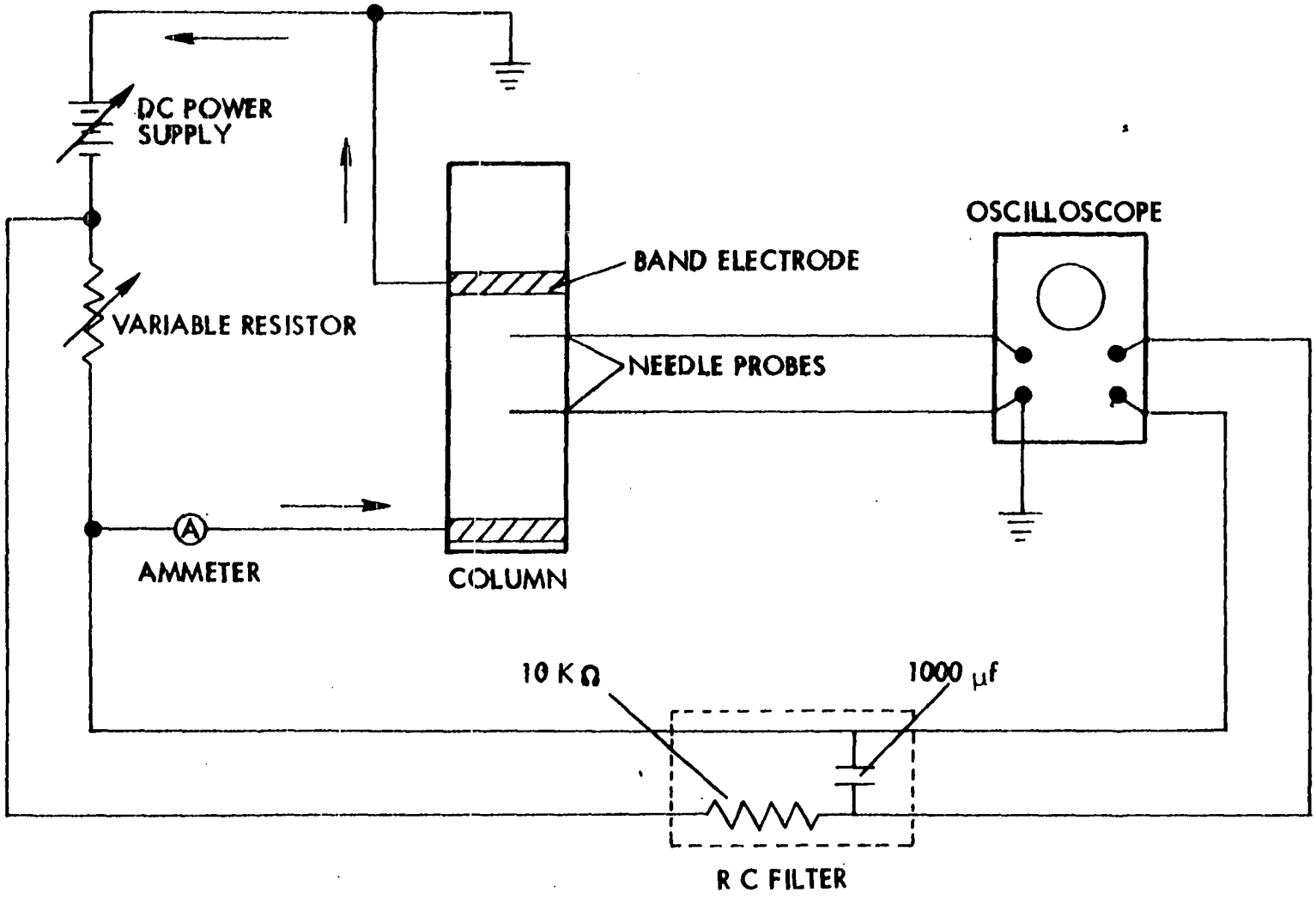
DC POWER SUPPLY
VARIABLE RESISTOR
AMMETER
A
COLUMN
BAND ELECTRODE
NEEDLE PROBES
OSCILLOSCOPE
10 KΩ
1000 μf
R C FILTER

measuring sub-circuit consisting of the fluid bed, the filter resistor, and the filter capacitor.

Potential field determination The electrical circuitry used in the experimental determination of the potential field in the fluidized bed is shown in Figure 11. Again, with the exception of the test section, the current circuit used in the determination of the potential field was the same as was used in the measurement of the interelectrode resistance with the negative terminal of the power supply grounded.

In the measuring circuit, leads were connected to the center electrode, the brass voltage probes, and the brass-screen wall electrode. Thus, the voltage drop could be measured between the center electrode and each probe, or between the center electrode and the brass-screen wall electrode. The particular voltage drop desired was measured on a Hewlett-Packard 410C voltmeter having an input impedance of approximately .11 megohms. Because of this extremely high resistance, negligible current flowed through the voltage probes. Although the measured voltages fluctuated randomly, the voltmeter needle appeared to dampen the fluctuations to some extent and an average voltage value could be read directly with the voltmeter.

Arcing experiment The apparatus and electrical circuitry used to visually observe arcing in the test section of Figure 5 is depicted schematically in Figure 12. The current and measuring circuits used were the same as were

Figure 11. Schematic of electrical circuit used to measure bed potential distribution

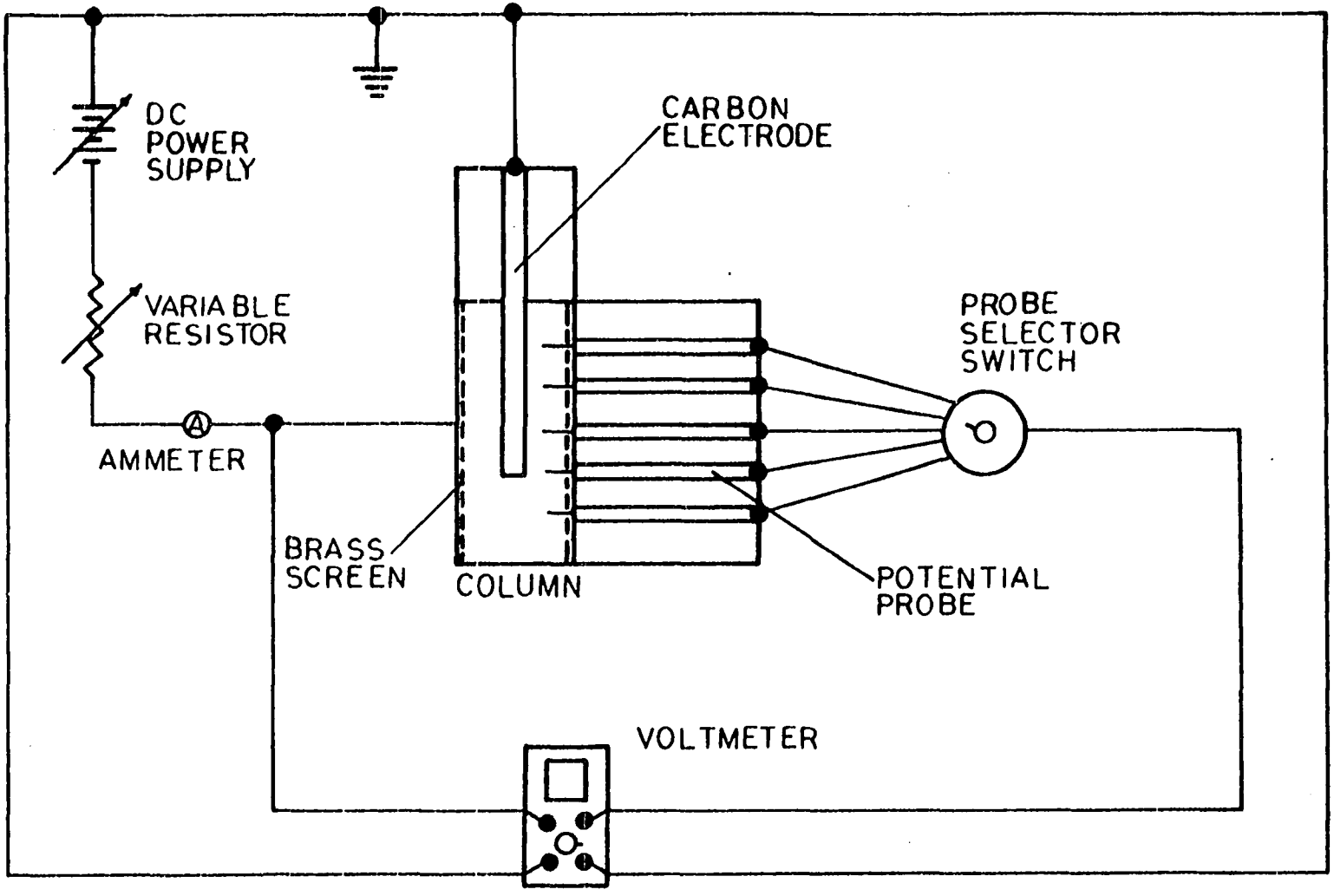
DC
POWER
SUPPLY
CARBON
ELECTRODE
VARIABLE
RESISTOR
PROBE
SELECTOR
SWITCH
AMMETER
BRASS
SCREEN
COLUMN
POTENTIAL
PROBE
VOLTMETER

Figure 12. Schematic of electrical circuit used in visual determination of arcing

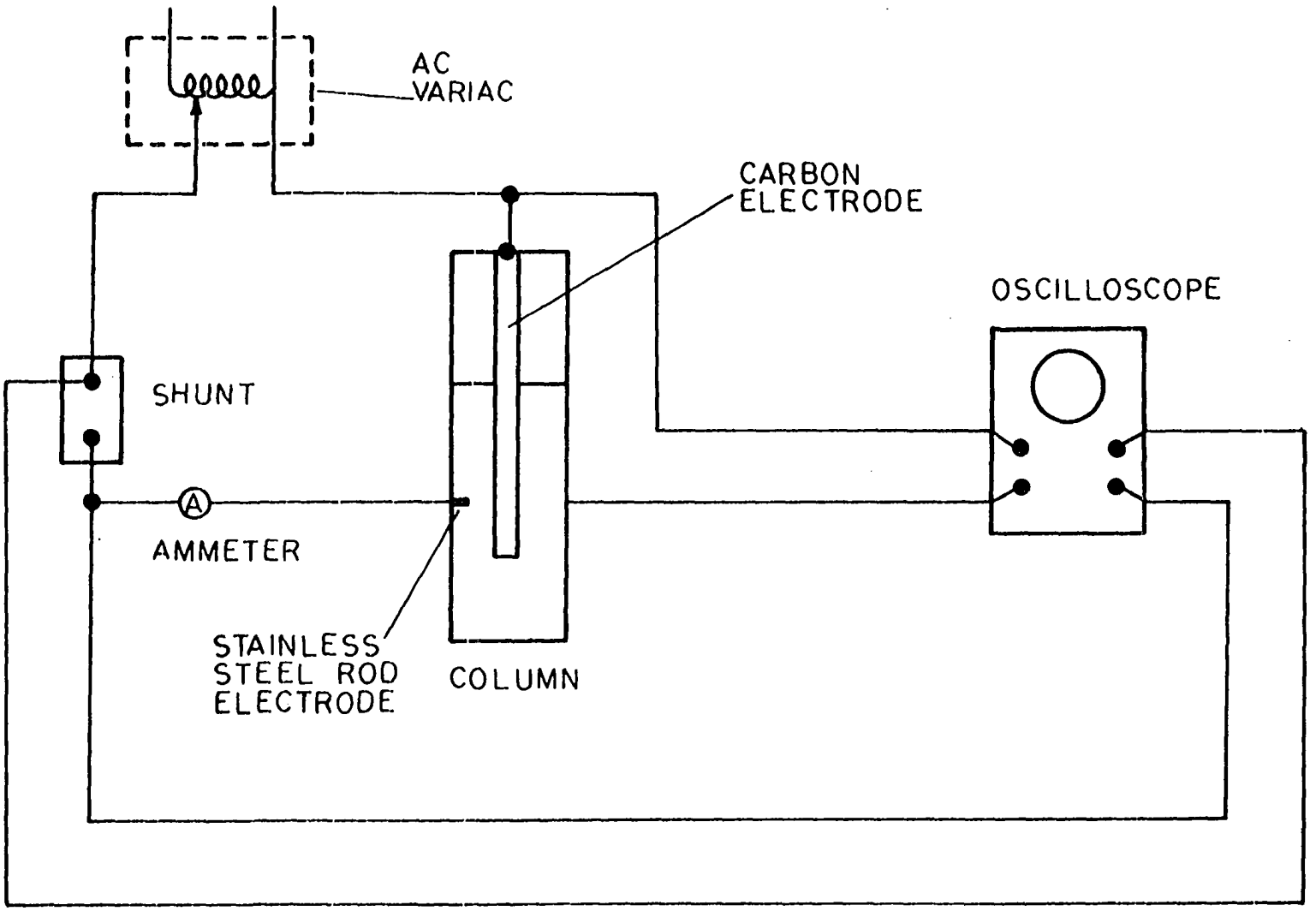
AC
VARIAC
CARBON
ELECTRODE
OSCILLOSCOPE
SHUNT
A
AMMETER
STAINLESS
STEEL ROD
ELECTRODE
COLUMN

employed in the measurement of the interelectrode resistance using AC excitation except for the inclusion of a Weston shunt (1 amp, 50 mv) between the Variac and the ammeter. This shunt was of use in obtaining a trace of the bed current waveform used in analysis of the voltage-current relationship.

Direct current excitation, using a current circuit exactly the same as in the measurement of the interelectrode resistance with the power supply negatively grounded, was also used.

Experimental Procedure

Preliminary procedure

Several basic preliminary steps were taken prior to each use of fluidization column. First, the column containing the appropriate test section was charged with calcined coke to the desired bed height. This was accomplished in the following manner. The coke was fluidized and allowed to settle. If the resulting bed height was not the desired height, coke was either added or removed, as the specific case warranted, and the bed refluidized and allowed to settle again. This procedure was repeated until the desired height was obtained.

The system was then purged to remove air and moisture which entered the system during charging of the column. This consisted of filling the gas holder with nitrogen and then venting the system gas to the atmosphere. This procedure was repeated three times.

Determination of interelectrode resistance

Measurement with gas flow The procedure followed for determining interelectrode resistance was identical in both the fluidized and fixed bed regions when gas was flowing through the bed. First, the test cell of Figure 2 was charged with calcined coke and the correct type of center electrode attached to the electrode holder. Then, the gas recycle system and the column were purged of air and moisture. Following this the upper and lower deflection beams of the oscilloscope were calibrated. The compressor was then started and the rotameters were adjusted to maintain the correct relative gas velocity.

The power supply was then turned on and the resistance of the decade resistance box adjusted to allow the desired level of current flow through the bed. This was accomplished by varying the resistance box settings until the approximate amperage desired was observed with the ammeter.

After the correct resistance setting was made, a period of 1 min. was allowed to elapse to allow for the time lag between the input and output signals of the RC filters in both the current and measuring circuits. Then the upper and lower oscilloscope beam deflections (proportional to the bed and decade box voltage drops), oscilloscope sensitivity settings, and the resistance setting of the decade box were noted and recorded. The bed current level was then changed again, and the above procedure repeated until the full range of data was collected.

The bed and decade box voltage drops were calculated by multiplying the respective oscilloscope beam deflections by the oscilloscope sensitivity settings. Bed current was then calculated by dividing the decade box voltage drop by the resistance setting of the decade box. The interelectrode resistance was then calculated by dividing the bed voltage drop by the bed current.

Measurement with no gas flow For interelectrode resistance measurements in a completely settled bed, the procedure used by Jones (24) was generally followed. First, nitrogen flow to the bed was started and the bed was fluidized for 1 min. at a velocity approximately three times the incipient fluidization velocity. Then the gas flow was completely stopped and the bed was allowed to settle for 3 min. Jones found that this settling period was necessary because the bed resistance decreased exponentially with time for approximately 3 min. after the gas flow was stopped. After this time period, the resistance remained essentially constant with time. When the bed had settled, the current through the bed was adjusted and the same procedure followed as for gas flow through the bed.

Determination of bed resistivity

Fluidized bed measurements The desired test cell was connected to the system and the needle probes inserted into the middle of the column. The column was then filled with the bed

material. This was followed by the standard operations of purging the system and calibrating the oscilloscope.

Next, the compressor was started and the correct gas flow rate to the column established. The desired current flow through the bed was then fixed and the output signal of the RC filter across the decade box was allowed to reach its final value. Because the probe voltage signal was not sent through an RC filter, its oscilloscope trace fluctuated randomly and the probe voltage drop could not be accurately read directly from the scope screen. Therefore, a picture of both the bed voltage and the decade box voltage drops was taken with a Polaroid camera mounted on the oscilloscope. An exposure time of 5 sec. was used. A representative picture is shown in Figure 13. The decade box voltage drop which showed up as a straight line was easily read from the picture. The resistance setting of the decade box was then noted and recorded. As in the interelectrode resistance measurements, bed current was then varied repeatedly until the experiment was completed.

Bed current was calculated by dividing the decade box voltage drop by its resistance setting. The probe voltage drop was then divided by the bed current to obtain the inter-probe resistance. Bed resistivity was calculated by multiplying the inter-probe resistance by the cross-sectional area of the column and then dividing by the distance between the measuring probes.

Figure 13. Representative picture of voltage traces

Upper trace: bed voltage drop, no RC filter smoothing
Lower trace: decade box voltage drop with RC filter smoothing

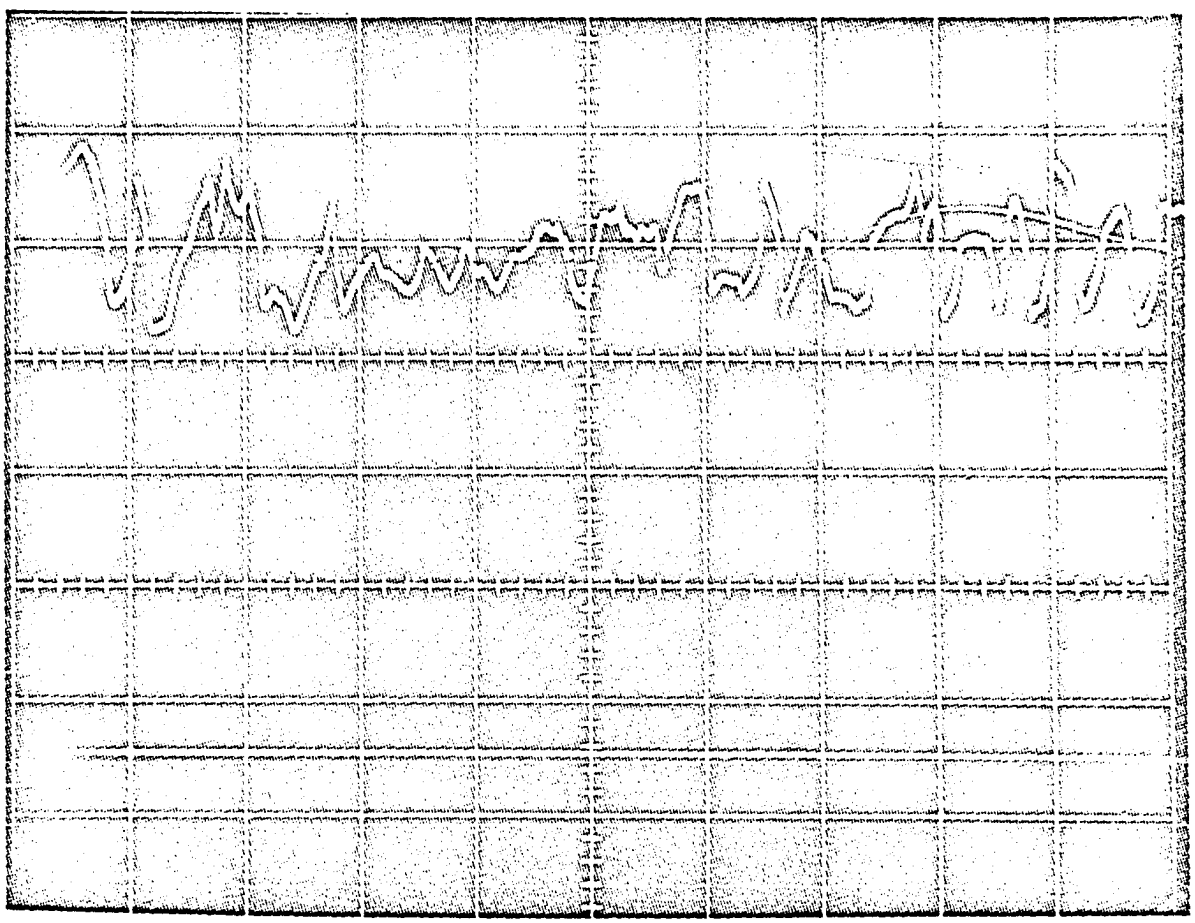

Unfluidized bed measurements In the fixed bed region, particle motion was absent. Therefore, the probe voltage drop could be read directly from the oscilloscope screen. For the case of no gas flow, the same measuring procedure was used as in the determination of interelectrode resistance with no gas flow.

Potential field verification

The distribution of electrical potential in a fluidized bed was experimentally determined with the test cell of Figure 6. After the column was filled with calcined coke and purged of air, the bed was fluidized and the desired bed current level in the current circuit was established. All of the probes were then positioned so that the tips of the probes were even with the wall of the column. Only one probe at a time was used in probing the bed. The other probes remained retracted. The initial position of the probe being used at any particular time depended upon the probe's location relative to the center electrode. If the probe to be used was located above the bottom of the center electrode, it was initially positioned so that it touched the center electrode. If the probe to be used was located below the bottom of the center electrode, the probe was initially positioned so that the probe tip was in the center of the column. The latter procedure was accomplished by positioning the probe guide so that it touched the outside

of the column wall. The probe was constructed so that the probe tip was in the center of the column when the probe guide was flush with the outer column wall.

After the probe was correctly located, the dial micrometer was positioned so that it touched the guide end of the probe. The dial micrometer was then set at zero to reference the location of the probe tip.

The probe was then moved outward to successive positions in the bed where measurements were desired. Near the exposed portion of the center electrode measurements were taken at 0.1 in. intervals. Near the outer electrode, where the voltage gradient was small, intervals of 0.25 in. were used.

At each probe position in the bed, the voltage drop between the center electrode and the probe tip and the overall voltage drop across the bed were measured on a voltmeter and recorded. The decade box resistance was also recorded.

Visual arc detection

The test cell of Figure 5 was used to visually determine the presence of arcing in the bed. Two types of current were used in the investigation. When direct current was passed through the bed the voltage across the bed was varied from 0 to 15 volts at several fluidizing velocities. When alternating current was used, the voltage across the bed was varied from 0 to 80 volts at the same fluidizing velocities used in the direct current experiment.

The procedure used in both types of experiments was the same. First all lights in the laboratory were turned off. A laboratory coat was draped around the column so that the residual light remaining in the laboratory would not interfere with the visual observance of arcing in the bed. The voltage across the bed was then increased from zero to the maximum voltage desired. At each voltage setting the bed in the vicinity of the wall electrode was checked for signs of arcing and the current through the bed noted and recorded. Also, at each voltage setting, a small radio was held close to the column to determine whether the electrical activity of the bed caused radio noise.

Ohmic characteristics

The voltage-current relationship (V-I relationship) in an electrofluid bed was investigated. The V-I relationship was studied at high temperature. A detailed description of the equipment used in the investigation was given by both Knowlton (29) and Ballain (1). Essentially, the system consisted of a stainless steel 4 in. inside diameter fluidized bed reactor, a gas recycle system similar to the one described above, and two power sources used to heat the reactor. One power source was utilized to heat the bed internally via direct resistance heating of the bed particles. Current was passed between a 1/2 in. diameter carbon rod immersed 12 in. into the center of the bed and the reactor wall.

The second heat source simply consisted of two Kanthal heaters which surrounded the reactor. An electrical schematic of the experimental circuit used is shown in Figure 14.

The bed was first filled with char and then fluidized with nitrogen at a velocity approximately two times the incipient fluidizing velocity of the bed. A voltage was then applied across the bed in 25 volt increments over the range of 25 to 150 volts by varying the setting of the internal heating Variac. The bed temperature was held relatively constant throughout the experiment at 1600°F. This was accomplished by using the internal heating power supply in conjunction with the external Kanthal heaters.

The Variac controlling the internal heating of the bed was set at 25 volts while the Variacs controlling the Kanthal heaters were adjusted until the bed temperature reached steady state at 1600°F. After the bed temperature had reached steady state, the bed current waveform and the waveform of the overall bed voltage drop were displayed on the 502A Tektronix dual beam oscilloscope. This was accomplished in the following manner. A Weston shunt, rated at 75 amps and 50 mv., was placed in the circuit between the Variac controlling the internal heating and the reactor. The alternating current waveform representative of the voltage drop across the shunt was displayed on one beam of the oscilloscope. This waveform had the shape of the bed current waveform since:

Figure 14. Schematic of electrical circuit used to obtain bed current and voltage waveforms

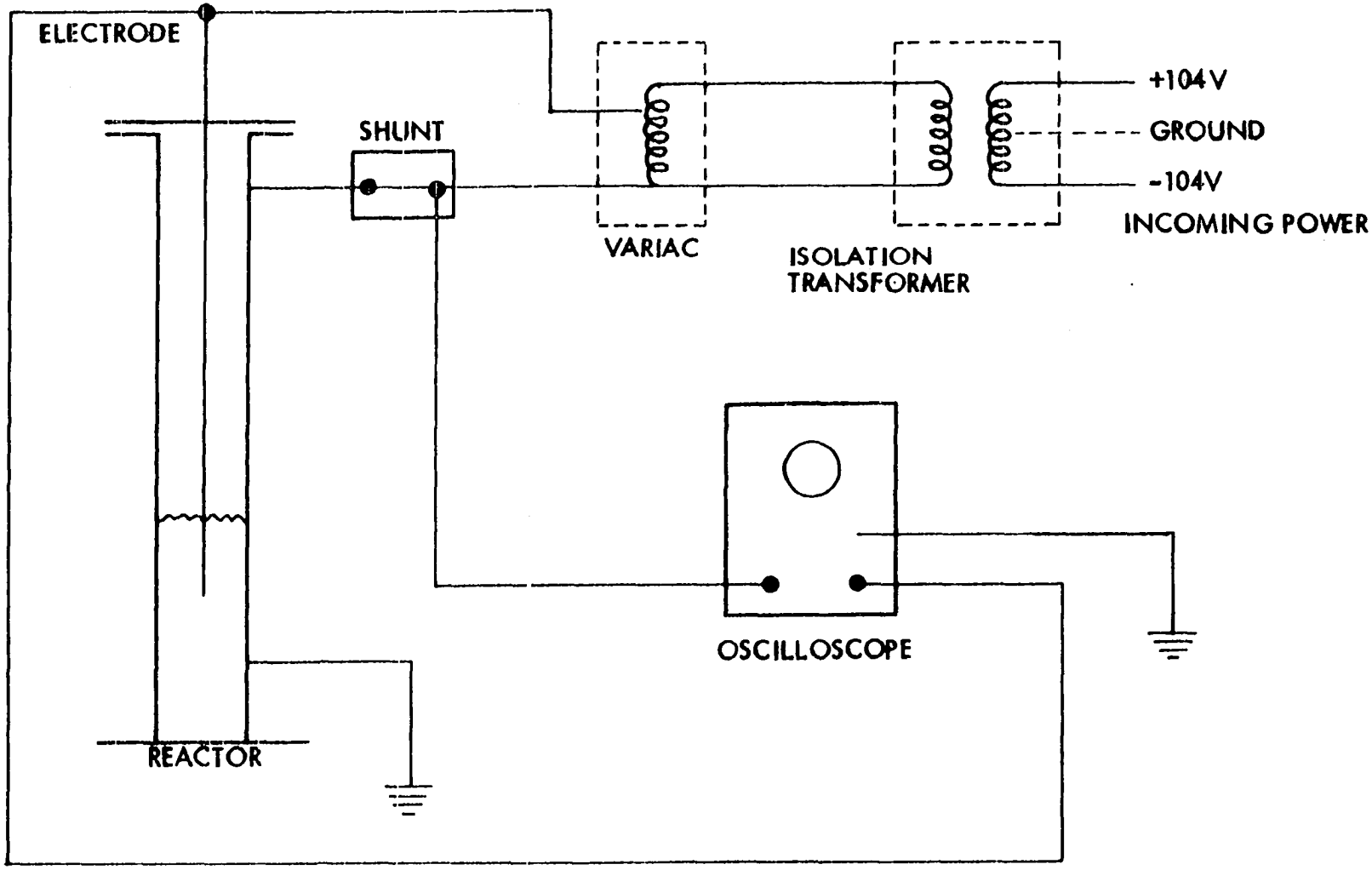
ELECTRODE
SHUNT
VARIAC
ISOLATION
TRANSFORMER
+104V
GROUND
-104V
INCOMING POWER
OSCILLOSCOPE
REACTOR

$$V_{shunt} = R_{shunt} I_{bed} .$$

The voltage waveform representative of the voltage drop across the bed was displayed simultaneously on the second beam of the oscilloscope. A photograph of the two waveforms was then taken with the Polaroid camera mounted on the oscilloscope. The X-Y function switch of the oscilloscope was then turned on. This enabled the voltage drop across the bed (ordinate) to be plotted versus the bed current (abscissa) on the scope screen. A photograph of this display was also taken. Representative pictures of the two different displays are shown in Figure 15.

After the two photographs were obtained, the Variac controlling the internal heating source was set at the next higher voltage that was desired. The external heaters were then adjusted downward until the desired steady state temperature was once again attained. Again, pictures of the voltage and current waveforms as well as the V-I plot were taken. This procedure was continued until the desired range of overall bed voltage drops had been covered.

The room temperature voltage-current relationship of a calcined coke bed fluidized with nitrogen when arcing was present was also investigated. The test cell and circuitry used in this instance are shown in Figures 5 and 12, respectively. In this experiment, a shunt (1 amp, 50 mv) was again required and was placed in the circuit between the Variac and the

Figure 15. Current-voltage relationship in an electrofluid reactor

Top picture: voltage-current relationship in electrofluid reactor at 1600°F, 4 in. diameter reactor

abscissa: bed current
ordinate: voltage drop across bed

Bottom picture: voltage waveform (upper trace) and current waveform (lower trace) in electrofluid bed at 1600°F, 4 in. diameter reactor

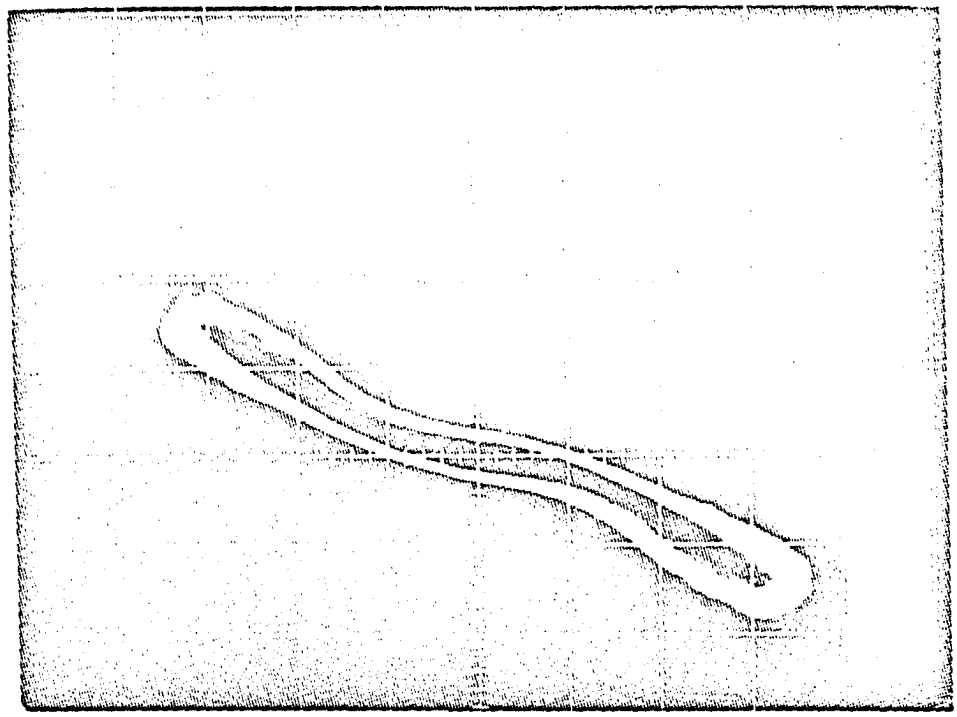

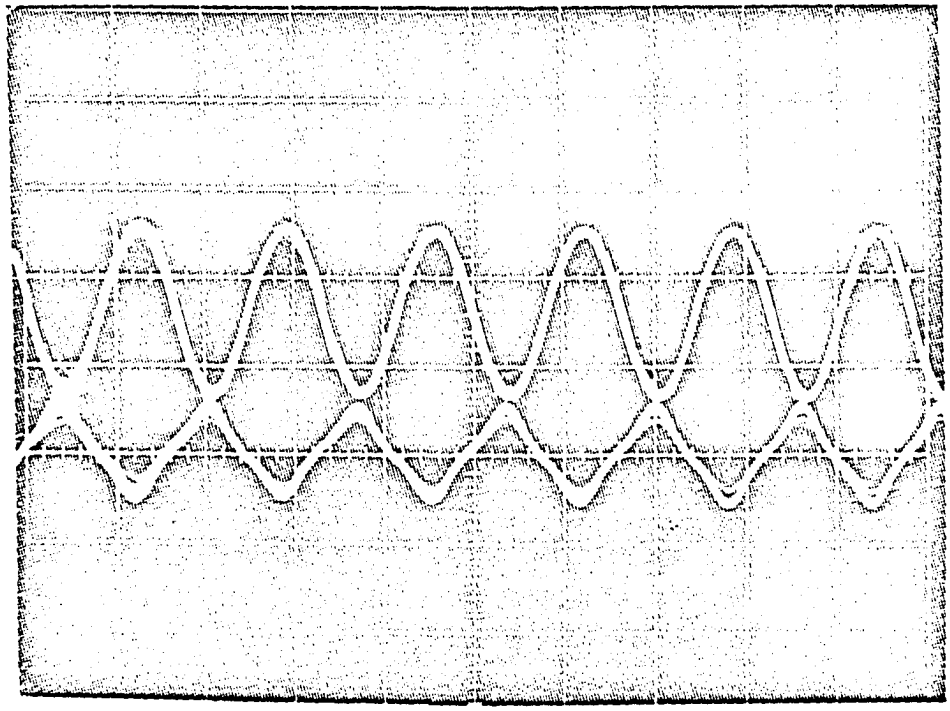

ammeter. The voltage drop across the bed was varied from 0 to 80 volts at 5 volt increments by changing the Variac settings. At each bed voltage setting, the voltage and current waveforms and the V-I plot were photographed with the oscilloscope camera as in the above procedure.

Determination of incipient fluidization velocity

The relative gas velocity variable used in the investigation is the ratio of the actual gas velocity through the column to the gas velocity at incipient fluidization. In order to determine the required relative velocity for a particular experiment, it was necessary to first determine the incipient fluidization velocity of the bed. The incipient fluidization velocity had to be determined for each different bed height, particle size, and column size.

A plot of the pressure drop through the bed versus gas velocity enabled the incipient fluidization velocity to be determined. As the gas velocity was increased in the unfluidized region of the bed, the pressure drop increased linearly with gas velocity. When the bed became fluidized the pressure drop became constant or increased only slightly upon further increases in gas velocity.

Then, pressure drops were taken at several gas velocities in both the fluidized and static regions of the bed and the results plotted. This gave a straight line in the static bed region and another straight line in the fluidized bed region.

The velocity at the intersection of the two lines was used as the incipient fluidization velocity. A typical pressure drop versus gas velocity plot is shown in Figure 16.

Bed Material

The bed material was composed of two size fractions of calcined coke obtained from the National Carbon Co. (grade No. 3-04). This material was part of that used by Glidden (9). A weight size distribution analysis of both fractions in shown in Table 1. This distribution was obtained by using Tyler standard testing sieves in conjunction with a Tyler Ro-tap sieve shaker. Each fraction sample was screened for 15 min. on the shaker. The large size fraction and the small size fraction were referred to as the -48/+65 Tyler mesh fraction and the -65/+100 Tyler mesh fraction respectively.

Table 1. Weight-size distribution of bed materials

Size, Tyler mesh	Weight per cent	
	-48/+65 fraction	-65/+100 fraction
+++/20	0.00	0.00
20/28	0.00	0.00
28/35	0.00	0.00
35/48	5.42	0.00
48/65	62.50	0.93
65/100	29.40	85.12
100/150	1.71	12.48
150/200	0.95	1.43
200/---	0.00	0.04

Figure 16. Bed pressure drop versus gas velocity plot for the determination of incipient fluidization velocity

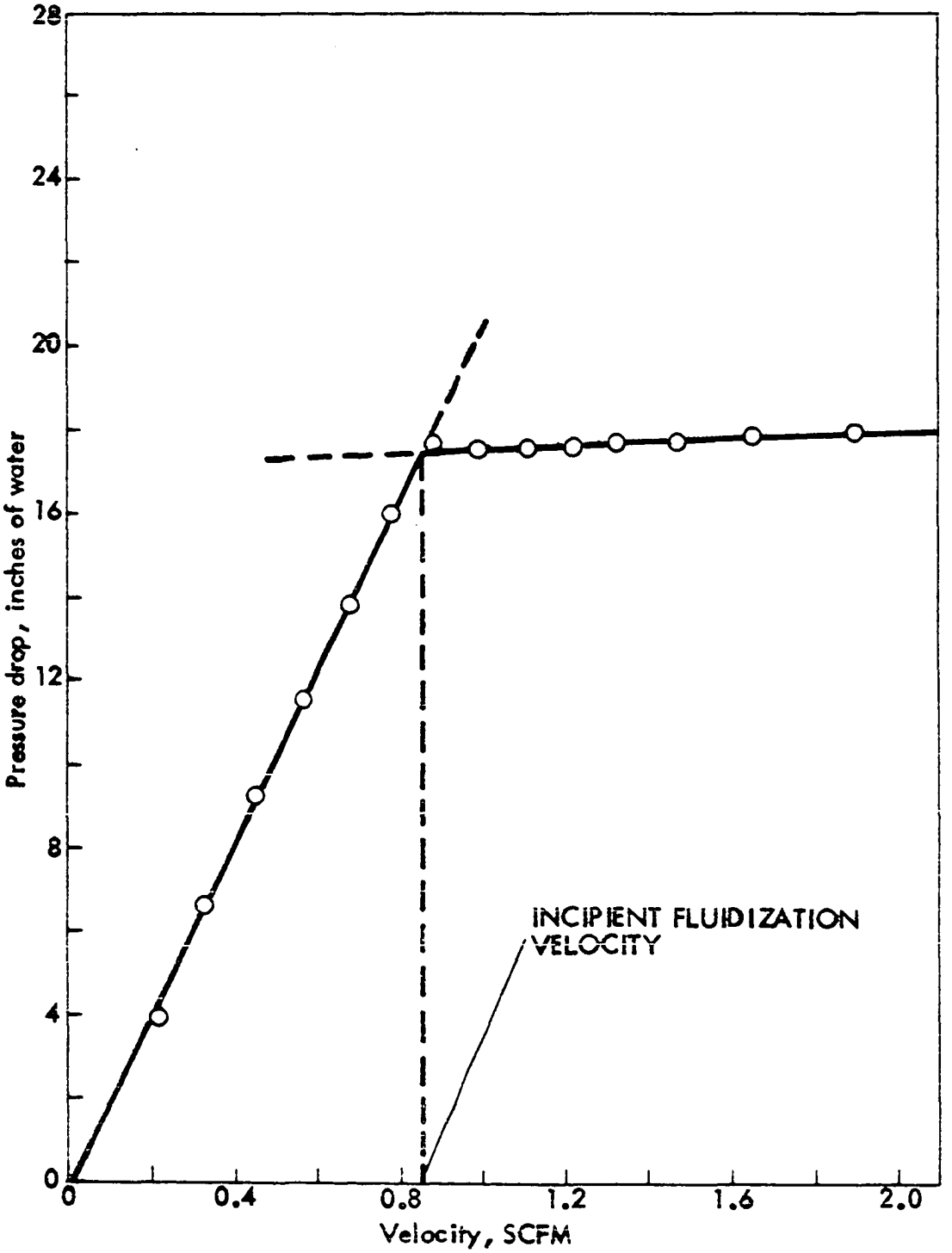
28
24
20
16
12
8
4
0
Pressure drop, inches of water
0
0.4
0.8
1.2
1.6
2.0
Velocity, SCFM
INCIPIENT FLUIDIZATION VELOCITY

The angle of repose and the standard deviation of the particle size of both fractions are shown in Table 2. The angle of repose was determined by the procedure used by Jones (24).

Table 2. Angle of repose and standard deviation of particle size

	Angle of repose, degrees	Standard deviation of particle size, in.
-48/+65 fraction	30° 40'	0.00187
-65/+100 fraction	34° 58'	0.00124

Calculation Methods

In the investigation, the interelectrode resistance was hypothesized to be the sum of several components, i.e.:

$$R_i = R_c + R_w + R_b \tag{6}$$

where R_c and R_w are the contact resistances between the bed and center electrode and between the bed and the brass-screen wall electrode, respectively. R_b denotes the bed resistance.

Since there is indication in the literature that the magnitude of the contact resistance is inversely proportional to the area available for current flow (17), and since the exposed

area of the wall electrode was greater than the exposed area of the center electrode, it was assumed that the contact resistance at the wall electrode was negligible compared to the contact resistance at the center electrode. With this assumption Equation 6 becomes:

$$R_i = R_c + R_b \quad . \tag{7}$$

Neither component of the interelectrode resistance could be measured independently of the interelectrode resistance. Therefore, a technique was developed in order to determine the relative contribution of each component to the interelectrode resistance. In this method, the bed resistance, R_b, was estimated independently and then subtracted from the experimentally determined interelectrode resistance to obtain the contact resistance, R_c.

Field theory calculation of contact resistance

The determination of the bed resistance component independently of the contact resistance was made utilizing electrical field theory. The field equation applicable to the experimental system used in the investigation (31, 35) was Laplace's equation:

$$\nabla^2\phi = \frac{\partial^2\phi}{\partial r^2} + \frac{1}{r}\frac{\partial\phi}{\partial r} + \frac{\partial^2\phi}{\partial\theta^2} + \frac{\partial^2\phi}{\partial z^2} = 0 \tag{8}$$

where ϕ is the potential function and r, θ, and z are the characteristic cylindrical coordinates. Laplace's equation

represents the steady state case of heat flow, current flux, or diffusion through a three-dimensional body.

The assumptions used in this development were:

(1) that the fluid bed material was homogeneous with respect to its resistivity, and

(2) that the voltage potential did not vary along the electrode surfaces.

A two-dimensional representation of a typical bed geometry over which Equation 8 was applied is shown in Figure 17. Because of the axial symmetry of the concentric electrode arrangement in the experimental apparatus,

$$\frac{\partial^2 \phi}{\partial \Theta^2} = 0 \tag{9}$$

and Equation 8 reduced to the two-dimensional form,

$$\frac{\partial^2 \phi}{\partial r^2} + \frac{1}{r} \frac{\partial \phi}{\partial r} + \frac{\partial^2 \phi}{\partial z^2} = 0 \tag{10}$$

as the defining equation for the system. Also, because of axial symmetry, only half of the column needed to be considered in applying Equation 10 to the bed region.

Laplace's equation as shown in Equation 10 was derived for the coordinate system A shown in Figure 17. However, coordinate system B was used in all cases in the investigation. Therefore, it was necessary to transform Equation 10 so that it applied to the coordinate system used. The radius variable,

Figure 17. Two-dimensional bed region over which Laplace's equation was applied

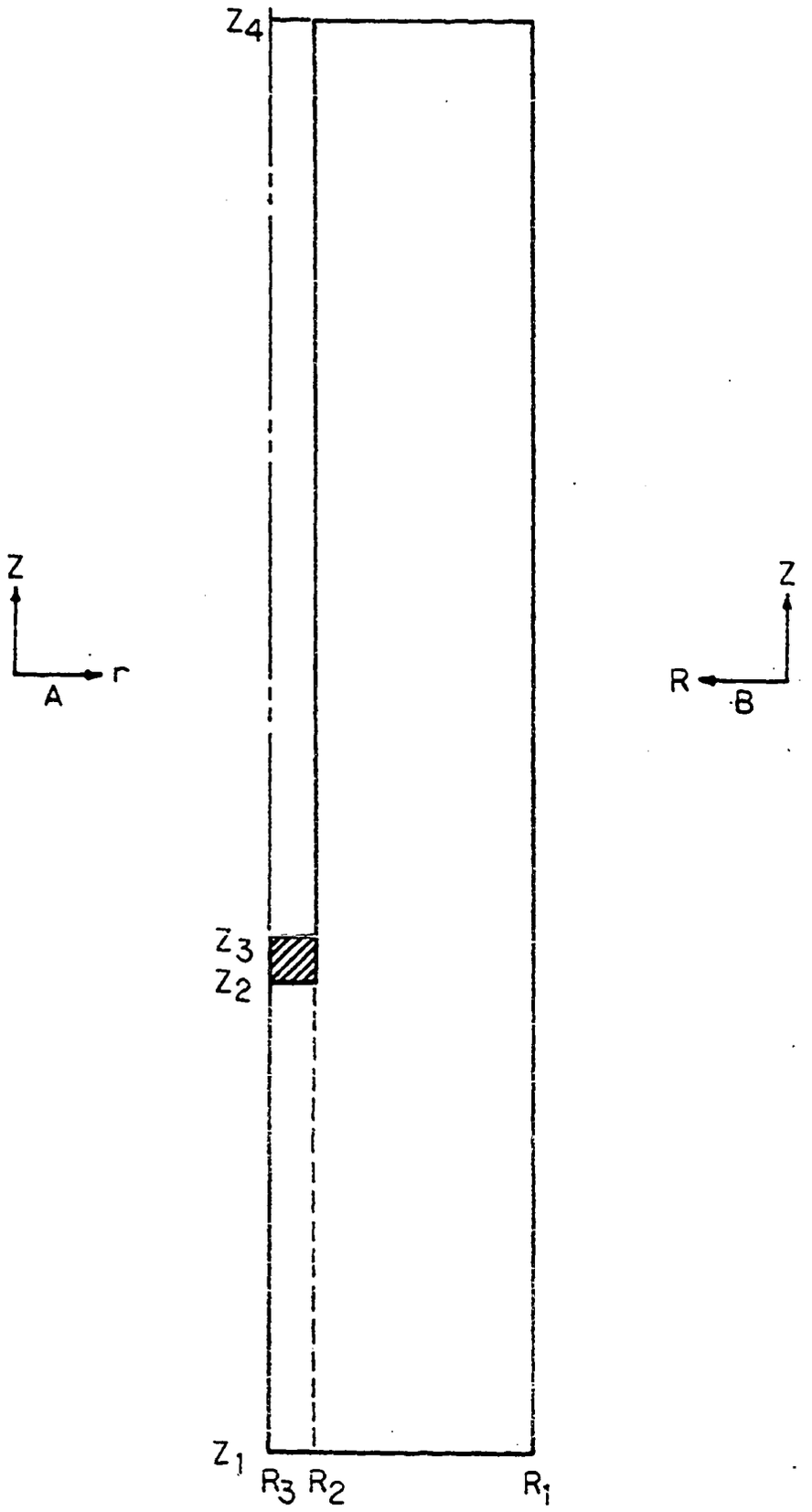
Z4
Z
r
A
Z
R
B
Z3
Z2
Z1
R3
R2
R1

R, in the transformed coordinate system was related to the derived radius variable, r, in the following manner:

$$R = k - r \tag{11}$$

where k is the magnitude of the bed radius. Using this transformation Laplace's equation becomes:

$$\frac{\partial^2 \phi}{\partial R^2} - \frac{1}{(K-R)} \frac{\partial \phi}{\partial R} + \frac{\partial^2 \phi}{\partial z^2} = 0 \quad . \tag{12}$$

The boundary conditions for the solution of Laplace's equation are usually of two types. The simplest type of boundary condition is where the potential, ϕ, is equal to a constant, K. That is,

$$\phi = K \quad . \tag{13}$$

Boundaries which are conductors give rise to boundary conditions of this type. A problem in which the entire boundary consists of potentials that are known is called a "Dirichlet Problem" (31).

The second type of boundary condition usually encountered in the solution of Laplace's equation is where the derivative of the potential normal to the boundary surface is zero. This boundary condition is expressed as:

$$\frac{\partial \phi}{\partial n} = 0 \tag{14}$$

and arises at boundaries which are insulators. If the boundary conditions at all boundaries of a region are given by Equation 14, the problem is called a "Neumann Problem" (31). In the bed region studied, the boundary conditions were a mixture of the types described above since both conducting and insulating surfaces were in contact with the bed. The boundary conditions for the solution of Equation 12 applied to the geometry of Figure 17 were:

$$\phi = 0 \qquad \text{at } R = R_1 \text{ between } z = z_1 \text{ and } z = z_4 \tag{15}$$

$$\frac{\partial \phi}{\partial z} = 0 \qquad \text{between } R = R_1 \text{ and } R = R_3 \text{ at } z = z_1 \tag{16}$$

$$\frac{\partial \phi}{\partial z} = 0 \qquad \text{between } R = R_1 \text{ and } R = R_2 \text{ at } z = z_4 \tag{17}$$

$$\frac{\partial \phi}{\partial R} = 0 \qquad \text{at } R = R_2 \text{ between } z = z_3 \text{ and } z = z_4 \tag{18}$$

$$\frac{\partial \phi}{\partial z} = 0 \qquad \text{between } R = R_2 \text{ and } R = R_3 \text{ at } z = z_2 \tag{19}$$

$$\phi = 1 \qquad \text{at } R = R_2 \text{ between } z = z_2 \text{ and } z = z_3 \tag{20}$$

$$\frac{\partial \phi}{\partial R} = 0 \qquad \text{at } R = R_3 \text{ between } z = z_1 \text{ and } z = z_2 \, . \tag{21}$$

Solution of Equation 12 subject to the above boundary conditions using conformal mapping and analytical methods were not feasible. Therefore, Laplace's equation was solved using numerical approximation. This involved replacing the differential equations by difference equations. The Liebmann iterative method in conjunction with an overrelaxation optimizing technique was used to solve the difference form of Laplace's equation. The steps involved in the above method are described in detail in Lapidus (31).

A program utilizing the above methods was developed to run on an IBM model 360/65 digital computer. This program approximated the solution of Equation 12 and located the constant potential lines which bounded regions over which 10 per cent of the total potential drop occurred.

The location of lines of constant current flux through the bed was also desired. These lines were orthogonal to the lines of constant potential. To obtain these constant flux lines Equation 12 was solved using different boundary conditions. Where the boundary had been an insulator in the determination of the constant potential lines it was now made a conductor (35). Similarly, where the boundary had been a conductor, it was now considered to be an insulator. Using this criteria the boundary conditions of Equations 15, 16, 17, 18, 19, 20, and 21 became:

$\frac{\partial \phi}{\partial R} = 0$ $\quad R = R_1$

between $z = z_1$ and $z = z_4$ (22)

$\phi = 0$ between $R = R_1$ and $R = R_3$

at $z = z_1$ (23)

$\phi = 1$ between $R = R_1$ and $R = R_2$

at $z = z_4$ (24)

$\phi = 1$ at $R = R_2$

between $z = z_3$ and $z = z_4$ (25)

$\phi = 1$ between $R = R_2$ and $R = R_3$

at $z = z_2$ (26)

$\frac{\partial \phi}{\partial R} = 0$ at $R = R_2$

between $z = z_2$ and $z = z_3$ (27)

$\phi = 0$ at $R = R_3$

between $z = z_1$ and $z = z_2$ (28)

In a sense the current flux distribution was solved using a potential field solution but with "orthogonal" boundary conditions. The solution located the boundaries of flux regions representing ten per cent of the current flow through the bed. Both the potential and flux lines were then plotted on the same graph using a Cal-Comp Simplotter.

A program used to obtain the constant potential and flux lines is shown in Appendix A.

When the correct solution of Laplace's equation is obtained and the potential and flux lines are correctly superimposed upon the region, it turns out that the capacitance of any curvilinear square in the region is exactly equal to that of any other curvilinear square. Therefore, Figure 18 actually represents a number of equal capacitors in series and in parallel. The capacitance of the entire region, C, can be related to the capacitance of a single curvilinear square by the relation:

$$C = \frac{m}{n} C_u \tag{29}$$

where m is the number of unit squares in parallel and n is the number of unit squares in series.

The capacitance of a unit curvilinear square was determined in the following manner. Selecting a curvilinear square bounded by lines of constant flux and constant potential which most approximated a geometrical rectangle, the radial position of the potential lines and the distance between the flux lines bounding the square were measured. In a three-dimensional system the rectangle is actually a hollow cylinder of inner radius, r_1, outer radius, r_2, and height 1. The capacitance of the cylinder which can be obtained from standard Physics or Electrical Engineering texts is:

$$C_u = \frac{2\pi l \varepsilon}{\ln r_2/r_1} \tag{30}$$

Figure 18. Constant potential and flux distributions in the electrical field for a 1 in. uninsulated electrode length

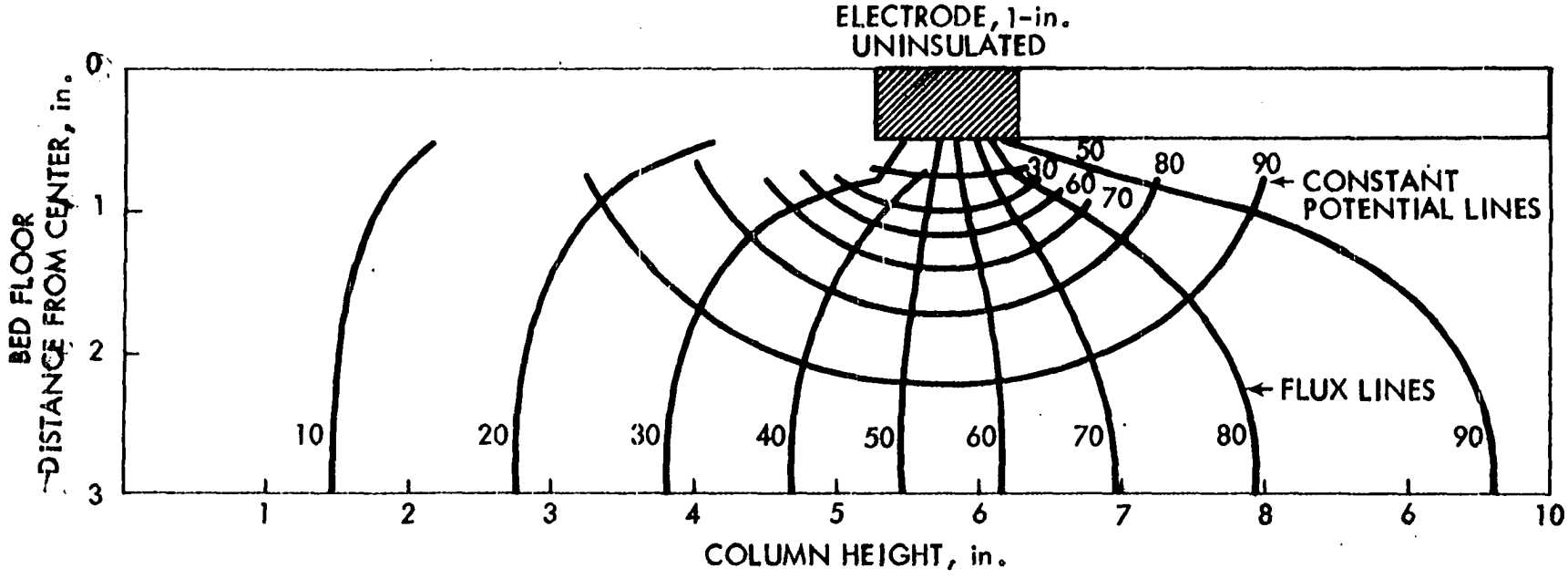
ELECTRODE, 1-in.
UNINSULATED
BED FLOOR
DISTANCE FROM CENTER, in.
0
1
2
3
10
20
30
40
50
60
70
80
90
CONSTANT POTENTIAL LINES
FLUX LINES
1
2
3
4
5
6
7
8
6
10
COLUMN HEIGHT, in.

where C_u is the capacitance of the curvilinear square, l is the distance between the flux lines bounding the curvilinear square, ε is the dielectric constant of the bed material, and r_1 and r_2 are the radial distances to the potential lines bounding the curvilinear unit square.

The total capacitance is then related to the bed resistance by the following equation (derived in Appendix B):

$$R_b = \frac{\rho}{C} \varepsilon \tag{31}$$

where R_b is the bed particle resistance, ρ is the resistivity of the bed material, ε is the dielectric constant of the bed material, and C is the total capacitance of the system.

It is not necessary to determine a value for ε to calculate R_b. This can be seen by first substituting Equation 30 in Equation 29 and then substituting the resulting expression into Equation 31. All of this substitution results in:

$$R_b = \frac{\rho\varepsilon}{m/n \frac{2\pi l\varepsilon}{\ln(r_2/r_1)}} \quad . \tag{32}$$

The dielectric constant thus cancels out of the expression giving:

$$R_b = \frac{\rho n \ln(r_2/r_1)}{m2\pi l} \tag{33}$$

as the expression which was used to calculate the bed particle resistance. Knowing R_b the bed contact resistance was then calculated by difference using Equation 7.

Restricted bed method of bed resistance calculation

A simple approximate method used to determine a value for the bed resistance was to apply the resistance equation:

$$R_b = \frac{\rho l}{A} , \tag{34}$$

where A is the cross sectional area perpendicular to current flow, to a differential volume element in the bed. This gave the following equation:

$$d\ R_b = \frac{\rho dr}{2\pi r} \tag{35}$$

assuming that ρ is the independent of r.

In this method the actual bed region available for current flow was considered to be restricted to a fraction of that actually available. This can be seen by observing Figure 19 which depicts the geometry of the system and the region of assumed current flow. This restricted region was the bed volume bounded by the wall electrode, the uninsulated portion of the center electrode, and the diagonal lines connecting the two electrodes. A limitation of the technique was that it was not applicable for the case of conduction from the electrode tip.

Integration of Equation 35 between the center electrode radius, r_o, and the radius of the column, D, gave:

$$R_b = \frac{\rho}{2\pi F} \ln \frac{DZ}{r_o (F+SD)} \tag{36}$$

Figure 19. Geometry used in derivation of approximate equation for determination of bed resistance

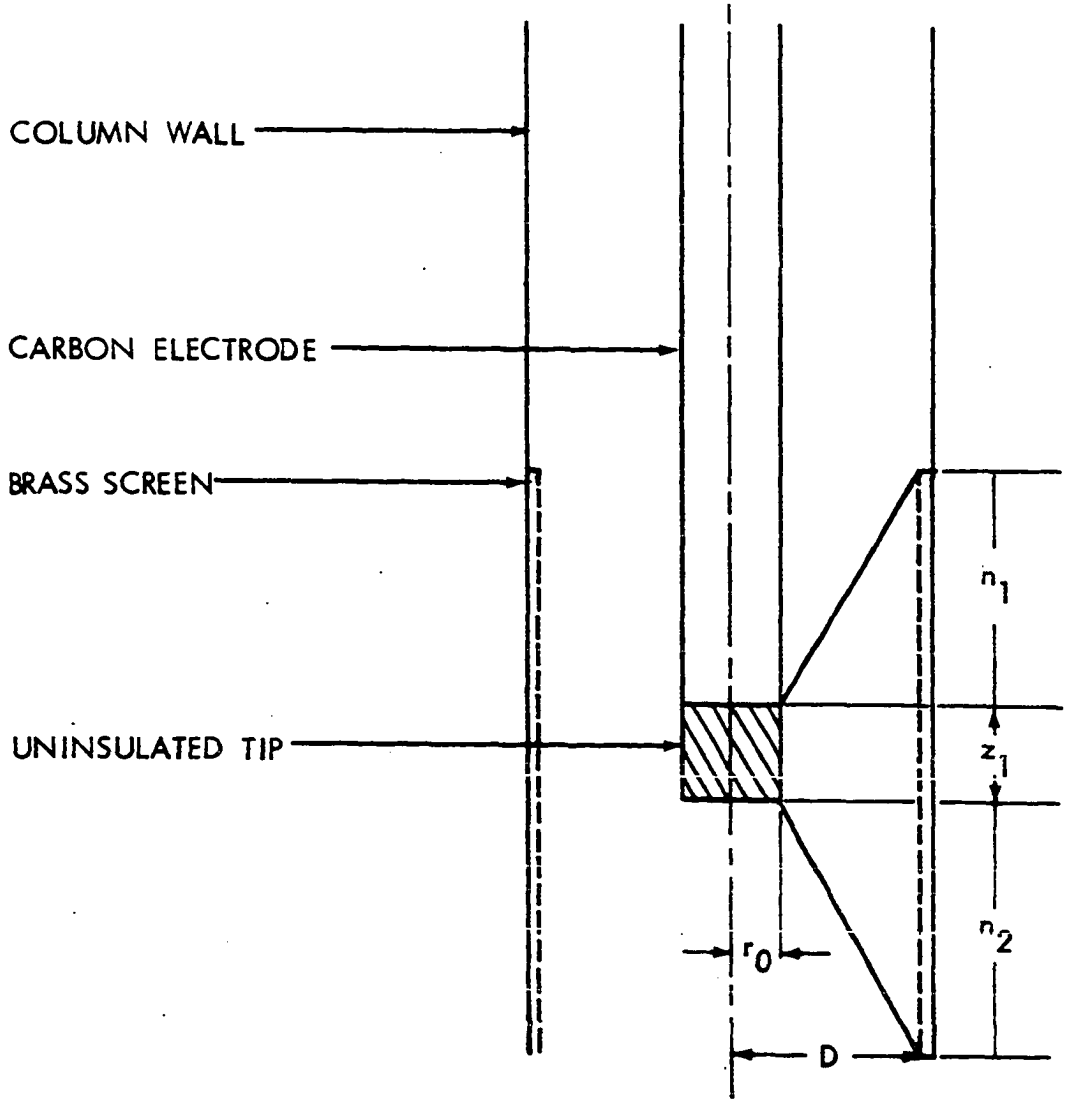
COLUMN WALL
CARBON ELECTRODE
BRASS SCREEN
UNINSULATED TIP
n_1
z_1
n_2
r_0
D

where ρ is the resistivity of the bed material,

$$S = (n_1 + n_2)/(D - r_o), \text{ and}$$

$$F = z - Sr_o.$$

Determination of standard deviation of particle size

The standard deviation of the particle size was determined using the formula:

$$\sigma_p = \left[\frac{1}{N-1}\left(\Sigma n_i D_i^2 - \frac{(\Sigma n_i D_i)^2}{N}\right)\right]^{1/2} \tag{37}$$

which for large N reduces to:

$$\sigma_p = \left[\frac{1}{N}(\Sigma n_i D_i^2) - D_p^2\right]^{1/2} . \tag{38}$$

The number of particles contained between any two adjoining mesh sizes, n_i, was calculated by the following relation, found in most standard Chemical Engineering Unit Operations texts:

$$n_i = \frac{m/d}{aD_i^3} . \tag{39}$$

The total number of particles in the mixture, N, was obtained by summing all of the particles in each particular mesh range.

The average diameter of particles within a particular size fraction, D_i, was taken to be the arithmetic average of the two adjoining mesh sizes. The average particle diameter of the mixture, D_p, was then determined using the relation:

$$D_p = \frac{\Sigma n_i D_i}{\Sigma n_i} . \tag{40}$$

RESULTS AND DISCUSSION

Interelectrode Resistance

The overall purpose of this investigation was to determine the nature of the interelectrode resistance in an electrofluid bed system. The objective of the first study undertaken was to investigate how certain operating parameters affected interelectrode resistance.

All measurements of interelectrode resistance were made at room temperature with -48/+65 Tyler mesh size calcined coke used as the bed material. The resistance was measured as a function of current density with relative gas velocity and exposed area of the center electrode as parameters. In all cases the current density used was the current density at the center electrode. Direct current with a negative ground was generally used, although the effect of both direct current with a positive ground and alternating current were also investigated. A 6 in. diameter Plexiglas column fitted with a brass-screen outer electrode was used to contain the bed.

The interelectrode resistance investigation was essentially conducted in three parts. The first two parts corresponded to an investigation of the effects of low (0.15 amps/sq. in. maximum) and high (12 amps/sq. in. maximum) current density on interelectrode resistance. The third part was concerned with the effect of the type and direction of current flow on inter-

electrode resistance.

Effect of low current density

In the low current density study, a 1 in. diameter carbon rod served as the center bed electrode. Measurements were made in fixed and fluidized beds with uninsulated center electrode lengths of 4, 1, and 1/4 in. These uninsulated electrode lengths correspond to configurations II, III, and IV, respectively, in Figure 20. Similar measurements were also made with only the tip of the center electrode uninsulated and with the tip uninsulated in conjunction with an uninsulated electrode length of 10.75 in. (configurations V and I, respectively, in Figure 20). The latter configuration was studied only in a fluidized bed. Vinyl electrical tape was used as the center electrode insulating material.

The unfluidized bed interelectrode resistance increased with increasing gas velocity and markedly so near the incipient fluidization velocity for configurations II, III and IV (Figures 21, 22, and 23). It did not appear to change with current density at small relative velocities. However, at the relative velocity nearest the incipient fluidization point, the interelectrode resistance appeared to decrease slightly with current density.

The fluidized bed resistance was much greater than its corresponding unfluidized bed resistance and decreased with both increasing gas velocity and current density (Figures 21,

Figure 20. Typical uninsulated center electrode areas

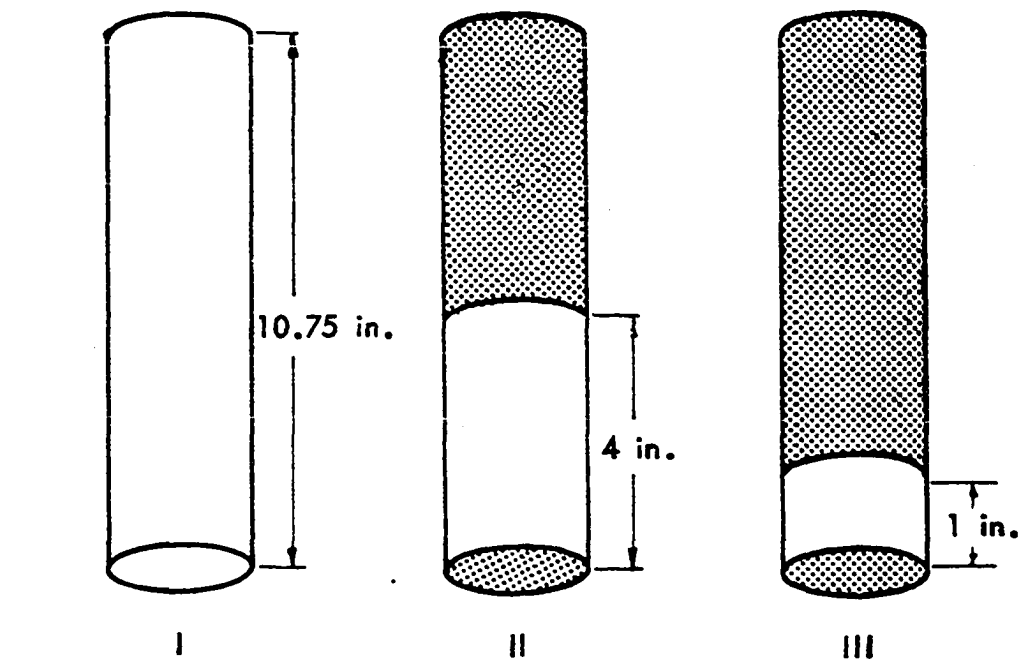
10.75 in.
4 in.
1 in.
I
II
III

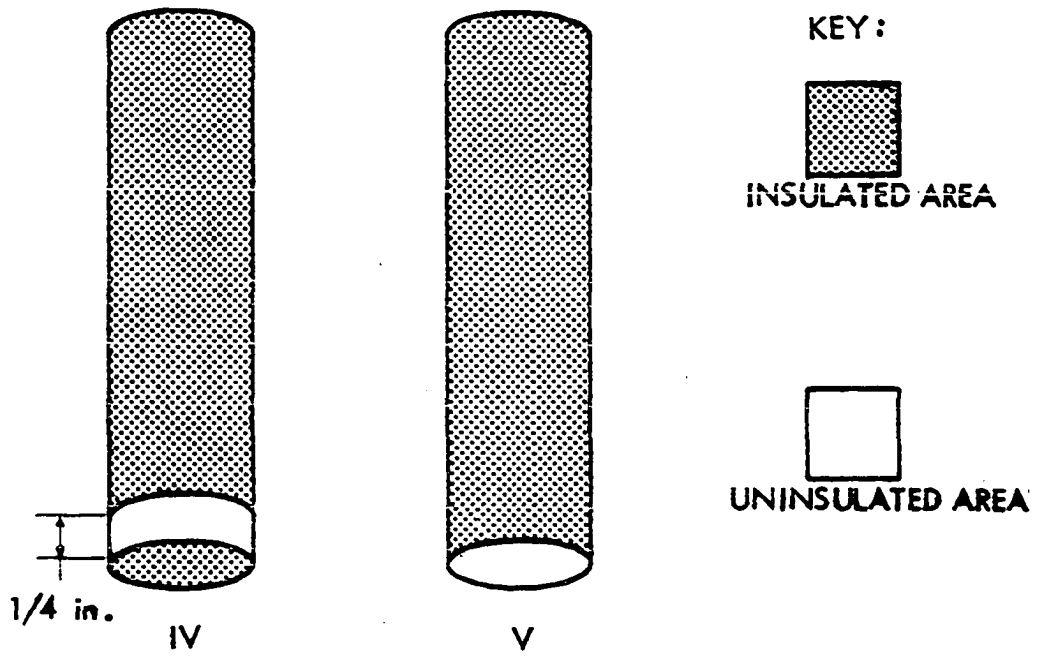
1/4 in.
IV
V
KEY:
INSULATED AREA
UNINSULATED AREA

Figure 21. Interelectrode resistance versus current density for 4 in. uninsulated electrode length (configuration II)

fluidized bed unfluidized bed

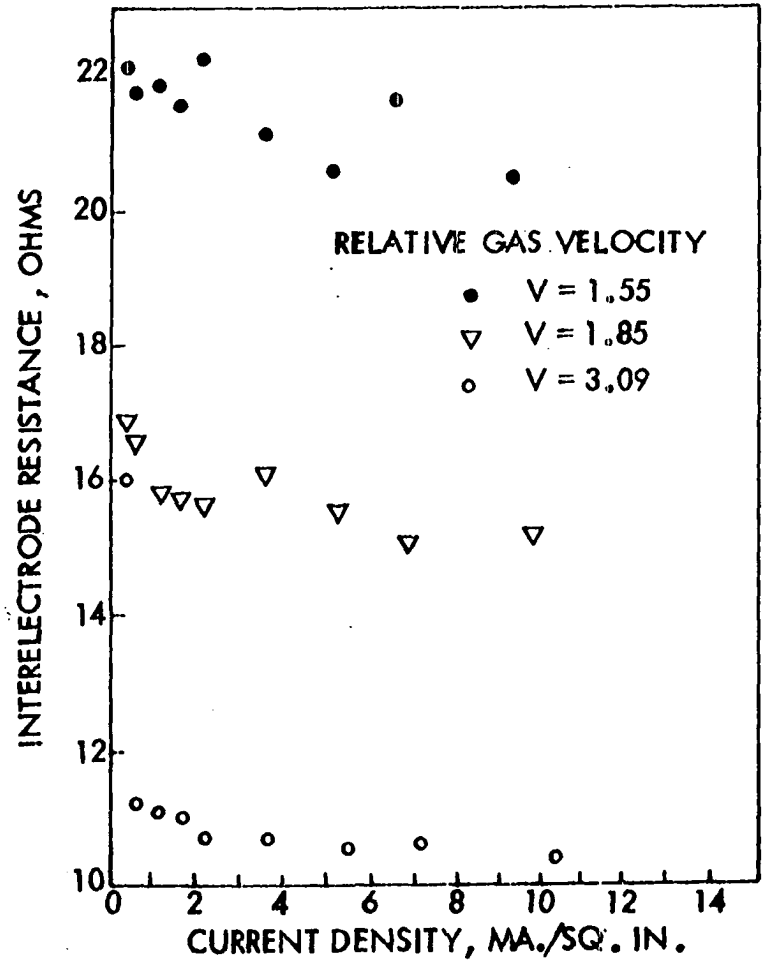
INTERELECTRODE RESISTANCE, OHMS
CURRENT DENSITY, MA./SQ. IN.
RELATIVE GAS VELOCITY
V = 1.55
V = 1.85
V = 3.09

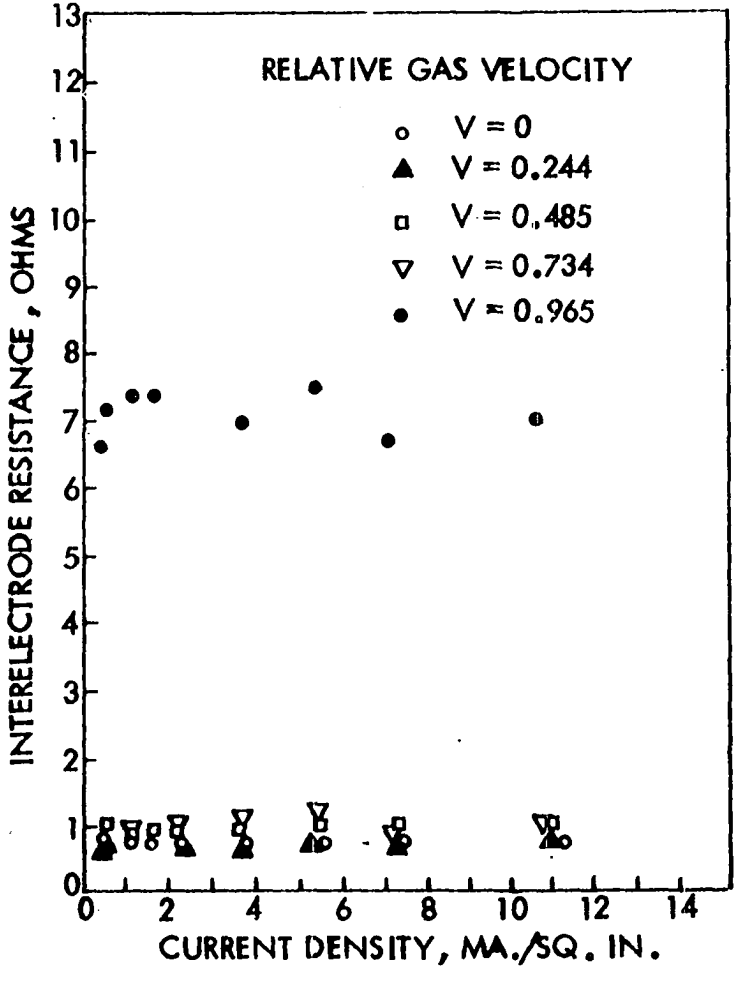
INTERELECTRODE RESISTANCE, OHMS
CURRENT DENSITY, MA./SQ. IN.
RELATIVE GAS VELOCITY
V = 0
V = 0.244
V = 0.485
V = 0.734
V = 0.965

Figure 22. Interelectrode resistance versus current density for 1 in. uninsulated electrode length (configuration III)

fluidized bed

unfluidized bed

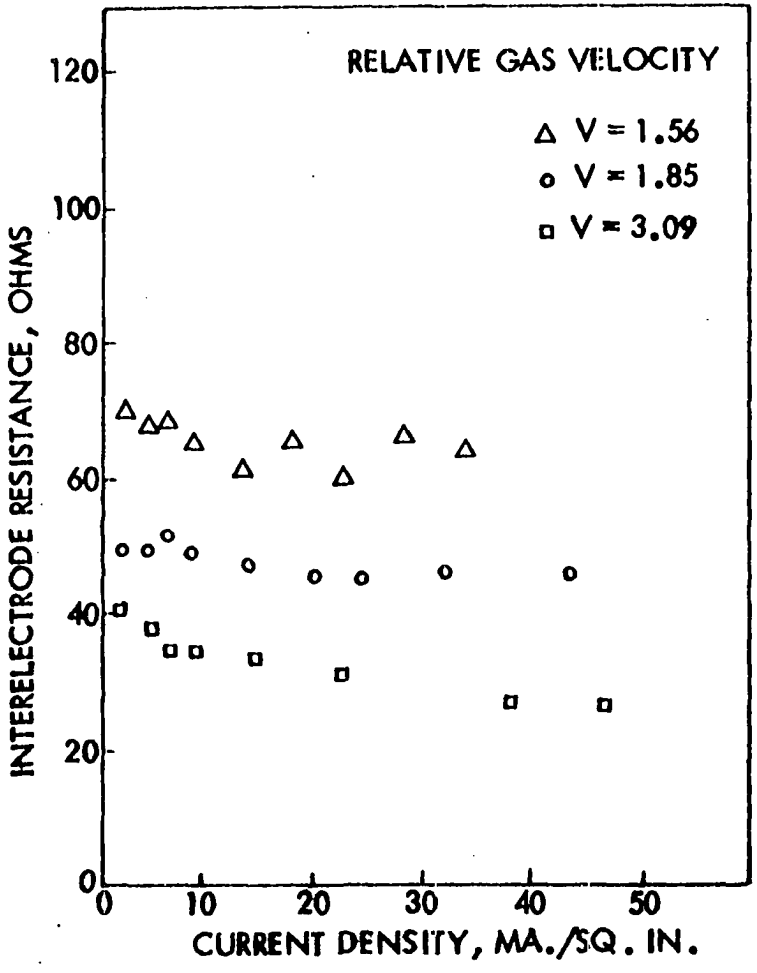
RELATIVE GAS VELOCITY
△ V = 1.56
o V = 1.85
□ V = 3.09
INTERELECTRODE RESISTANCE, OHMS
CURRENT DENSITY, MA./SQ. IN.
0
20
40
60
80
100
120
0
10
20
30
40
50

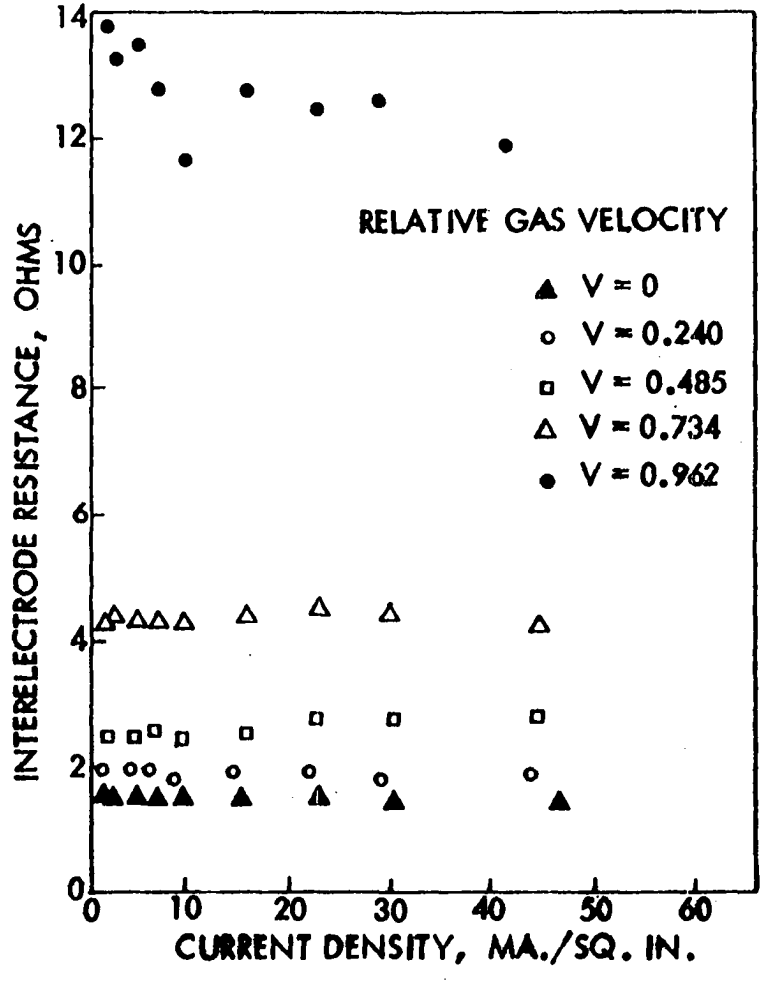
RELATIVE GAS VELOCITY
▲ V = 0
o V = 0.240
□ V = 0.485
△ V = 0.734
● V = 0.962
INTERELECTRODE RESISTANCE, OHMS
CURRENT DENSITY, MA./SQ. IN.
0
2
4
6
8
10
12
14
0
10
20
30
40
50
60

Figure 23. Interelectrode resistance versus current density for 1/4 in. uninsulated electrode length (configuration IV)

fluidized bed unfluidized bed

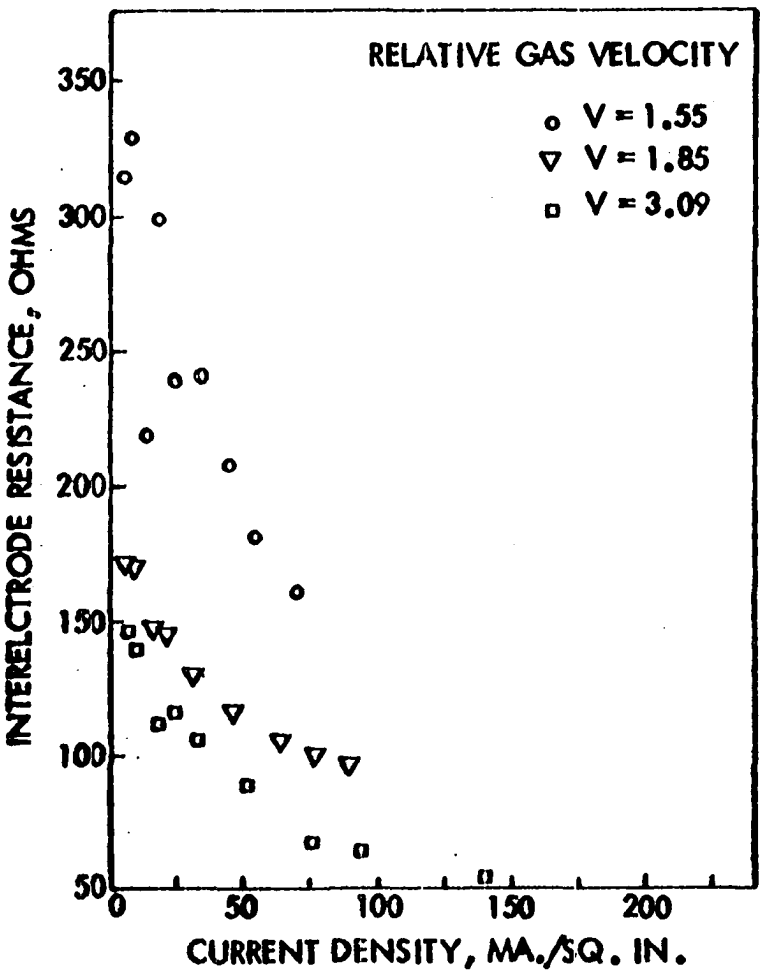
RELATIVE GAS VELOCITY
V = 1.55
V = 1.85
V = 3.09
INTERELCTRODE RESISTANCE, OHMS
CURRENT DENSITY, MA./SQ. IN.
350
300
250
200
150
100
50
0
50
100
150
200

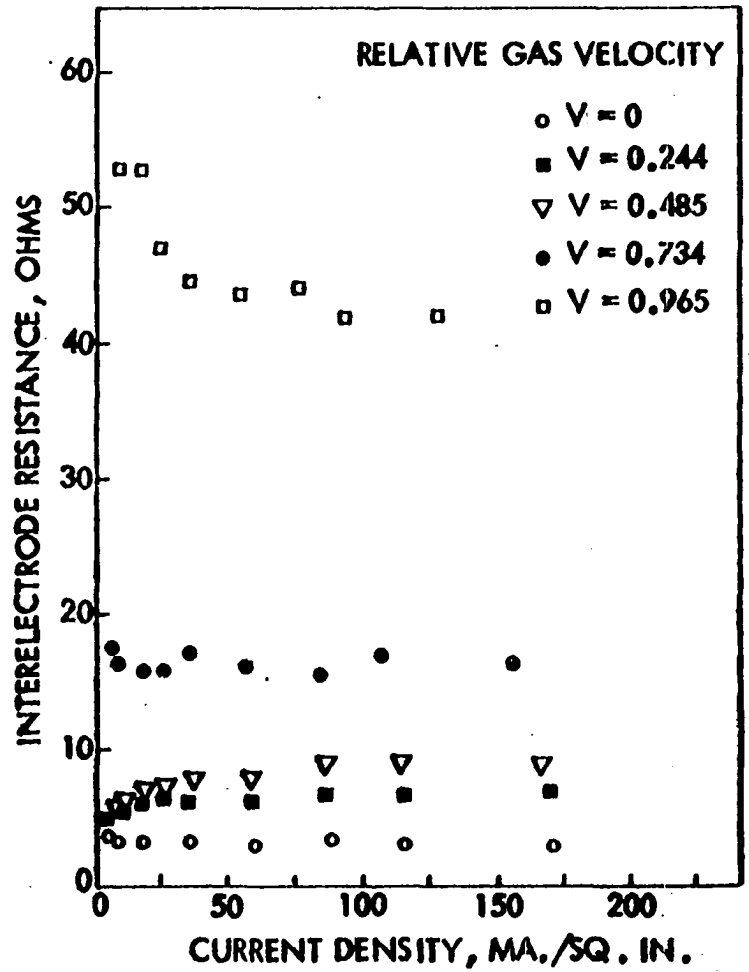
RELATIVE GAS VELOCITY
V = 0
V = 0.244
V = 0.485
V = 0.734
V = 0.965
INTERELECTRODE RESISTANCE, OHMS
CURRENT DENSITY, MA./SQ. IN.
60
50
40
30
20
10
0
50
100
150
200

22, 23 and 24). For the case of configuration IV, the decrease with current flow was quite non-linear. For configurations I, II, and III, however, this non-linearity was not observed.

The interelectrode resistance in the fluidized bed appeared to be inversely proportional to the exposed area of the center electrode (Figure 25). This result was obtained by plotting interelectrode resistance for configurations II, III and IV versus the reciprocal of the exposed center electrode area with relative velocity as a parameter and at a constant current density of 10 ma./sq. in.

The results obtained when only the flat tip of the electrode was exposed (configuration V) were different from those obtained when the sides of the electrode were exposed. For example, the resistance of the unfluidized and fluidized beds was of the same order of magnitude (Figure 26). And, although the exposed area was the same as for the case of configuration IV, the interelectrode resistance for configuration V was much higher than the resistance for configuration IV. The interelectrode resistance was also a non-linear function of current density, even in the unfluidized bed, and did not vary with gas velocity. The reasons for these "deviations" are not apparent, but may be due to a stagnant gas flow region or a high bed porosity region immediately beneath the electrode tip.

Figure 24. Interelectrode resistance versus current density for 10.75 in. uninsulated electrode length with tip uninsulated (configuration I)

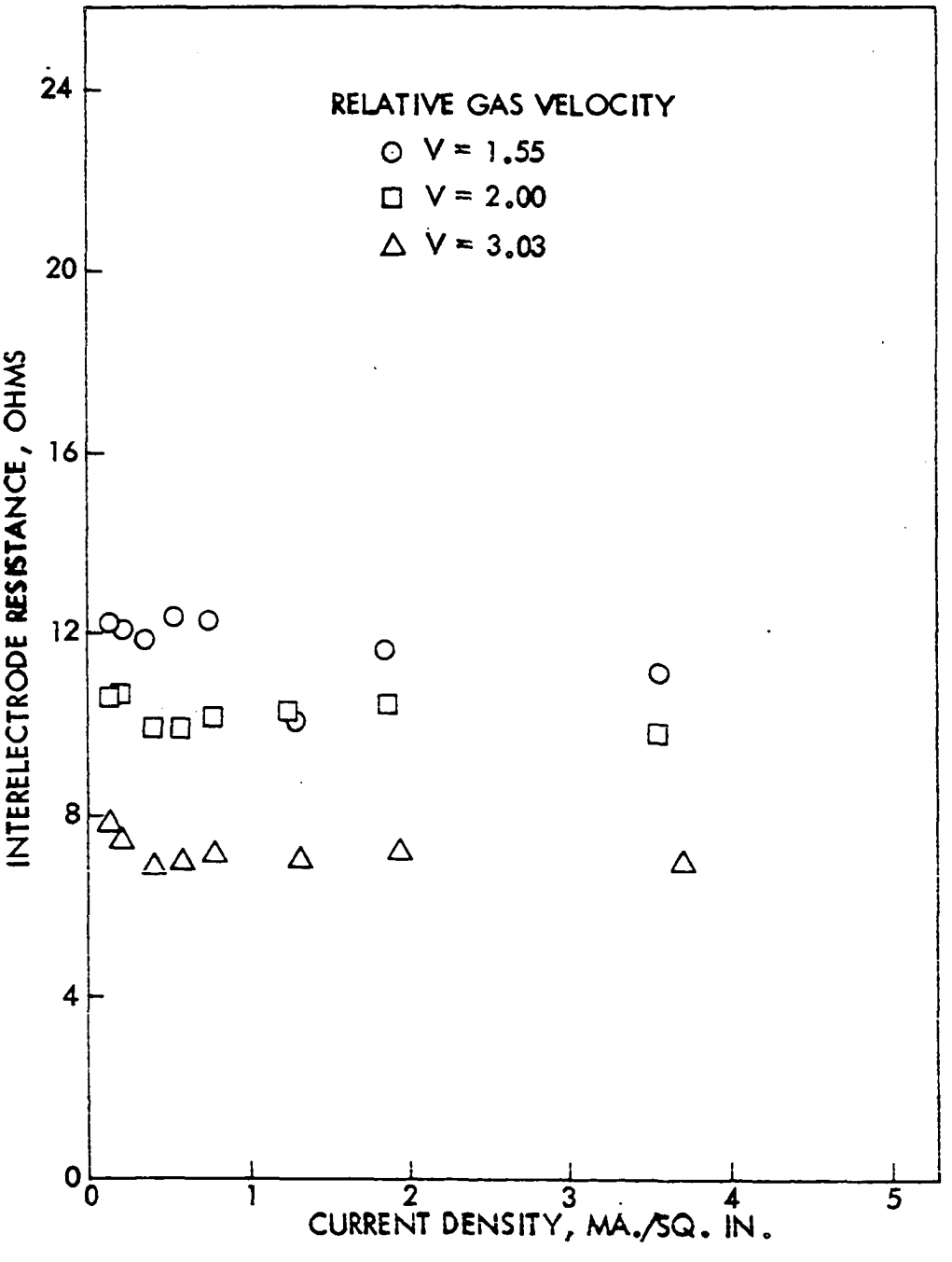
RELATIVE GAS VELOCITY
○ V = 1.55
□ V = 2.00
△ V = 3.03
INTERELECTRODE RESISTANCE, OHMS
24
20
16
12
8
4
0
0
1
2
3
4
5
CURRENT DENSITY, MA./SQ. IN.

Figure 25. Interelectrode resistance versus the reciprocal of exposed center electrode area at a constant bed current of 10 ma.

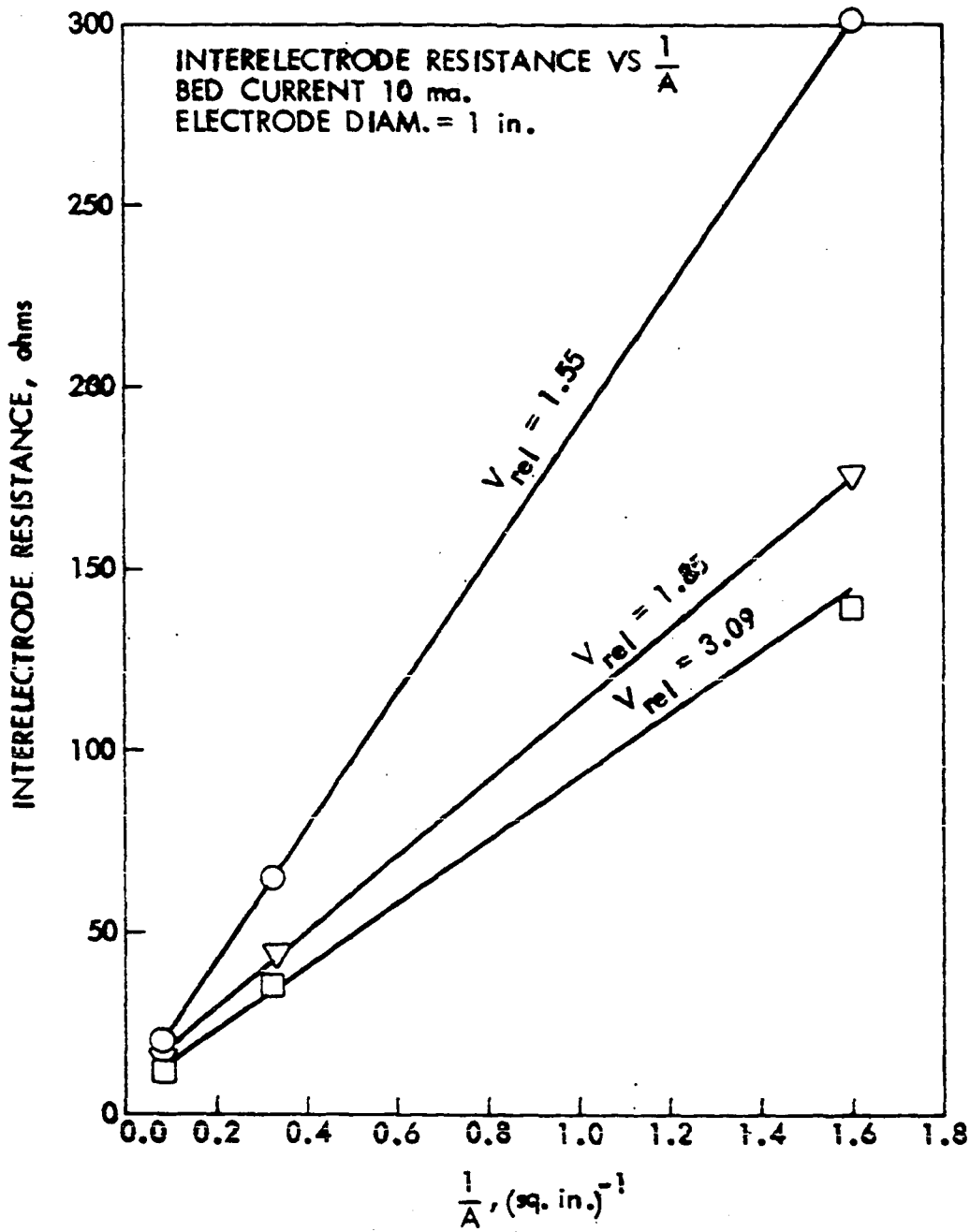
INTERELECTRODE RESISTANCE VS 1/A
BED CURRENT 10 ma.
ELECTRODE DIAM. = 1 in.
INTERELECTRODE RESISTANCE, ohms
300
250
200
150
100
50
0
0.0
0.2
0.4
0.6
0.8
1.0
1.2
1.4
1.6
1.8
1/A, (sq. in.)⁻¹
V rel = 1.55
V rel = 3.09

Figure 26. Interelectrode resistance versus current density for tip uninsulated (configuration V)

fluidized bed

unfluidized bed

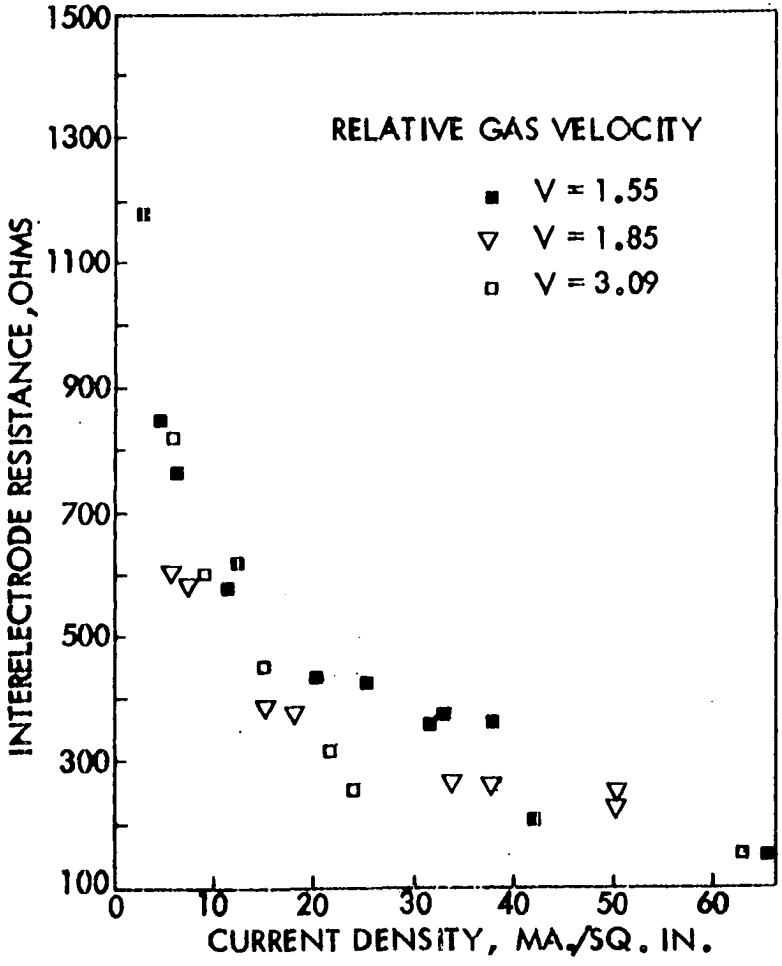
RELATIVE GAS VELOCITY
V = 1.55
V = 1.85
V = 3.09
INTERELECTRODE RESISTANCE, OHMS
CURRENT DENSITY, MA./SQ. IN.
1500
1300
1100
900
700
500
300
100
0
10
20
30
40
50
60

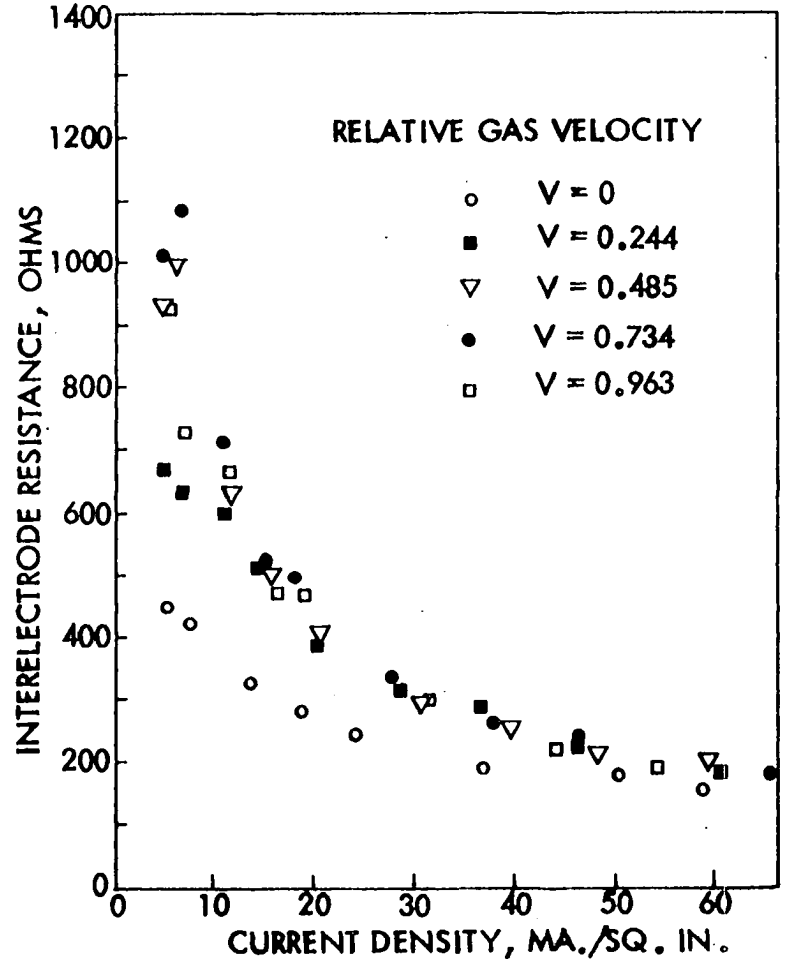
RELATIVE GAS VELOCITY
V = 0
V = 0.244
V = 0.485
V = 0.734
V = 0.963
INTERELECTRODE RESISTANCE, OHMS
CURRENT DENSITY, MA./SQ. IN.
1400
1200
1000
800
600
400
200
0
10
20
30
40
50
60

The actual bed current used in the above runs ranged from 0 to 130 ma. The largest current density achieved at the exposed surface of the center electrode in these runs was approximately 0.14 amps/sq. in. This was for configuration IV and was with a bed current of approximately 100 ma.

Effect of high current density

In order to achieve current densities significantly higher than those used in the low current density study, extremely small center electrodes were used. This was done in an attempt to increase the current density at the center electrode to levels approximating those which might exist in commercial electrofluid reactors, yet with only milliamperes of current actually flowing through the bed. This also allowed the determination of interelectrode resistance as a function of current density over a larger range than had been previously studied.

A 1 in. diameter brass electrode holder was designed to hold small center electrodes 0.040 and 0.0625 in. in diameter and 4 in. in length (Figure 27). Three different center electrode materials were used: tungsten (0.040 in. in diameter), steel and brass (both 0.0625 in. in diameter). Measurements were made only in the fluidized bed and with only two uninsulated electrode configurations. These corresponded to the flat tip uninsulated and 1/4 in. uninsulated along the electrode length.

Figure 27. Drawing of small diameter electrode holder and small electrode

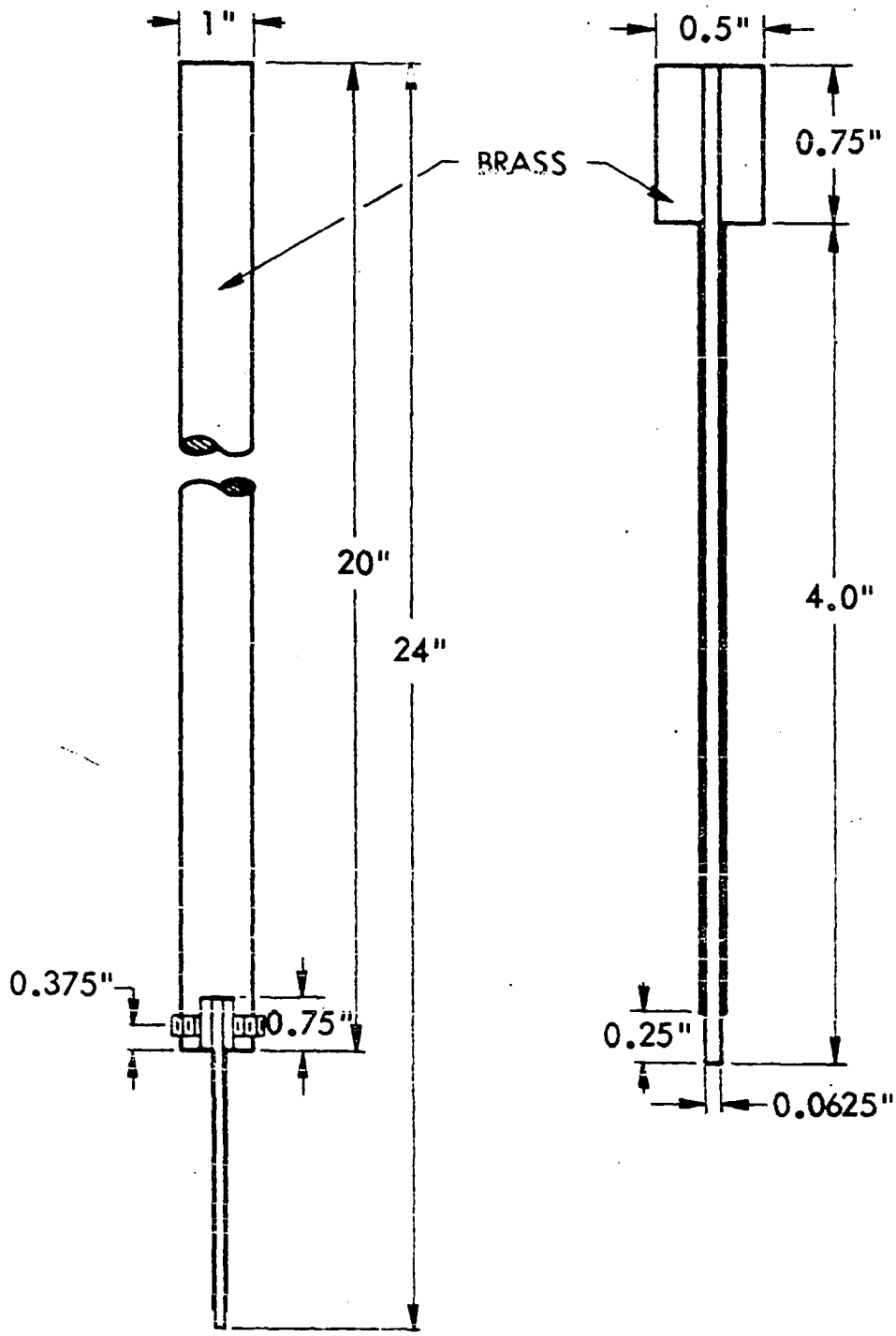
1"
0.5"
0.75"
BRASS
20"
24"
4.0"
0.375"
0.75"
0.25"
0.0625"

The results of the runs in which a 1/4 in. length of the electrode was uninsulated are shown in Figures 28, and 29, where interelectrode resistance is plotted versus current density at three relative velocities. In these runs the current density range was extended to over 2 amps/sq. in. for the steel and brass electrodes and to 4 amps/sq. in. for the smaller tungsten electrode. The maximum bed current used was approximately 100 ma.

The shape of these curves is approximately the same as the shape of the curves for the 1 in. diameter carbon electrode with a 1/4 in. length uninsulated. That is, the interelectrode resistance decreases non-linearly with increasing current density. However, the interelectrode resistance of the small electrodes was much greater at a particular relative velocity than that of the large electrode. Also, the magnitude of the interelectrode resistance with the tungsten electrode was greater than that of the steel and brass electrodes. This result would be expected if interelectrode resistance is inversely proportional to the reciprocal of the exposed area since the diameter of the tungsten electrode was smaller than the diameter of both the brass and steel electrodes.

Runs were also made with all three electrodes having only the bottom tip uninsulated (Figures 30 and 31). Because of the small area available for current flow, the current densities were extended to over 4 amps/sq. in. for the steel and brass

Figure 28. Interelectrode resistance versus current density for tungsten electrode, 1/4 in. electrode length uninsulated

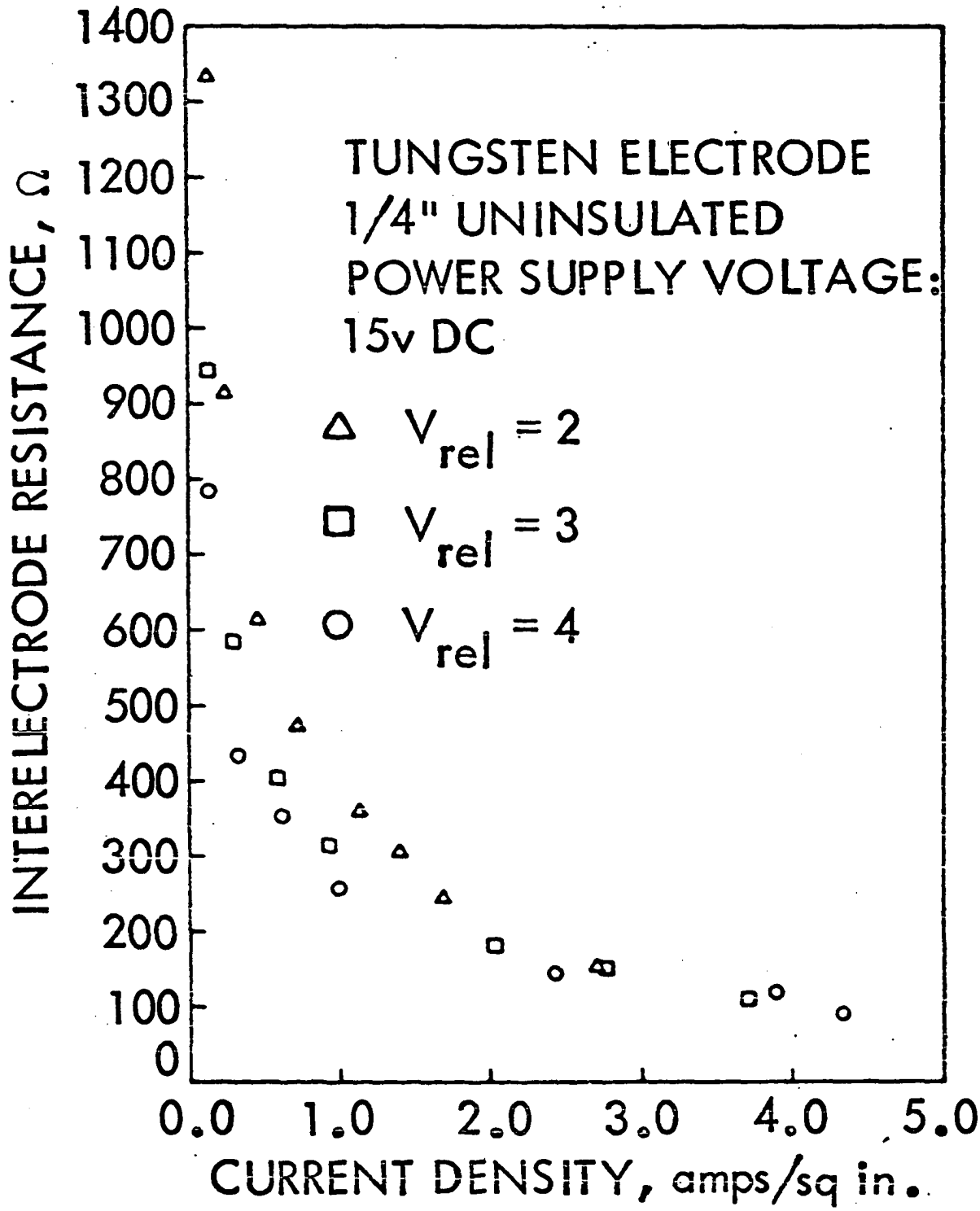
INTERELECTRODE RESISTANCE, Ω
1400
1300
1200
1100
1000
900
800
700
600
500
400
300
200
100
0
TUNGSTEN ELECTRODE
1/4" UNINSULATED
POWER SUPPLY VOLTAGE:
15v DC
△ $V_{rel} = 2$
□ $V_{rel} = 3$
○ $V_{rel} = 4$
0.0
1.0
2.0
3.0
4.0
5.0
CURRENT DENSITY, amps/sq in.

Figure 29. Interelectrode resistance versus current density for 1/4 in. insulated electrode length

brass electrode steel electrode

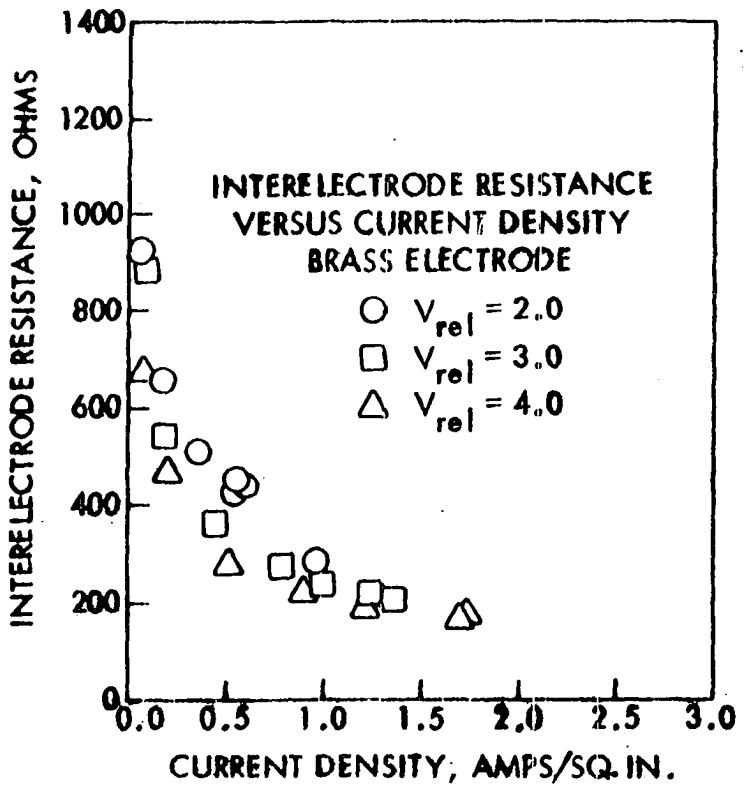
INTERELECTRODE RESISTANCE VERSUS CURRENT DENSITY
BRASS ELECTRODE
V_{rel} = 2.0
V_{rel} = 3.0
V_{rel} = 4.0
INTERELECTRODE RESISTANCE, OHMS
CURRENT DENSITY, AMPS/SQ. IN.
0
200
400
600
800
1000
1200
1400
0.0
0.5
1.0
1.5
2.0
2.5
3.0

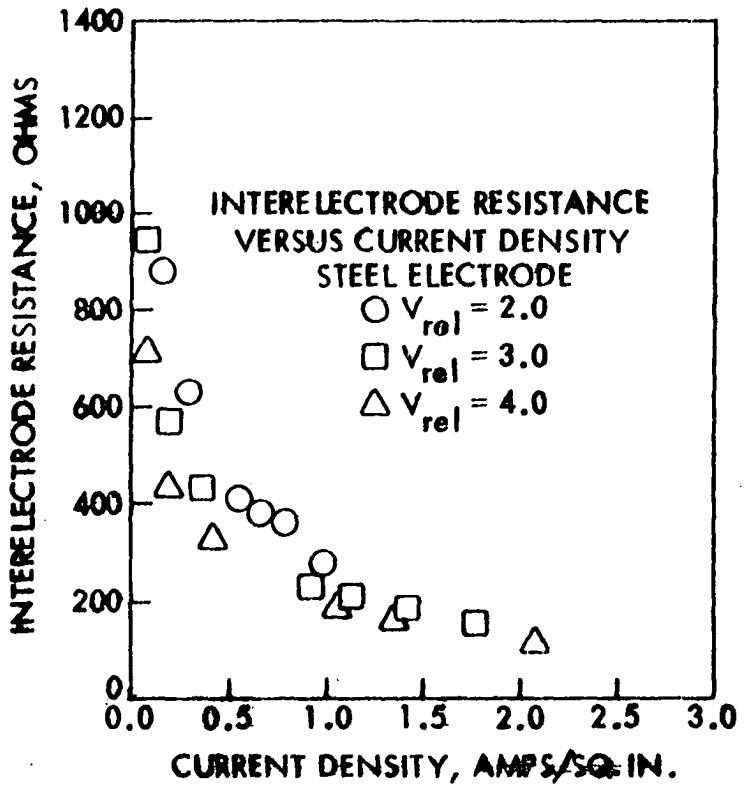
INTERELECTRODE RESISTANCE VERSUS CURRENT DENSITY
STEEL ELECTRODE
V_{rel} = 2.0
V_{rel} = 3.0
V_{rel} = 4.0
INTERELECTRODE RESISTANCE, OHMS
CURRENT DENSITY, AMPS/SQ. IN.
0
200
400
600
800
1000
1200
1400
0.0
0.5
1.0
1.5
2.0
2.5
3.0

Figure 30. Interelectrode resistance versus current density, tip uninsulated, tungsten electrode (1/25 in. diameter)

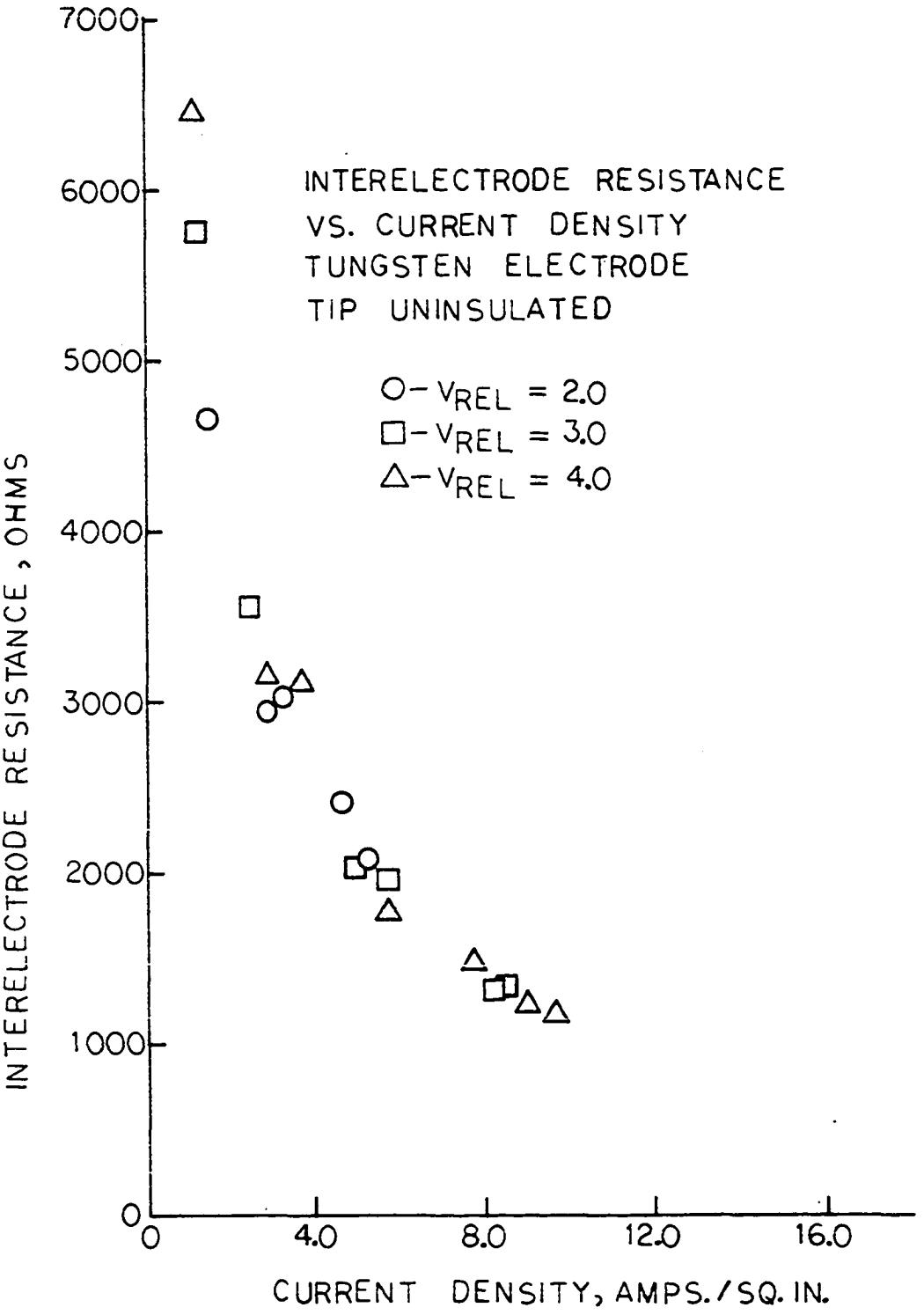
INTERELECTRODE RESISTANCE
VS. CURRENT DENSITY
TUNGSTEN ELECTRODE
TIP UNINSULATED
O- VREL = 2.0
□- VREL = 3.0
△- VREL = 4.0
INTERELECTRODE RESISTANCE, OHMS
7000
6000
5000
4000
3000
2000
1000
0
0
4.0
8.0
12.0
16.0
CURRENT DENSITY, AMPS./SQ. IN.

Figure 31. Interelectrode resistance versus current density, tip uninsulated

brass electrode
(1/16 in. diameter)

steel electrode
(1/16 in. diameter)

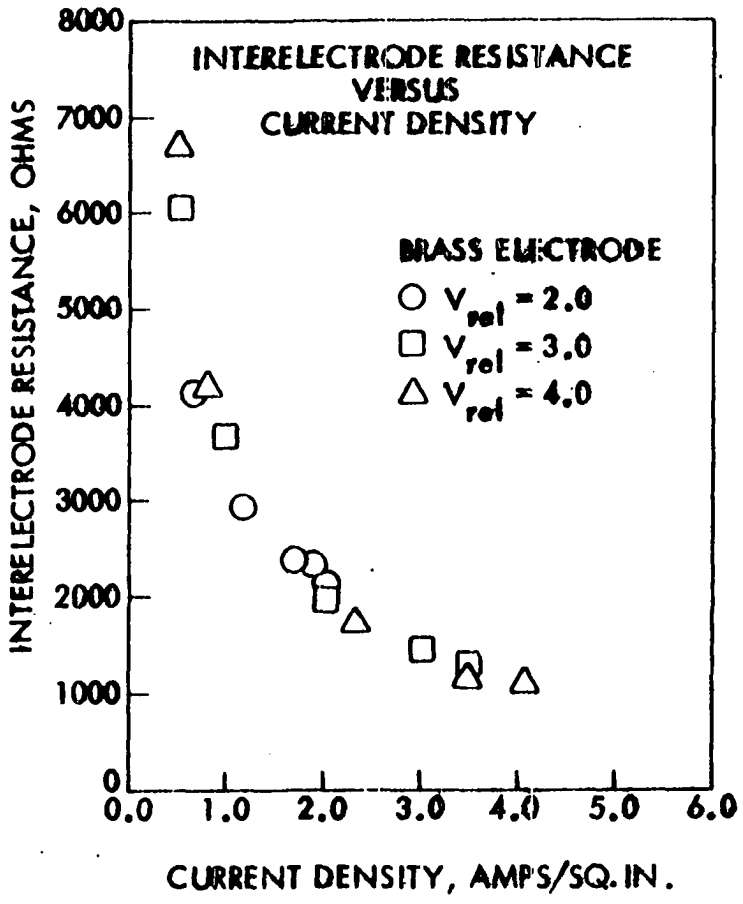
INTERELECTRODE RESISTANCE VERSUS CURRENT DENSITY
BRASS ELECTRODE
V_{rel} = 2.0
V_{rel} = 3.0
V_{rel} = 4.0
INTERELECTRODE RESISTANCE, OHMS
8000
7000
6000
5000
4000
3000
2000
1000
0
0.0
1.0
2.0
3.0
4.0
5.0
6.0
CURRENT DENSITY, AMPS/SQ. IN.

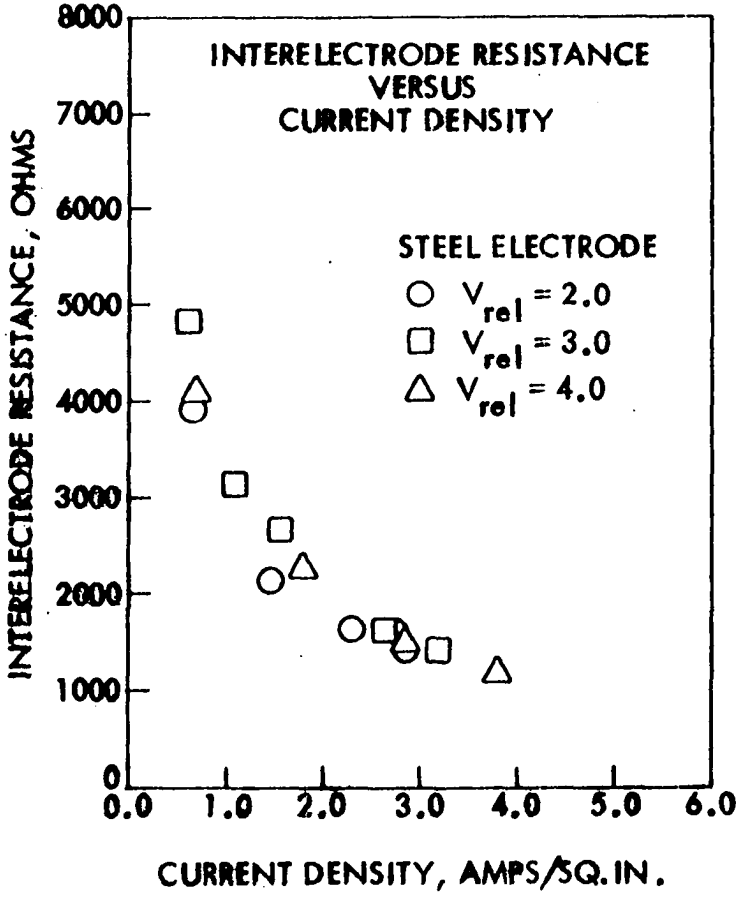
INTERELECTRODE RESISTANCE VERSUS CURRENT DENSITY
STEEL ELECTRODE
V_{rel} = 2.0
V_{rel} = 3.0
V_{rel} = 4.0
INTERELECTRODE RESISTANCE, OHMS
8000
7000
6000
5000
4000
3000
2000
1000
0
0.0
1.0
2.0
3.0
4.0
5.0
6.0
CURRENT DENSITY, AMPS/SQ. IN.

electrodes and to 12 amps/sq. in. for the tungsten electrode. Again, the shape of interelectrode resistance versus current density curve was the same as that for the case of the uninsulated tip of the 1 in. diameter carbon electrode. Furthermore, the interelectrode resistance did not appear to depend upon relative velocity just as was observed with the 1 in. diameter electrode. Also, the value of the interelectrode resistance at any particular current density was the same for the tungsten electrode as it was for the larger brass and steel electrodes.

While checking the electrical continuity of the system before a small electrode run in which only the tip was uninsulated, it was found that no current could be made to flow through an unfluidized bed. Further investigation led to the conclusion that no electrical contact was being made between the tip of the electrode and the bed. Fluidization of the bed caused bed-electrode contact to be made although the resistance was still quite high. Thus, it would appear that as the bed particles settle after fluidization is stopped, a small gap is left between the electrode and the bed particles directly beneath the electrode tip. This would account for the infinite resistance observed in the unfluidized bed.

Effect of current direction and current type

In the third part of the interelectrode resistance investigation experiments were conducted to determine how (1) alternating current and (2) reversing the direction of

direct current flow through the bed would affect the inter-electrode resistance curve. In this part runs were made using direct current with a negative ground and then the runs were repeated using a positive ground. This had the effect of reversing the current flow through the bed. Alternating current was then passed through the bed at the same conditions used in the direct current runs and the results of the three runs compared. A carbon center electrode 1 in. in diameter was used in these runs.

The results of the direct current case are shown in Figures 32 and 33 for the same uninsulated electrode length but different current polarities. As is easily seen, the two curves are of the same form and magnitude. Consequently, it was concluded from comparing the two curves that changing the direction of direct current flow through the bed had no effect on the interelectrode resistance.

The results of the alternating current run are shown in Figure 34, again for the same uninsulated electrode length as for the direct current tests. The DC filters used in the previous two experiments to dampen out the voltage fluctuations resulting from bubbling and particle motion could not be used for alternating current flow through the bed (in an alternating current regime the filters acted as voltage attenuators). The scatter of the data shown in Figure 34 is probably due to the lack of filter smoothing.

Figure 32. Interelectrode resistance versus current density for 1/4 in. uninsulated electrode length (direct current negative ground)

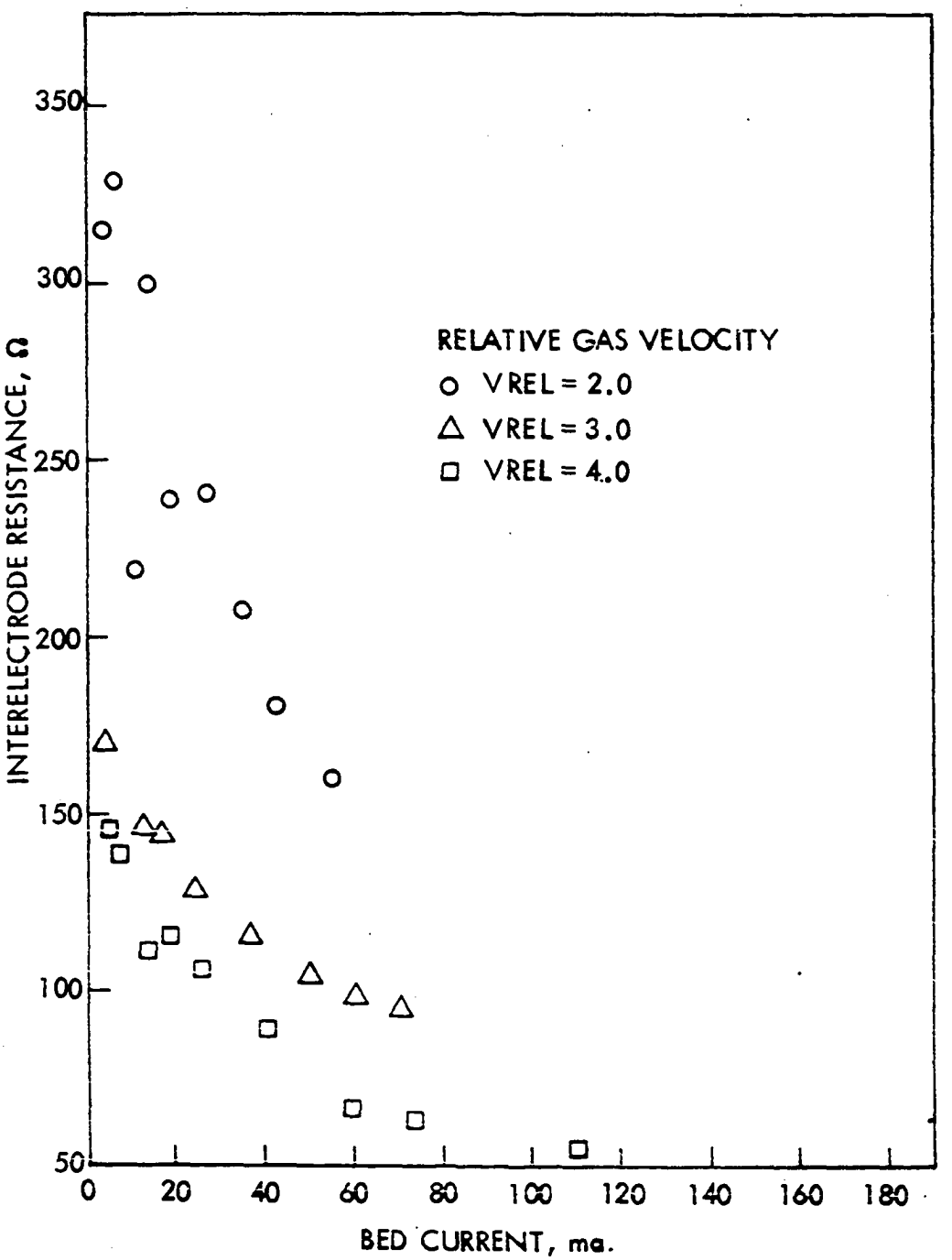
INTERELECTRODE RESISTANCE, Ω
350
300
250
200
150
100
50
0
20
40
60
80
100
120
140
160
180
BED CURRENT, ma.
RELATIVE GAS VELOCITY
VREL = 2.0
VREL = 3.0
VREL = 4.0

Figure 33. Interelectrode resistance versus current density for 1/4 in. uninsulated electrode length (direct current positive ground)

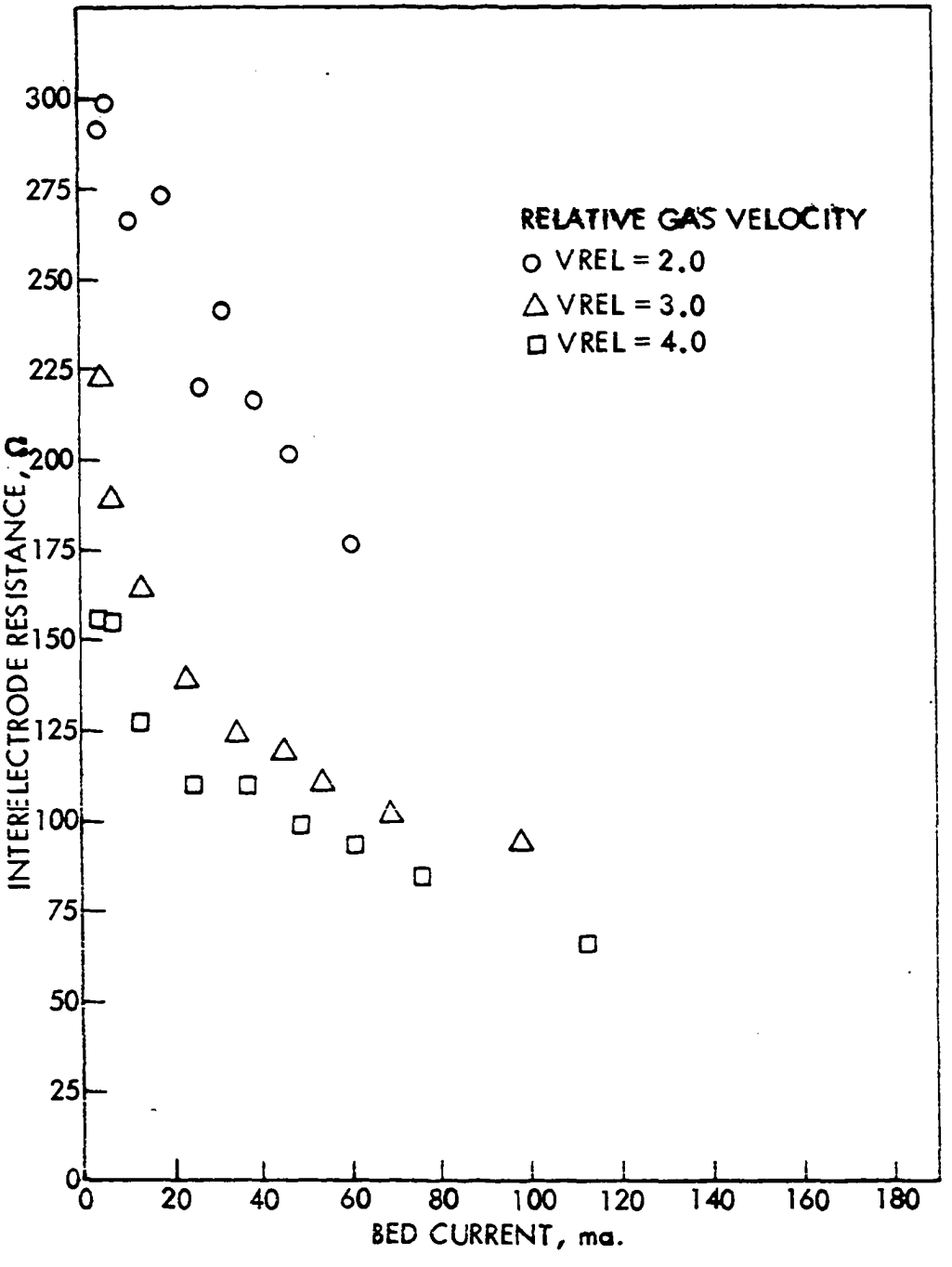
RELATIVE GAS VELOCITY
○ VREL = 2.0
△ VREL = 3.0
□ VREL = 4.0
INTERELECTRODE RESISTANCE, Ω
BED CURRENT, ma.
0
25
50
75
100
125
150
175
200
225
250
275
300
0
20
40
60
80
100
120
140
160
180

Figure 34. Interelectrode resistance versus current density for 1/4 in. uninsulated electrode length (alternating current)

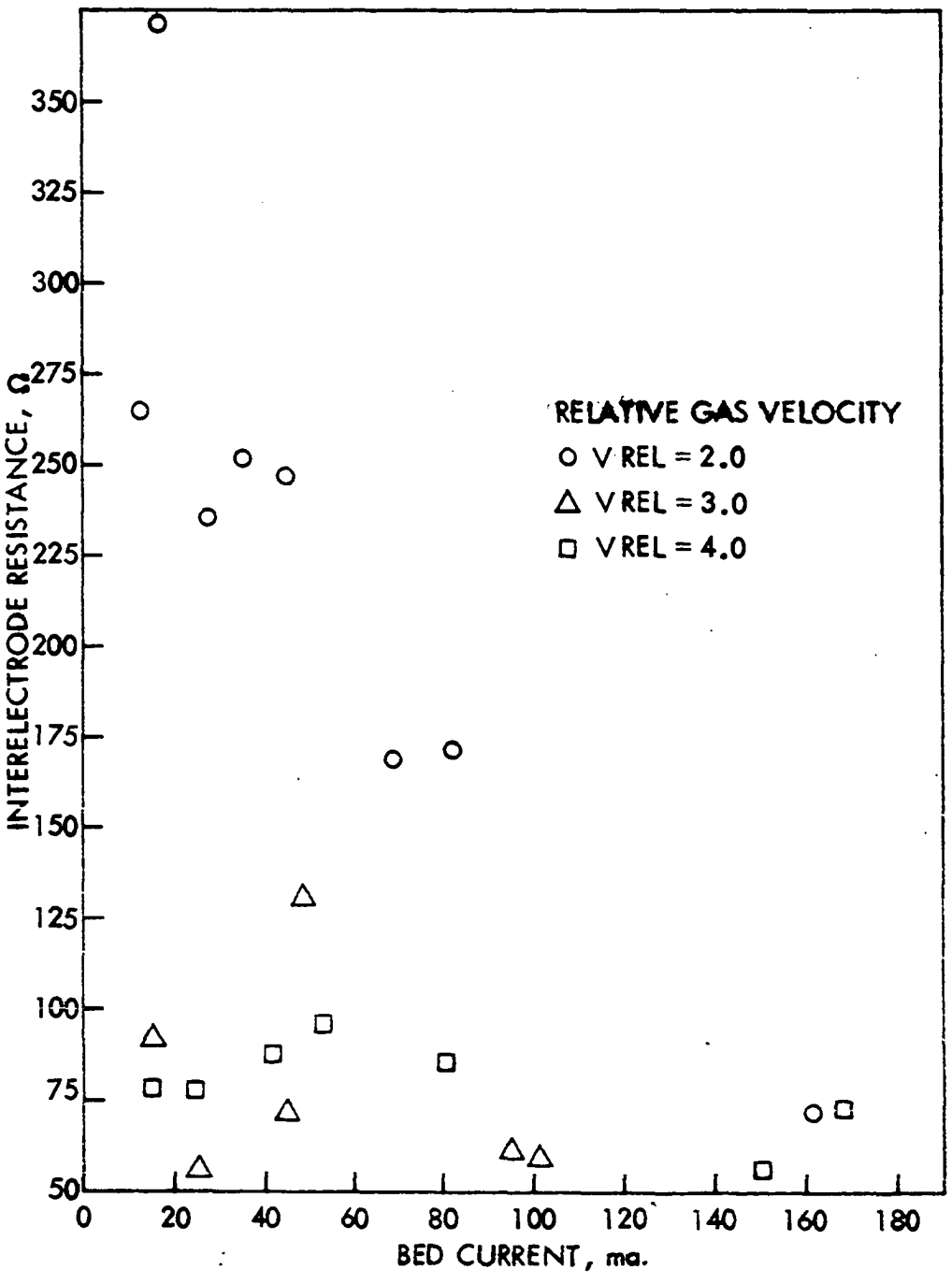
INTERELECTRODE RESISTANCE, Ω
350
325
300
275
250
225
200
175
150
125
100
75
50
0
20
40
60
80
100
120
140
160
180
BED CURRENT, ma.
RELATIVE GAS VELOCITY
V REL = 2.0
V REL = 3.0
V REL = 4.0

Comparison of the alternating current case with the two direct current cases is difficult because of the scatter in Figure 34. At a relative velocity of two, the shape and magnitude of the resistance versus current curve in Figure 34 agree well with the corresponding curves in Figures 32 and 33. However, at the two higher relative velocities there is no apparent trend toward a decrease in interelectrode resistance with increasing bed current for the alternating current case. This contrasts sharply with the decreasing curves shown in the direct current plots (Figures 32 and 33).

Much better agreement between direct current and alternating current runs can be seen by comparing Figures 35 and 36. Figure 35 shows the interelectrode resistance versus current density curve for direct current (positive ground) with the electrode tip insulated. Figure 36 depicts the same curve for alternating current. Again, a 1 in. diameter carbon center electrode was used. Comparison of these two figures shows a decrease of interelectrode resistance with increasing current density for both current regimes. Also, the magnitudes of the interelectrode resistance at a particular current density agree well. For example, at a current density of 0.06 amps/sq. in. the magnitudes of the interelectrode resistances of both curves is approximately 275-300 ohms. As a result of these experiments, it would appear that the type of current being passed through the bed does not affect interelectrode resistance.

Figure 35. Interelectrode resistance versus current density for tip uninsulated (direct current positive ground)

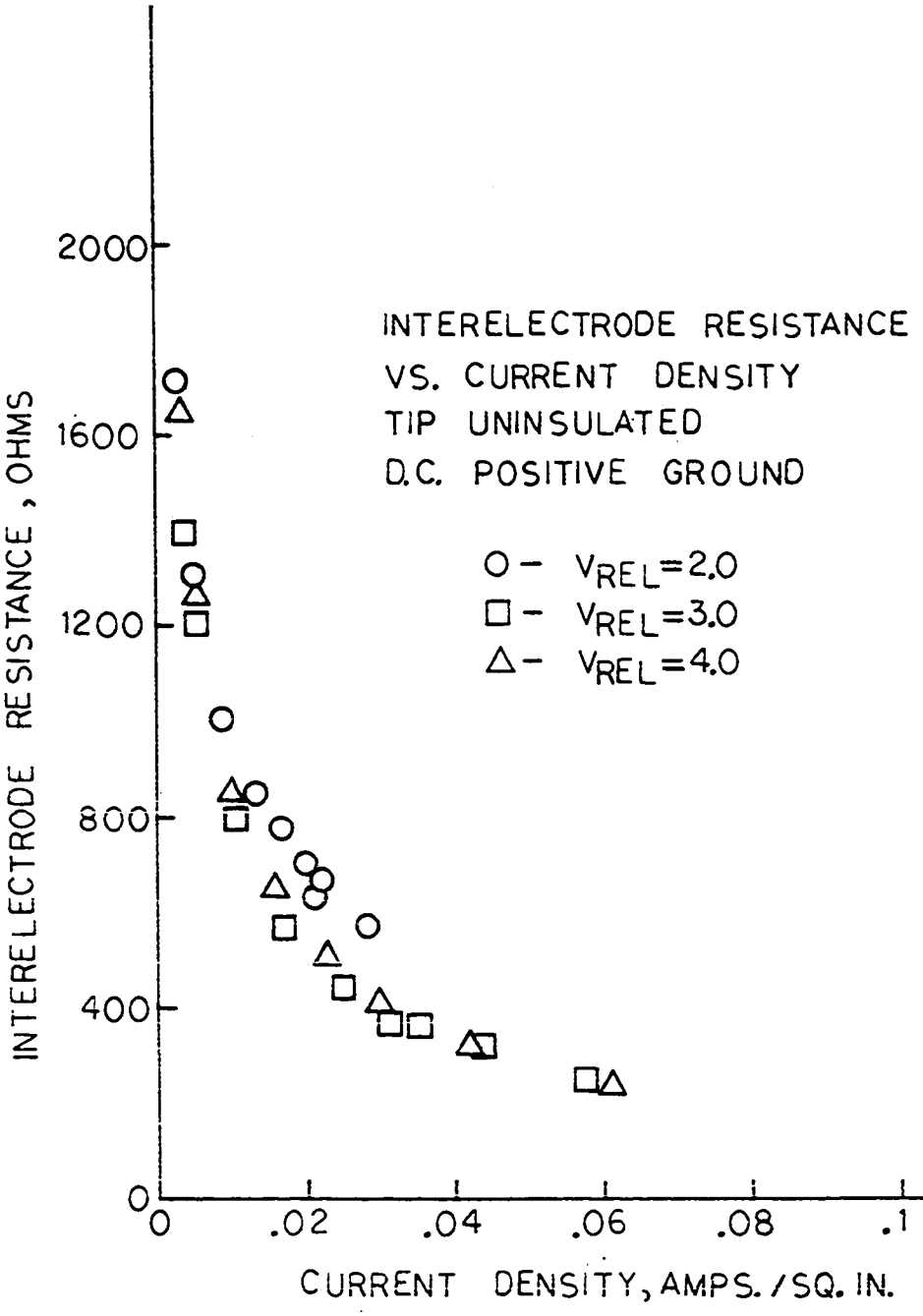
INTERELECTRODE RESISTANCE
VS. CURRENT DENSITY
TIP UNINSULATED
D.C. POSITIVE GROUND
○ - V_{REL}=2.0
□ - V_{REL}=3.0
△ - V_{REL}=4.0
INTERELECTRODE RESISTANCE, OHMS
2000
1600
1200
800
400
0
0
.02
.04
.06
.08
.1
CURRENT DENSITY, AMPS./SQ. IN.

Figure 36. Interelectrode resistance versus current density for tip uninsulated (alternating current)

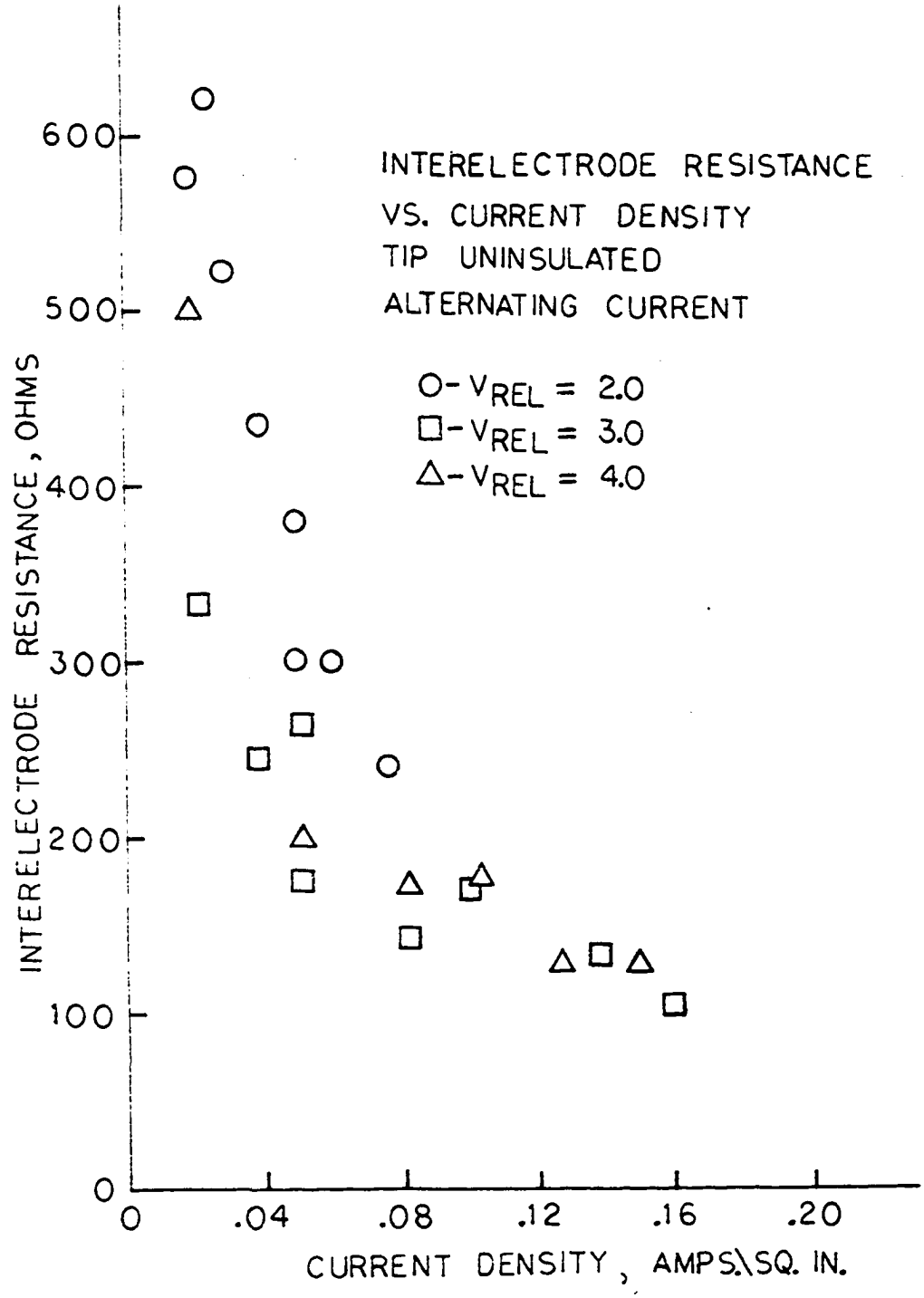
INTERELECTRODE RESISTANCE
VS. CURRENT DENSITY
TIP UNINSULATED
ALTERNATING CURRENT
O- VREL = 2.0
□- VREL = 3.0
△- VREL = 4.0
INTERELECTRODE RESISTANCE, OHMS
600
500
400
300
200
100
0
0
.04
.08
.12
.16
.20
CURRENT DENSITY, AMPS\SQ. IN.

Bed Resistivity

A study was undertaken to determine bed resistivity at different bed conditions by investigating the effect of system operating variables on resistivity. Jones (24) investigated the effect of velocity and column diameter on bed resistivity but confined his research to 2 and 4 in. column diameters. In order to extend this work, a study investigating the effect of velocity on bed resistivity in 4 and 6 in. diameter Plexiglas columns was undertaken. This study compared the data from the 4 and 6 in. diameter columns to the smaller diameter column data obtained by Jones. Also, an empirical expression for predicting bed resistivity obtained by Jones was tested to see if it was valid for these larger diameters.

In the second part of the study, the effect of bed current density on bed resistivity was measured with relative gas velocity as a parameter. Both parts of the study were used to obtain values of bed resistivity to be used in calculating bed resistance values from Equations 33 and 36.

Effect of velocity and column diameter on bed resistivity

A four-point probe method was used to measure bed resistivity as a function of column diameter and gas velocity. Direct current was passed axially through the fluidized bed between two copper-strip electrodes 13 in. apart attached to the column wall. Two probes (No. 17 bead sewing needles spaced

1-1/2 in. apart) were inserted through the side of the column wall into the bed and the voltage drop across the portion of the bed spanned by the probes was measured. A large resistance was placed in series with the voltage probes so that negligible current flowed through probes. Bed resistivity was then calculated using Ohm's Law.

This study was an extension of the work of Jones (24) to larger column diameters. Jones reported an overall decrease in fluidized bed resistivity with increasing column diameter in his work with 2 and 4 in. diameter columns. This investigation was made to determine whether the bed resistivity would continue to decrease with increasing column diameter.

Using the 4 and 6 in. diameter test cells (Figures 4 and 3), runs were made at two different levels of bed height and particle size. The bed heights used were 13-3/4 in. and 4-3/8 in. as measured between the upper surface of the settled bed and the voltage probes. The particle sizes of calcined coke used in the runs were -65/+100 and -48/+65 Tyler mesh size fractions. Nitrogen was used as the fluidizing gas in all runs.

Measurements of the bed resistivity were taken while varying the velocity of the gas over the settled and fluidized bed regions. As the velocity of the gas was increased in the settled bed region, the bed resistivity rose and reached a maximum just beyond the incipient fluidization velocity. The resistivity then decreased to a minimum before rising again. This behavior agreed with the results of Jones.

The results of the measurements with -65/+100 Tyler mesh size coke are plotted along with the results of Jones in Figure 37. The results of the measurements with -48/+65 Tyler mesh size coke are shown in Figure 38. Both plots show an overall decrease of bed resistivity with an increase in column diameter. Also, a comparison of the plots shows that the bed resistivity of the larger particles is less than that of the smaller particles.

An important result of these experiments can be seen in Figure 37. The trough in the bed resistivity versus velocity curve in the fluidized region is much wider for the 6 in. diameter column than for the 4 in. or the 2 in. diameter columns. Moreover, the minimum point in the curve for the larger diameter column appears at a higher velocity than for the smaller columns. The relatively "flat" region in the curve would appear to be a satisfactory region of operation for large industrial electrofluid reactors because velocity changes would not cause large changes in resistance with corresponding changes in voltage.

The rise in the resistivity after the minimum point seems to coincide with the onset of slugging in the bed. Since large diameter columns slug at higher velocities than small diameter columns, the results seem reasonable.

Jones developed an expression correlating the relative minimum resistivity (the ratio of the resistivity at the

Figure 37. Bed resistivity versus velocity for -65/+100 Tyler mesh size calcined coke

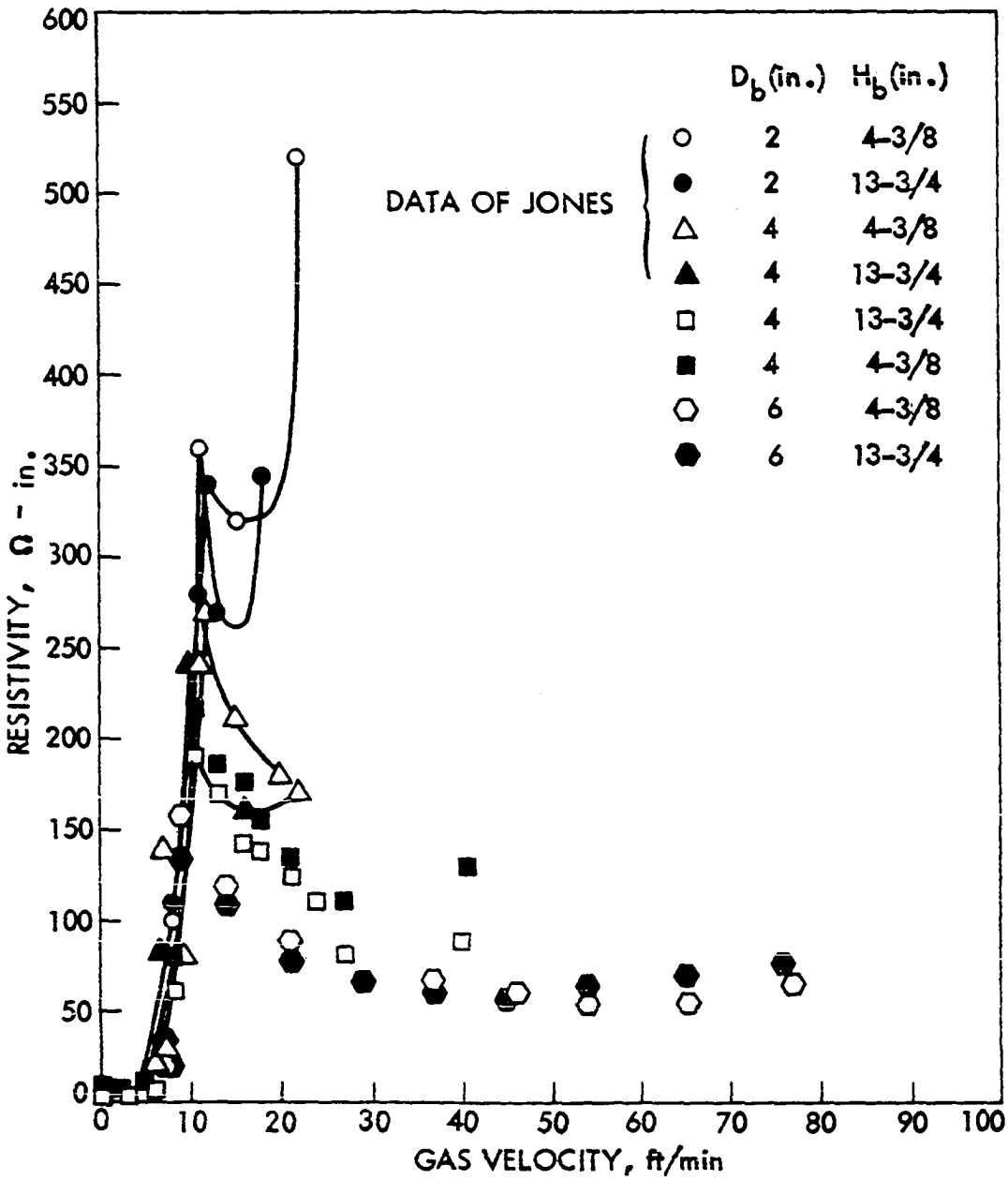
DATA OF JONES
D_b(in.) H_b(in.)
2 4-3/8
2 13-3/4
4 4-3/8
4 13-3/4
4 13-3/4
4 4-3/8
6 4-3/8
6 13-3/4
RESISTIVITY, Ω - in.
GAS VELOCITY, ft/min
0
50
100
150
200
250
300
350
400
450
500
550
600
0
10
20
30
40
50
60
70
80
90
100

Figure 38. Bed resistivity versus velocity for -48/+65 Tyler mesh calcined coke

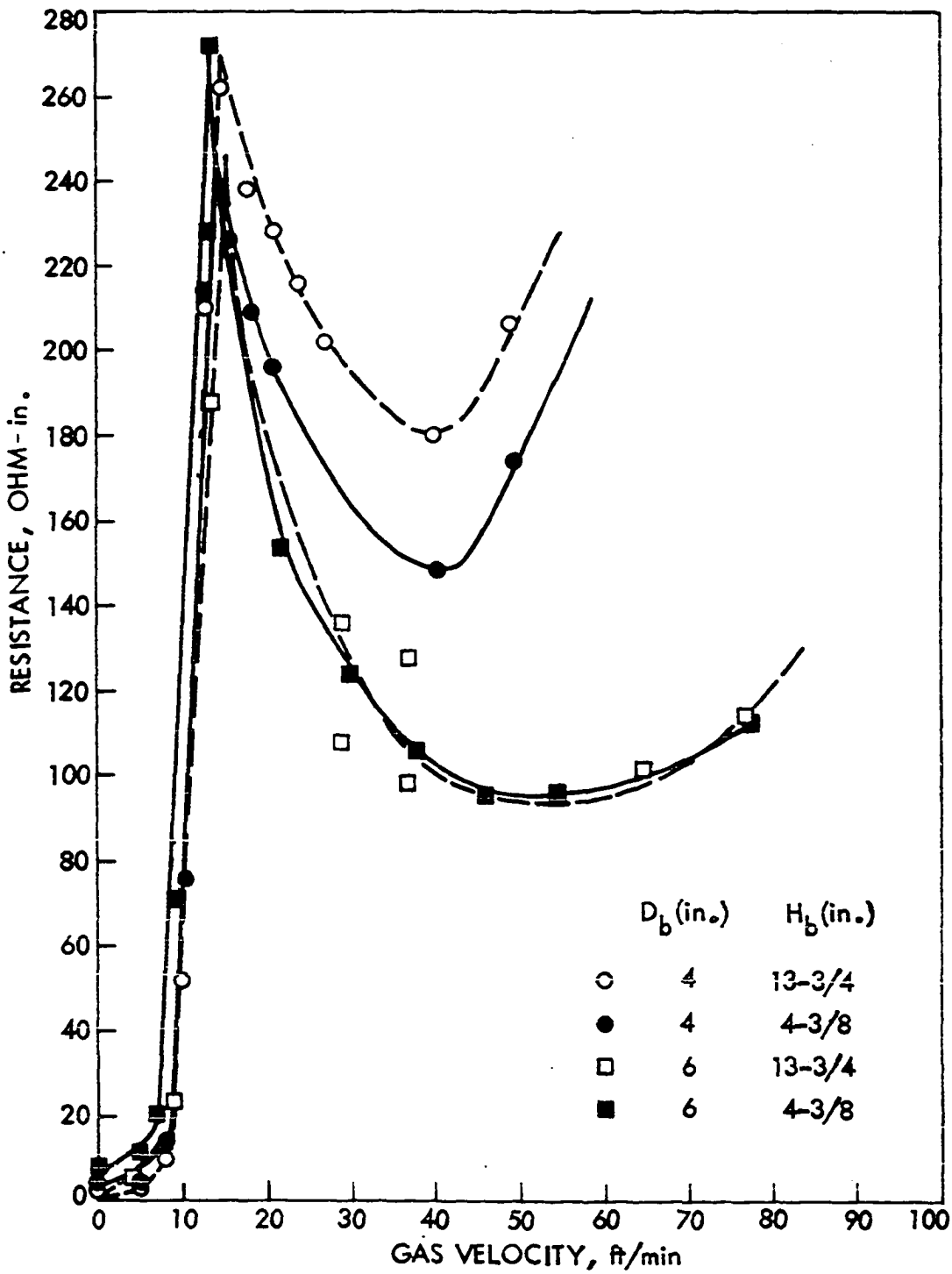
RESISTANCE, OHM-in.
GAS VELOCITY, ft/min
0
20
40
60
80
100
120
140
160
180
200
220
240
260
280
0
10
20
30
40
50
60
70
80
90
100
D_b(in.)
H_b(in.)
4
13-3/4
4
4-3/8
6
13-3/4
6
4-3/8

minimum point in the resistivity versus velocity curve to the resistivity at no gas flow) with column diameter, tangent of the angle of repose of the bed material, and standard deviation of the particle size (Figure 39). The correlation may prove to be important for predicting the resistance of fluidized beds from the column diameter and easily measured solid properties of the bed material if the correlation can be extended to larger column diameters. In the case of the 4 in. and 6 in. column diameters this seems to be the case, since the data put the correlation fairly well (Figure 40).

Effect of current density on bed resistivity

The four-point probe method was used to measure the bed resistivity as a function of current density. A settled bed height of 21.5 in. was used and -48/+65 Tyler mesh size calcined coke was used as the bed material. The maximum bed current used was approximately 100 ma.

Measurements of the resistivity were made in two ways. Runs were made both with and without a "dummy" center electrode in the test cell to see if the presence of the electrode had an effect upon the bed resistivity. Results of the runs were plotted as bed volume resistivity versus current density with relative gas velocity as a parameter (Figure 41). The current density was calculated as the current flowing through the bed per unit cross sectional area of the column.

Figure 39. Observed versus predicted values of minimum relative resistivity (data of Jones) for 2 in. and 4 in. diameter

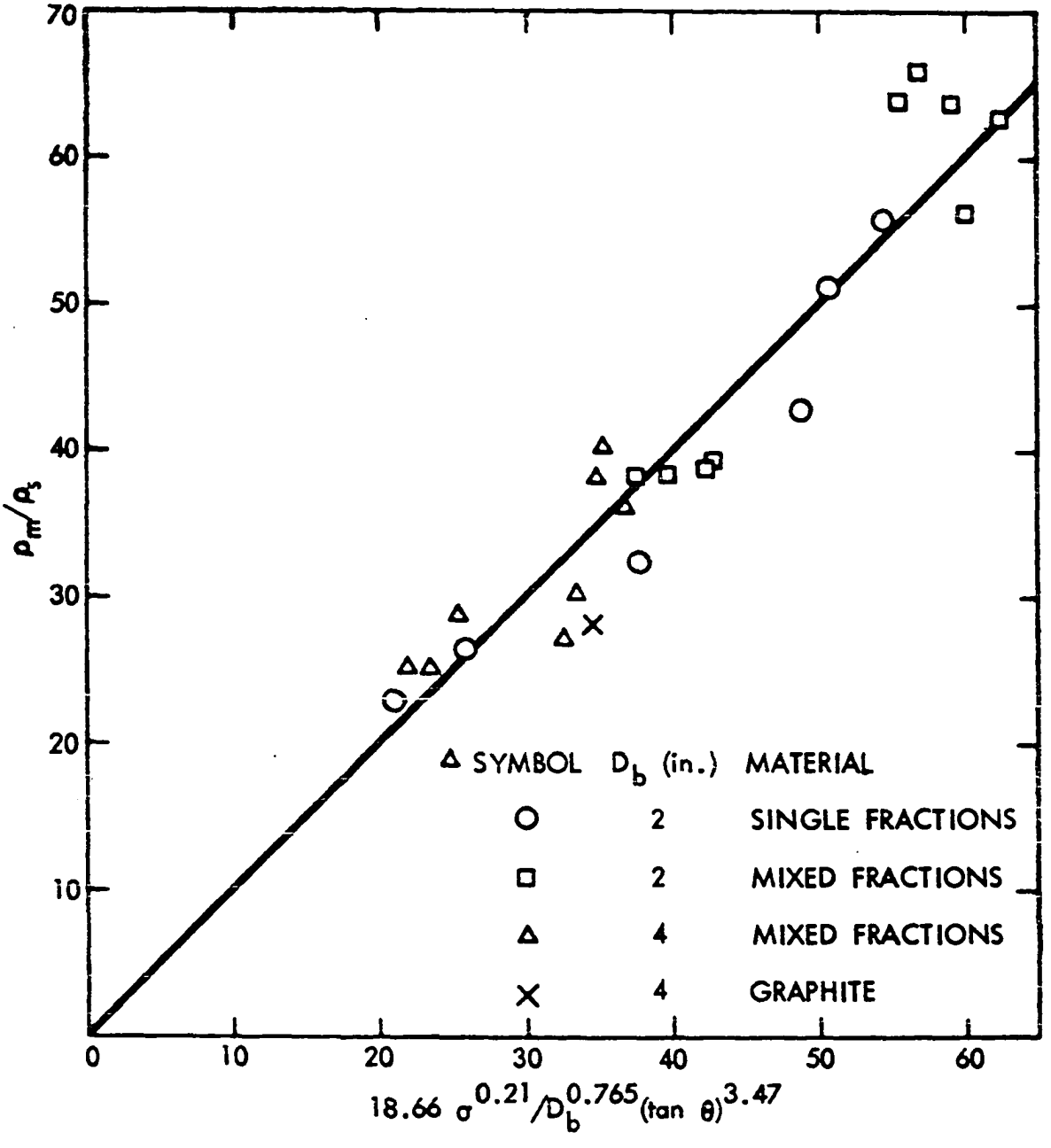
70
60
50
40
30
20
10
0
10
20
30
40
50
60
ρ_m/ρ_s
$18.66\ \sigma^{0.21}/D_b^{0.765}(\tan\theta)^{3.47}$
SYMBOL D_b (in.) MATERIAL
2 SINGLE FRACTIONS
2 MIXED FRACTIONS
4 MIXED FRACTIONS
4 GRAPHITE

Figure 40. Observed versus predicted values of minimum relative resistivity for 4 and 6 in. columns

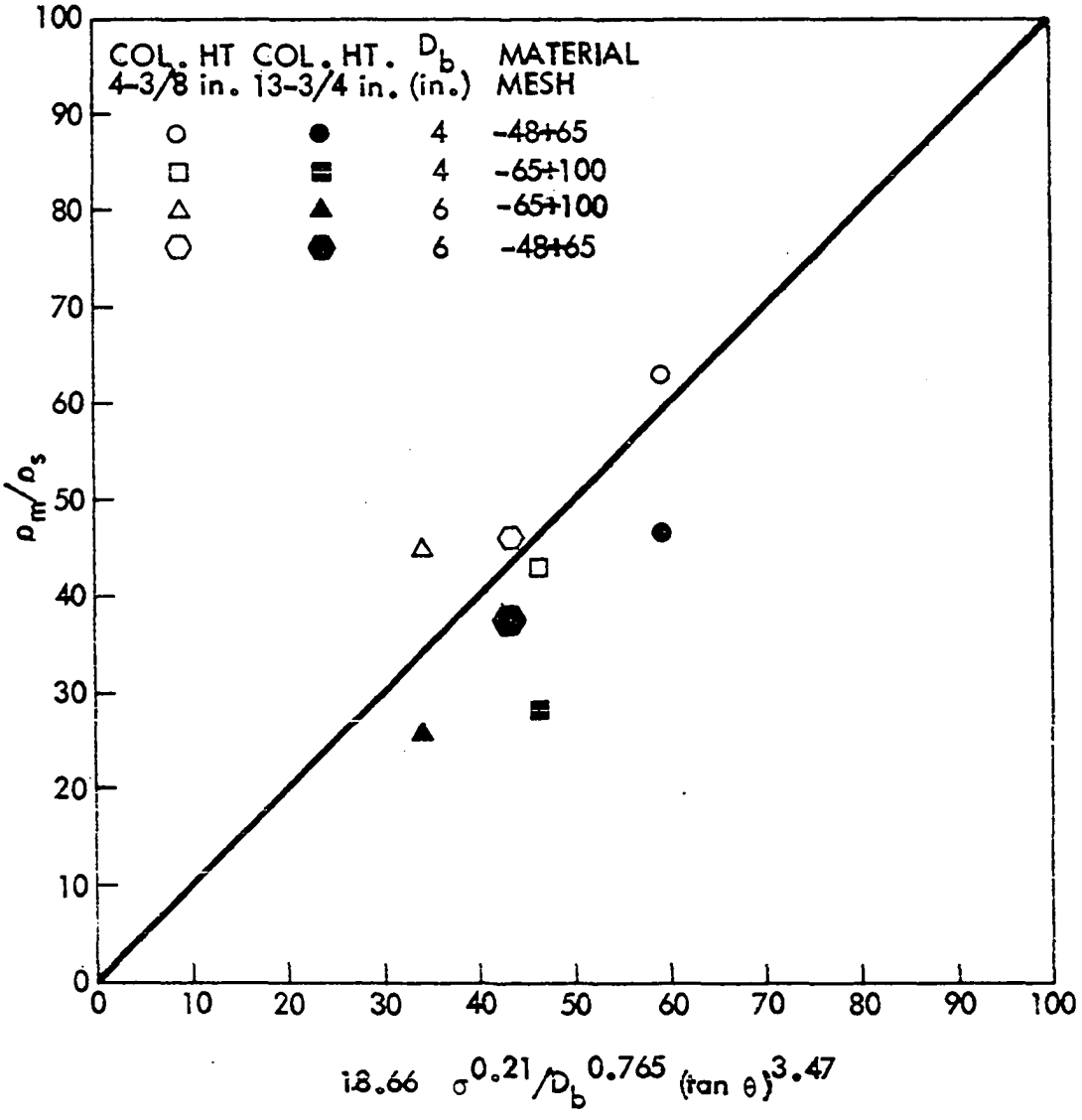
COL. HT 4-3/8 in.
COL. HT. 13-3/4 in.
D_b (in.)
MATERIAL MESH
4 -48+65
4 -65+100
6 -65+100
6 -48+65
ρ_m/ρ_s
$18.66\ \sigma^{0.21}/D_b^{0.765}\ (\tan\theta)^{3.47}$
0
10
20
30
40
50
60
70
80
90
100

Figure 41. Bed volume resistivity versus current density

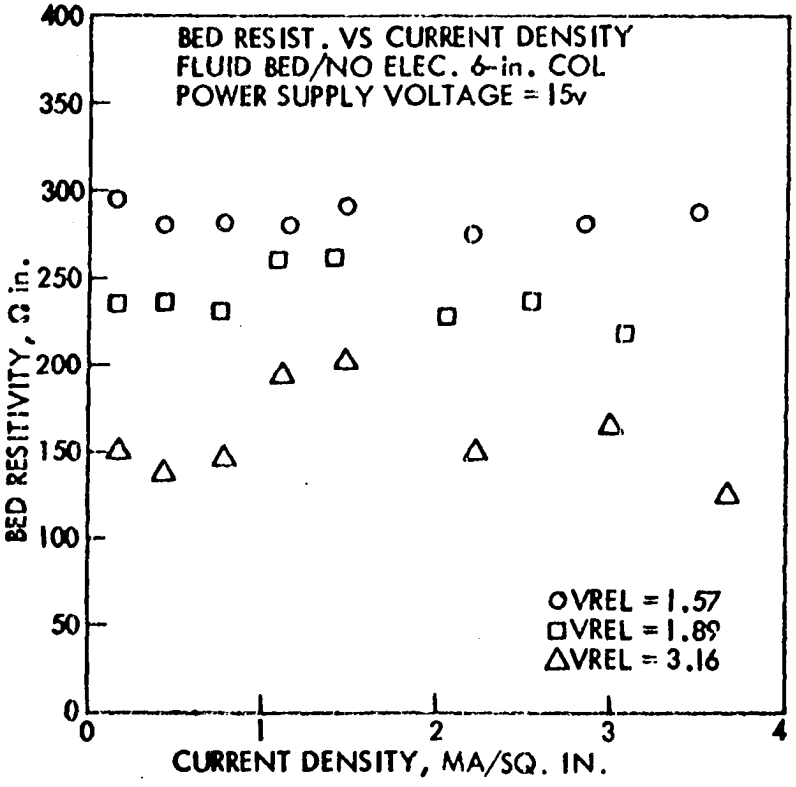
BED RESIST. VS CURRENT DENSITY
FLUID BED/NO ELEC. 6-in. COL
POWER SUPPLY VOLTAGE = 15v
BED RESITIVITY, Ω in.
CURRENT DENSITY, MA/SQ. IN.
OVREL = 1.57
□VREL = 1.89
ΔVREL = 3.16
400
350
300
250
200
150
100
50
0
0
1
2
3
4

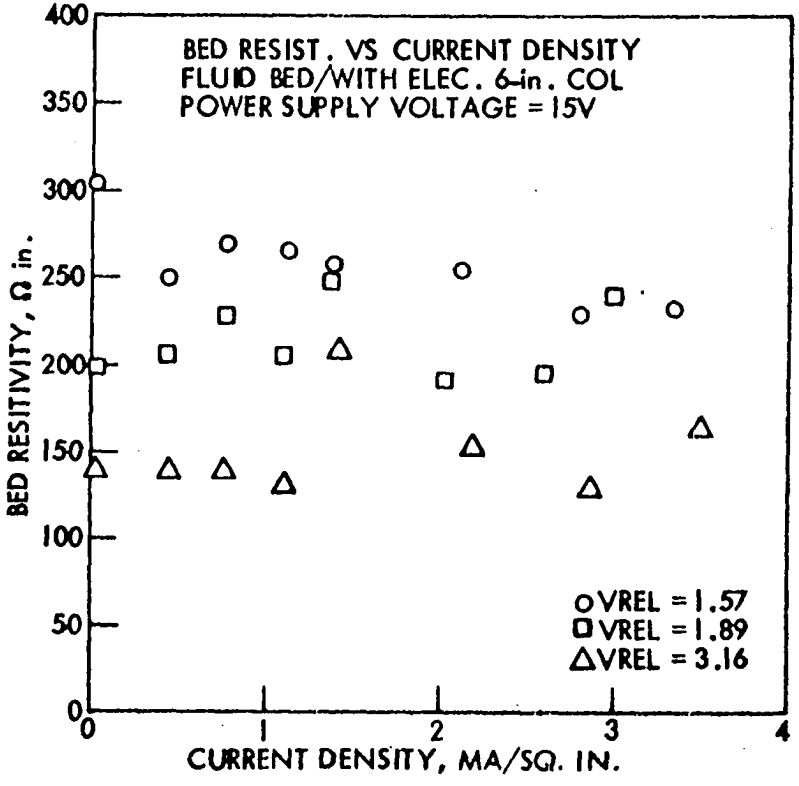
BED RESIST. VS CURRENT DENSITY
FLUID BED/WITH ELEC. 6-in. COL
POWER SUPPLY VOLTAGE = 15V
BED RESITIVITY, Ω in.
CURRENT DENSITY, MA/SQ. IN.
OVREL = 1.57
□VREL = 1.89
ΔVREL = 3.16
400
350
300
250
200
150
100
50
0
0
1
2
3
4

The results show that the insertion of the electrode in the bed had no apparent effect upon the resistivity of the bed. As with the interelectrode resistance, the bed resistivity decreased with increasing relative gas velocity in the fluidized bed region. Although there was much scatter in the data, no apparent trend of bed resistivity with current density was noted. Therefore, it would seem that the decreasing behavior of the interelectrode resistance with increasing current density should be attributed to the contact resistance.

Verification of Laplacian Field Model

In order to effect a separation of contact resistance from bed resistance a Laplacian potential field model of the bed was proposed. If this model was valid, the technique described in Calculation Methods could then be used to calculate the bed resistance. The contact resistance could then be calculated by subtracting the bed resistance from the interelectrode resistance.

Assuming that Laplacian potential field model of the bed was valid was equivalent to assuming that the solution to Laplace's equation:

$$\nabla^2 \phi = 0 \tag{41}$$

would accurately predict the distribution of potential (or voltage) between the center and wall electrodes in the bed. It was also necessary to assume (1) that the bed was

homogeneous with respect to its resistivity and (2) that the potential of the bed adjacent to a given electrode surface was uniform.

A number of measurements were taken to verify this model. A special test cell (Figure 6) built for this purpose was fitted with five probes so as to determine the radial voltage potential at various axial positions of the bed. Measurements were made with a 16 in. bed of calcined coke of -48/+65 Tyler mesh size. A relative gas velocity of two was used. Measurements were made at room temperature and pressure using a DC power supply to establish the bed field.

In a typical run, one of the voltage probes was first positioned so that it touched the center electrode while the other probes were retracted. The probe was then moved outward to successive radial positions. At each position the location of the probe tip was determined and the voltage drop between the probe and the center electrode and the total voltage drop were measured. The same probing procedure was then repeated using the other four probes.

The potential field was probed for four different electrode configurations. In the first configuration the center electrode was completely uninsulated. A constant bed current of 100 ma. was used in this case. The results are shown in Figure 42. In this plot and the plots for the other three configurations the fraction of the experimentally obtained voltage drop

Figure 42. Experimental vs. theoretical bed voltage profiles for a completely uninsulated center electrode

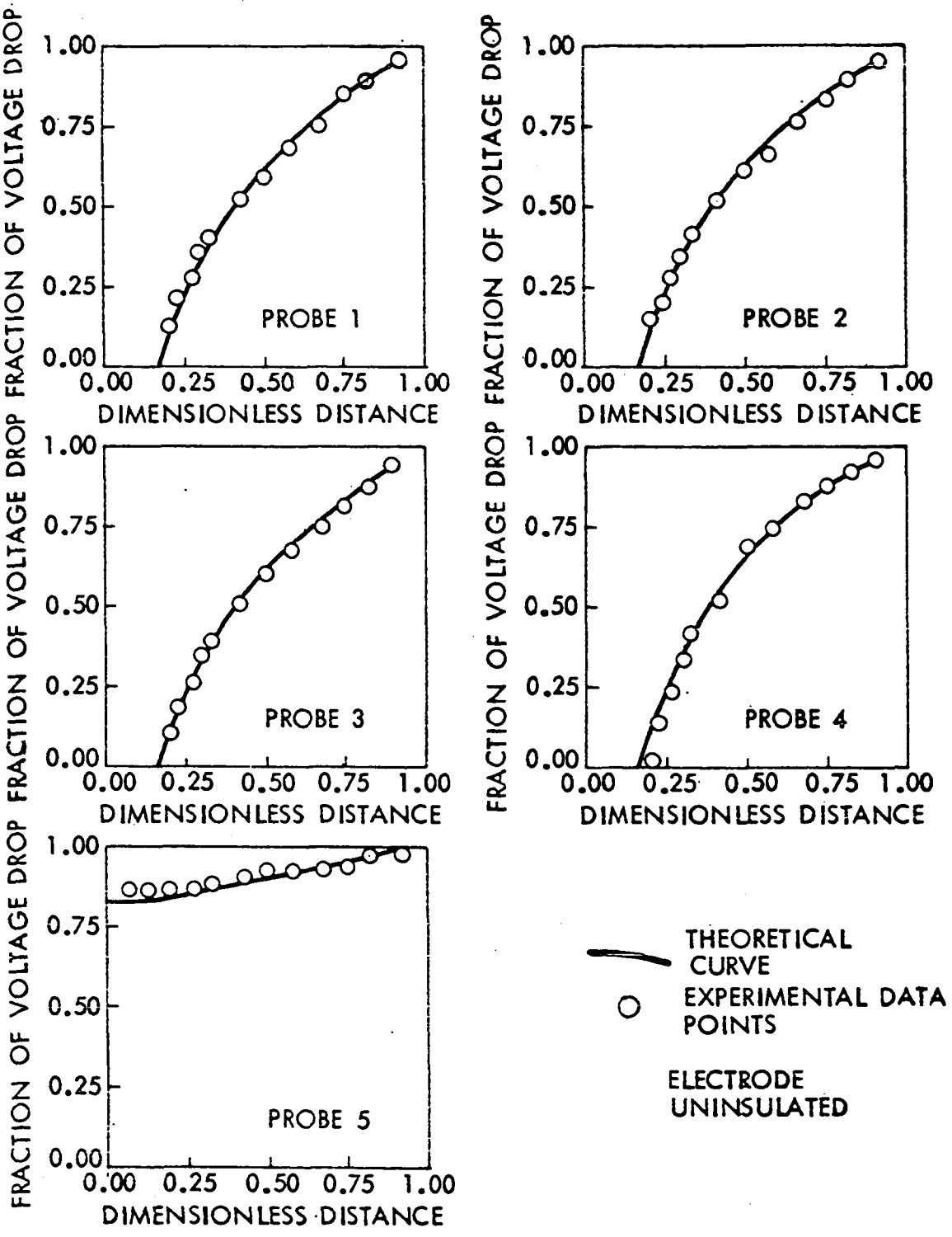
FRACTION OF VOLTAGE DROP
1.00
0.75
0.50
0.25
0.00
PROBE 1
0.00 0.25 0.50 0.75 1.00
DIMENSIONLESS DISTANCE
PROBE 2
PROBE 3
PROBE 4
PROBE 5
THEORETICAL CURVE
EXPERIMENTAL DATA POINTS
ELECTRODE UNINSULATED

occurring between the center electrode and the probe tip is plotted versus the dimensionless radial position of the tip. The latter is the ratio of the radial position of the tip to the inside radius of the column. Experimentally obtained values are denoted by small circles while the smooth curve represents values predicted by Laplace's equation. The predicted values agreed quite closely with the measured values for all five probes.

In the second configuration the center electrode was completely insulated except for a 1/4 in. length immediately opposite the fourth probe from the top. Again, a bed current of 100 ma. was used. The results shown in Figure 43 show that the predicted and observed values agree well for this configuration also.

In the third configuration the center electrode was again completely uninsulated except for a 1/4 in. length opposite the top probe. As in the other two cases a 100 ma. current was passed through the bed. And, again, no discernable deviation between the measured and predicted values was noted (Figure 44).

In configuration four the electrode was completely insulated except for the flat tip at its end. The electrode was shortened in this configuration so that the fourth probe from the top could be used to probe the region 1/2 in. below the electrode tip. For this configuration the overall resistance

Figure 43. Experimental vs. theoretical bed voltage profiles for 1/4 in. section of center electrode uninsulated across from probe 4

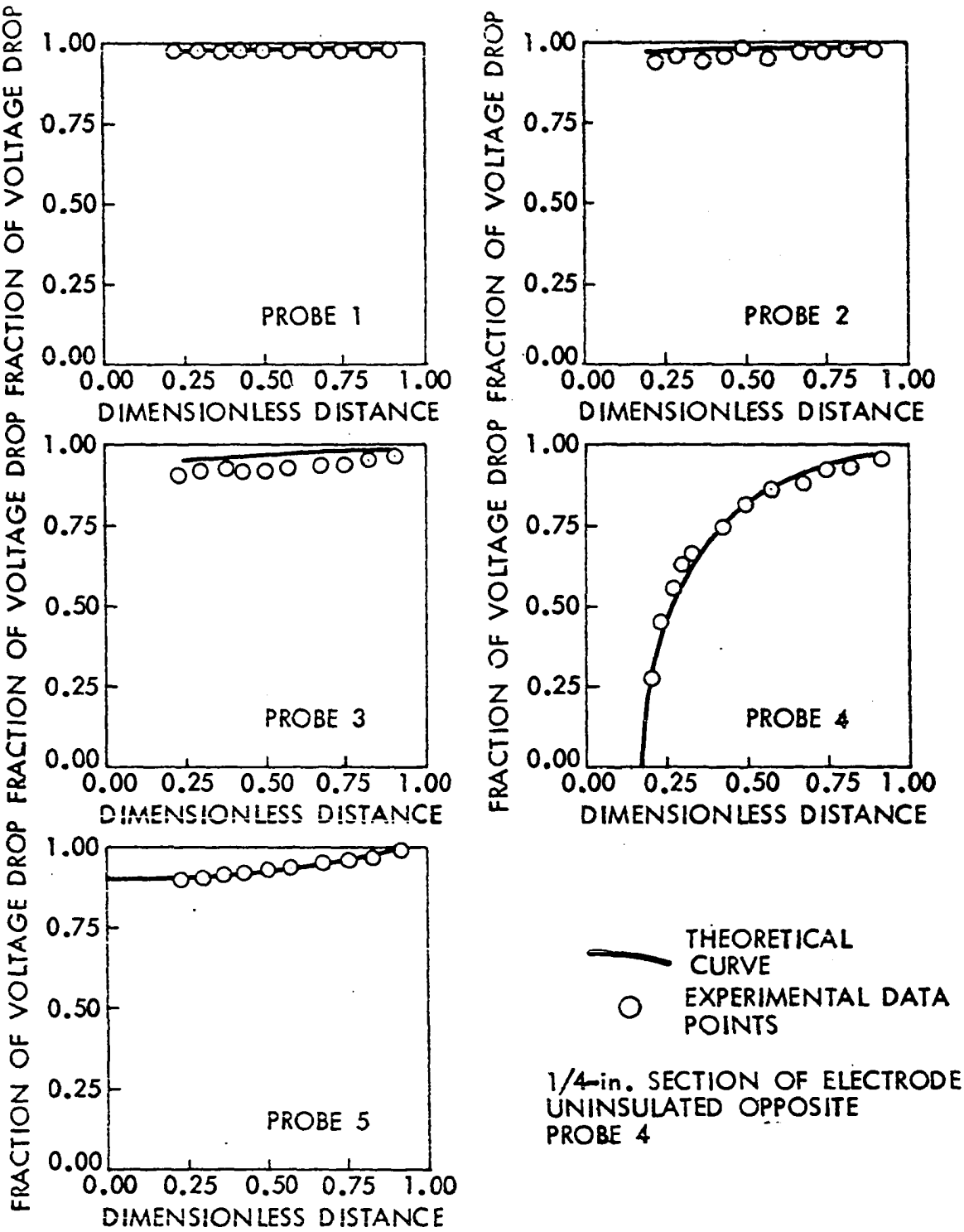
FRACTION OF VOLTAGE DROP
1.00
0.75
0.50
0.25
0.00
PROBE 1
0.00 0.25 0.50 0.75 1.00
DIMENSIONLESS DISTANCE
PROBE 2
PROBE 3
PROBE 4
PROBE 5
THEORETICAL CURVE
EXPERIMENTAL DATA POINTS
1/4-in. SECTION OF ELECTRODE UNINSULATED OPPOSITE PROBE 4

Figure 44. Experimental vs. theoretical bed voltage profiles for a 1/4 in. section of center electrode uninsulated across from probe 1

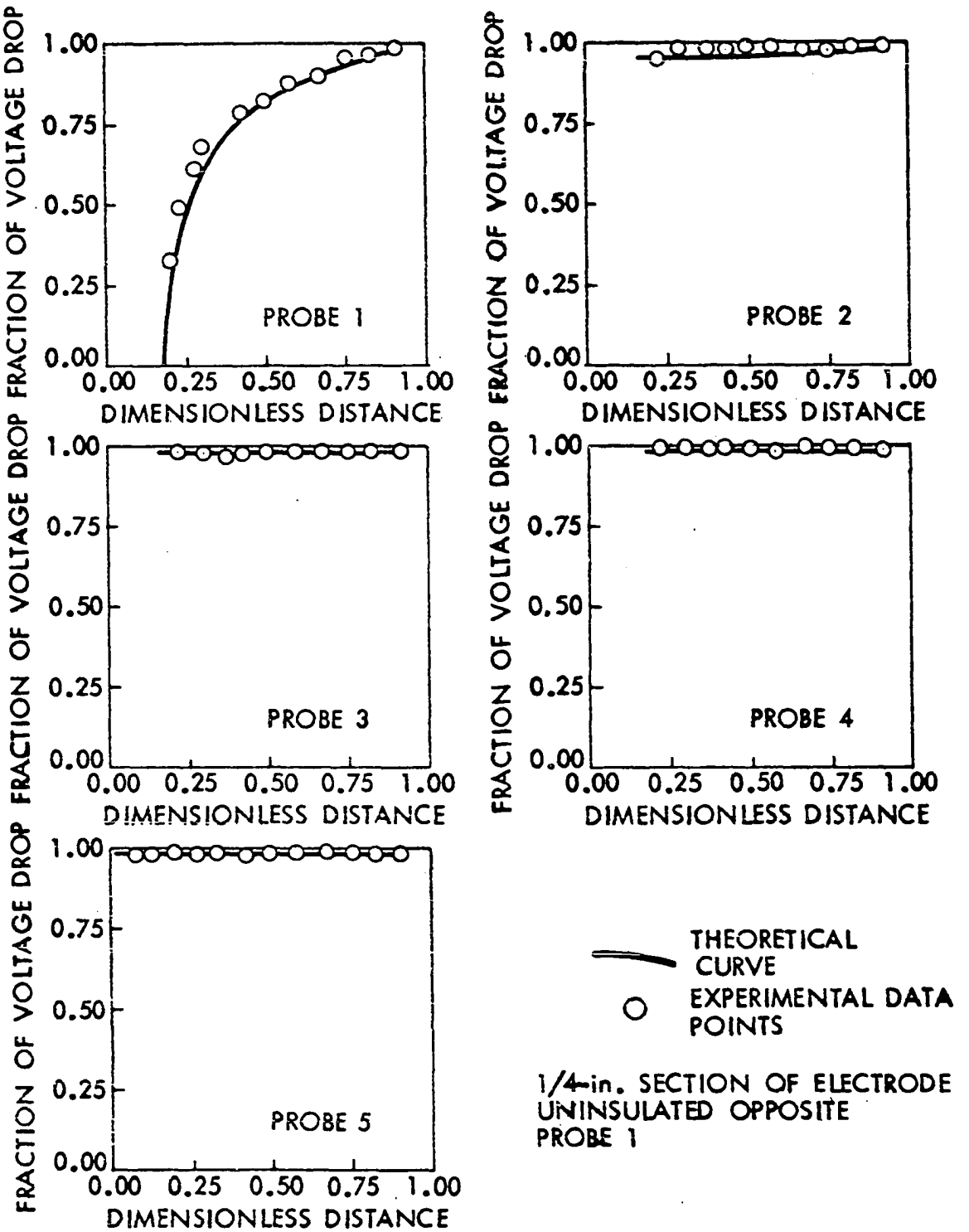
FRACTION OF VOLTAGE DROP
1.00
0.75
0.50
0.25
0.00
PROBE 1
PROBE 2
PROBE 3
PROBE 4
PROBE 5
0.00 0.25 0.50 0.75 1.00
DIMENSIONLESS DISTANCE
THEORETICAL CURVE
EXPERIMENTAL DATA POINTS
1/4-in. SECTION OF ELECTRODE UNINSULATED OPPOSITE PROBE 1

resistance of the system was much higher than in the other configurations so that the bed current was limited to only 30 ma. In this case all probes showed agreement with the predicted values except for the probe in the region beneath the center electrode (Figure 45).

The generally good agreement between measured and predicted values provides strong support for the potential field model. Also, the close agreement indicates that the calcined coke bed is homogeneous with respect to its resistivity except for the region beneath the center electrode tip.

Comparison of Bed Resistance Calculation Methods

Knowing values for the bed resistivity at several velocities, it was next attempted to determine the relative magnitudes of the bed and contact resistances. The method employed was to determine a value for the bed resistance and then determine the contact resistance by difference using Equation 7.

Two methods were used to determine a value for the bed resistance for various geometries. A major assumption made in each method was that the volume resistivity of the bed was the same throughout all regions of the bed.

The first method used was to apply field theory by solving Laplace's equation numerically to find the bed potential distribution and relating this to the bed resistance. The

Figure 45. Experimental versus theoretical bed voltage profiles for uninsulated center electrode tip

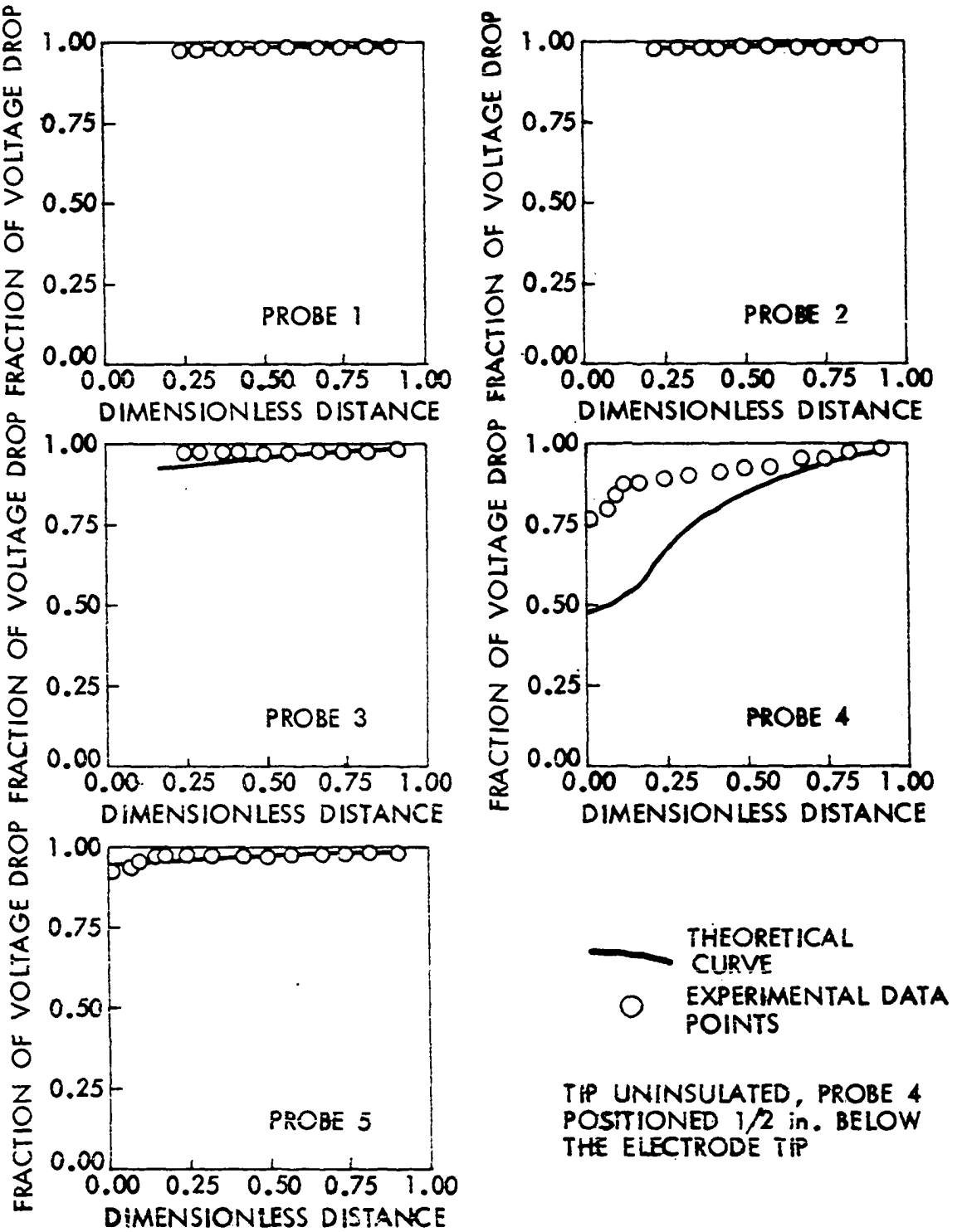
FRACTION OF VOLTAGE DROP
1.00
0.75
0.50
0.25
0.00
PROBE 1
0.00 0.25 0.50 0.75 1.00
DIMENSIONLESS DISTANCE
PROBE 2
PROBE 3
PROBE 4
PROBE 5
THEORETICAL CURVE
EXPERIMENTAL DATA POINTS
TIP UNINSULATED, PROBE 4 POSITIONED 1/2 in. BELOW THE ELECTRODE TIP

second (restricted bed) method was derived analytically. Both techniques are described in detail in the Calculation Methods section of the thesis. Of the two methods used as means of calculating the bed resistance, the restricted bed method is much faster and easier to use. It was derived from the defining equation for resistivity

$$R = \frac{\rho l}{A} \quad . \tag{42}$$

A limitation of this equation is that it assumes no distortion of the electrical field through a given medium.

The field theory treatment is the more rigorous of the two methods and has wider applicability. Furthermore, the field theory method supplies more information than just the bed resistance.

A comparison of values for the bed resistance obtained by the restricted bed method and by field theory is shown for three different electrode configurations in Table 3. The resistance values are for a 6 in. cylindrical column with a 1 in. diameter center electrode and a 16 in. long wall electrode. The bed height was also 16 in. The three different electrode configurations refer to the different electrode lengths which were uninsulated. These lengths were 1/4 in., 1 in., and 10.75 in. Using the field theory model as a reference, Table 3 indicates that the restricted bed method approximates the bed resistance well at large uninsulated

Table 3. Resistance of different electrode configurations in ohms, bed resistivity taken as 275 ohm-in.

	Uninsulated electrode length		
	1/4 in.	1 in.	10.75 in.
Restricted bed	35.7	21.5	6.31
Field theory	25.6	19.1	5.67
% Difference	39%	12.5%	11.3%

electrode lengths, but is in error at short uninsulated electrode lengths.

The field theory method gives consistently lower values for bed resistance than the restricted bed method. This is due to the fact that the portion of the bed region available for current flow in the restricted bed model is less than that actually available. This can be seen by looking at Figure 19. This limited bed region causes the higher resistances associated with the restricted bed model shown in Table 3.

Contact Resistance

Comparison of bed and contact resistances

A plot of interelectrode resistance versus current density at a relative velocity of 3.1 for two uninsulated areas is shown in Figure 46. Superimposed on this plot is the value of bed resistance for both uninsulated electrode lengths as calculated

Figure 46. Interelectrode and bed resistance versus current density for tip uninsulated and 1/4 in. length uninsulated

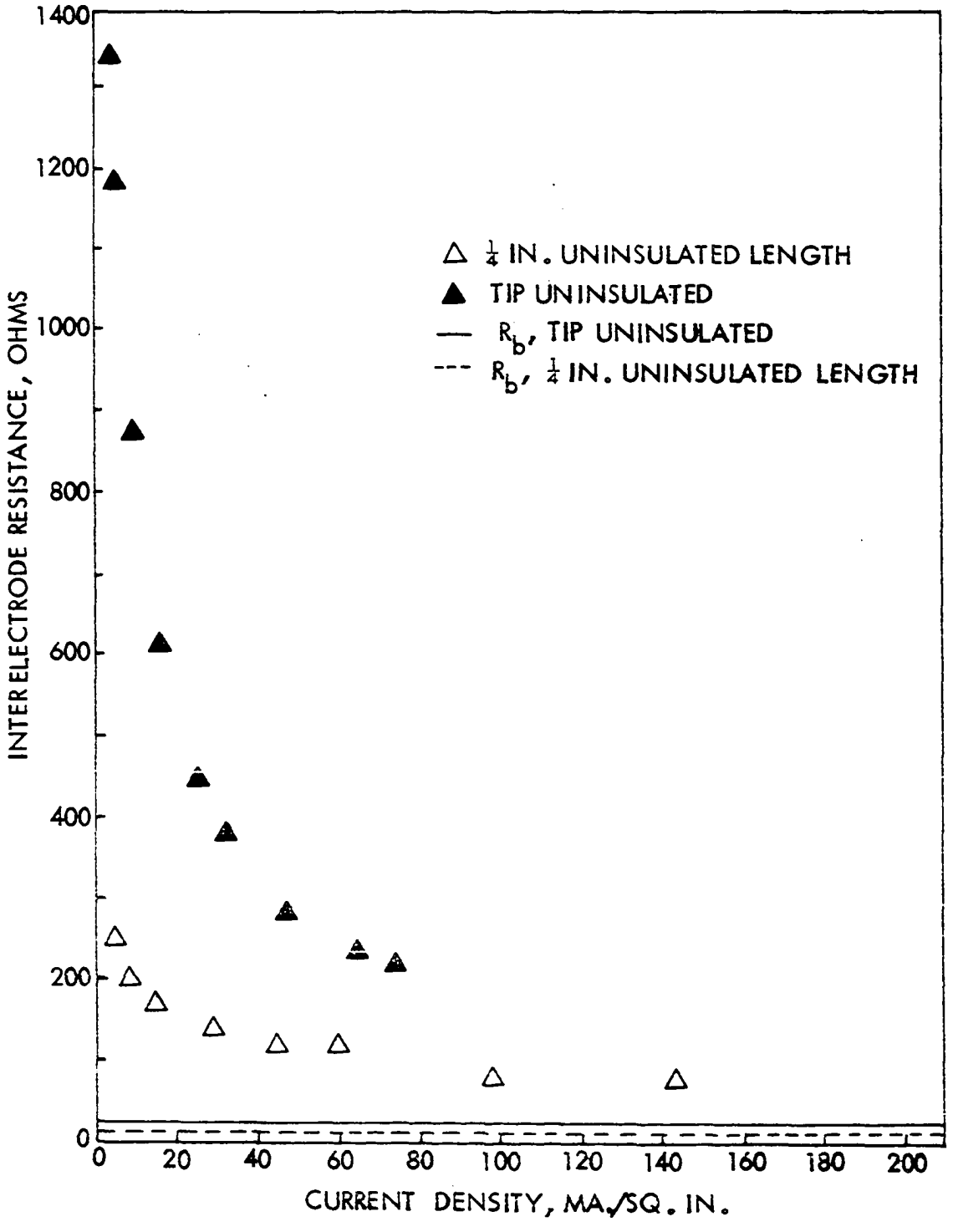
1400
1200
1000
800
600
400
200
0
INTER ELECTRODE RESISTANCE, OHMS
△ ¼ IN. UNINSULATED LENGTH
▲ TIP UNINSULATED
— R_b, TIP UNINSULATED
--- R_b, ¼ IN. UNINSULATED LENGTH
0
20
40
60
80
100
120
140
160
180
200
CURRENT DENSITY, MA./SQ. IN.

by the field theory method. This shows graphically the relative magnitudes of interelectrode resistance and the contact resistance. The difference between the interelectrode resistance curve and the bed resistance line is the contact resistance. The figure clearly shows that the contact resistance is the larger of the interelectrode resistance components for these configurations, and appears to be the component of interelectrode resistance which varies non-linearly with current density.

At higher current densities there is a flattening of the interelectrode resistance curve in Figure 46. This flattening occurs in nearly every interelectrode resistance versus current density curve. For the case of the 1/4 in. uninsulated length the interelectrode resistance curve is nearly constant with current density at current densities above 100 ma/sq. in.

In Table 4 the contact resistance, bed resistance and the ratio of the contact resistance to the bed resistance is listed for several electrode configurations of large and small diameter electrodes. The ratio was calculated at the maximum current used in each run, or equivalently, at the maximum current density. This point occurred where the interelectrode resistance versus current density curve was flattest.

Table 4 shows that the ratio of contact to bed resistance varies between 1 and 4.35 except for the case where the flat tip of the 1 in. diameter carbon electrode was uninsulated.

Table 4. Comparison of bed resistance and contact resistance at maximum current with relative velocity, electrode exposure, and electrode diameter as parameters

Electrode	Diameter in.	Exposure length, in.	V_{rel}	Maximum current, ma.	Maximum current density A/sq. in.	R_c, ohms	R_b, ohms	R_c/R_b
Tungsten	1/25	1/4	4	130	4.25	65	35	1.63
			3			60	40	1.5
			2			109	51	2.12
Steel	1/16	1/4	4	105	2.1	85	35	2.43
			3			100	40	2.5
			2			149	51	2.92
Brass	1/16	1/4	4	100	1.9	85	35	2.43
			3			110	40	2.75
			2			149	51	2.92
Carbon	1	1/4	4	120	0.15	50	15	4.33
			3			80	17	4.7
			2			93	21.5	4.35
Carbon	1	1	4	160	0.05	22.3	9.7	2.3
			3			26	11	2.36
			2			58	14	4.14
Carbon	1	TIP	4	50	0.07	197	18	10.9
			3			195	20	9.75
			2			294	26	11.30
Carbon	1	10.75	3.2	130	0.004	3.45	3.25	1.15
			1.9			5.6	4.2	1.33
			1.6			5.6	5.6	1.0

In this case the ratio was approximately 10. The abnormally high ratio at the tip is caused by the same phenomenon which resulted in high resistance in the interelectrode resistance versus current density runs mentioned before. The table shows that contact resistance is at least equal to and usually 2 to 4 times greater than the bed resistance at the maximum currents used. Also, there appears to be a general decrease in the ratio with increasing relative velocity. Although the comparisons of contact resistance and bed resistance were made at conditions where interelectrode resistance is not changing rapidly with current, the comparisons are somewhat suspect because they were not made at the same current density.

Variation along electrode length

Several runs were made at room temperature in a 6 in. Plexiglas column to determine how the contact resistance varied along the center electrode surface. The bed consisted of -48/+65 Tyler mesh size calcined coke with a 19 in. fluidized bed height. A 1/4 in. wide uninsulated band of the 1 in. diameter carbon center electrode surface was exposed at several points along the electrode length from the tip of the electrode to a point 16 in. above the tip. A 16 in. length of brass screen attached to the inside of the column wall was used as the other electrode.

The measured interelectrode resistance was plotted versus bed current with relative velocity as a parameter at each

electrode position. The current and relative velocity ranges used in all runs were 0 to 100 ma. and 1.57 to 3.16, respectively, the bed resistance was calculated by the restricted bed method. The contact resistance between the center electrode and the bed was then determined by difference and was calculated for a particular current level and relative velocity. The results of this calculation showed that the contact resistance dropped sharply immediately above the electrode tip and then rose again several inches from the tip--the point of increase depending upon the relative velocity through the bed (Figures 47 and 48). This dependence on velocity suggests a possible correlation of contact resistance with the pattern of gas flow along the electrode.

For all three velocities, the contact resistance was a minimum at the highest current level used and a maximum at the lowest level. The greatest variation of contact resistance with length occurred near the tip of the electrode and near the top of the bed. The sharp decrease in contact resistance over a short electrode length near the tip is evident in all figures and was previously noted. However, Figure 48 shows rapid variation of contact resistance with length near the upper part of the bed at low bed currents. In the center part of the electrode (especially at the higher bed currents) contact resistance variation with length was much less severe than at the ends.

Figure 47. Contact resistance versus distance along center electrode

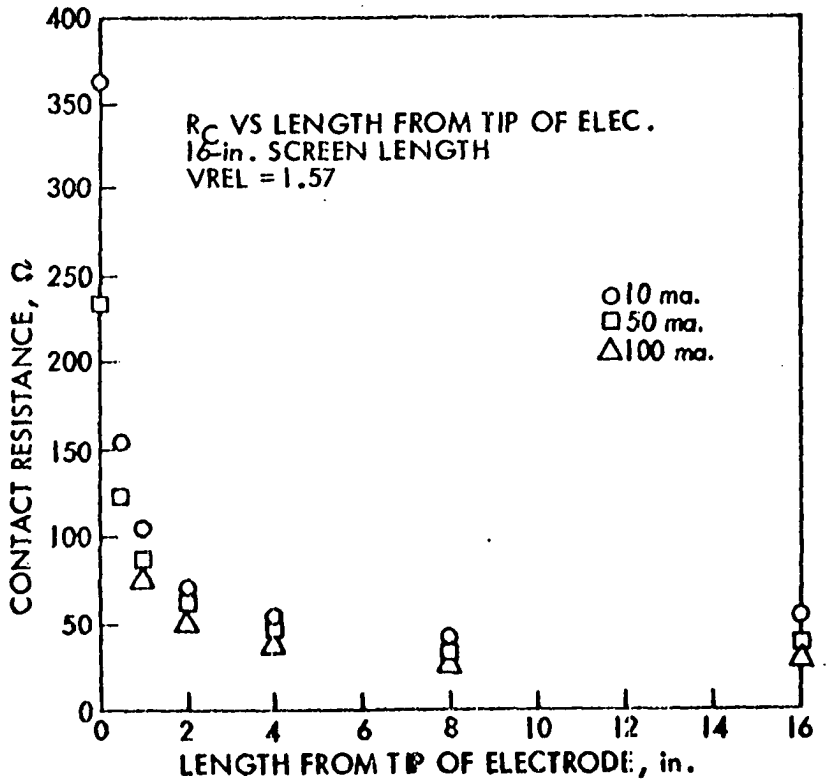
R_C VS LENGTH FROM TIP OF ELEC.
16-in. SCREEN LENGTH
VREL = 1.57
○ 10 ma.
□ 50 ma.
△ 100 ma.
CONTACT RESISTANCE, Ω
LENGTH FROM TIP OF ELECTRODE, in.
400
350
300
250
200
150
100
50
0
0
2
4
6
8
10
12
14
16

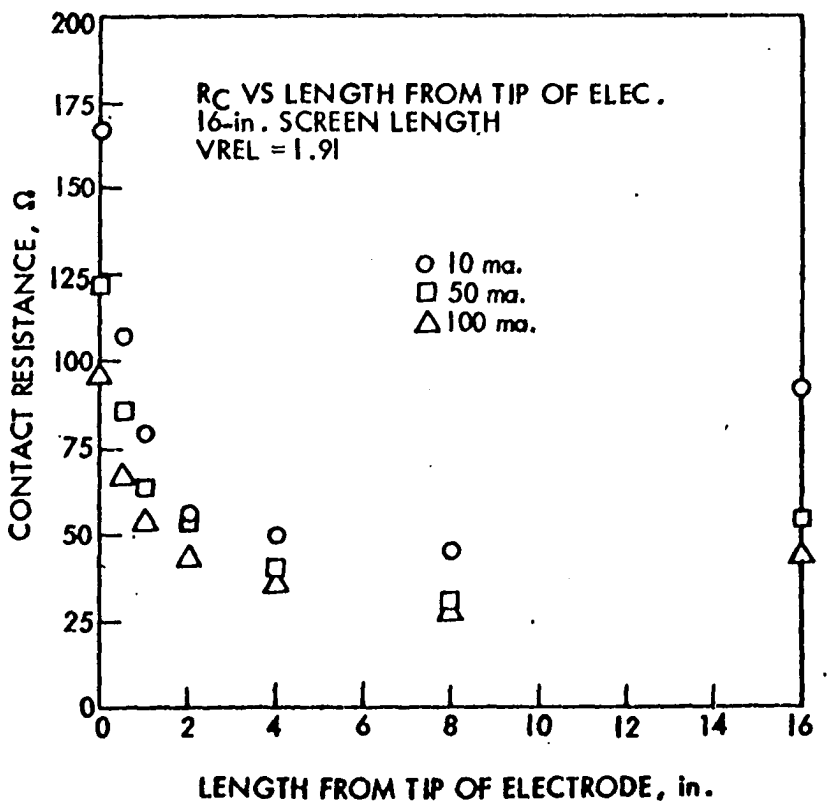
R_C VS LENGTH FROM TIP OF ELEC.
16-in. SCREEN LENGTH
VREL = 1.91
○ 10 ma.
□ 50 ma.
△ 100 ma.
CONTACT RESISTANCE, Ω
LENGTH FROM TIP OF ELECTRODE, in.
200
175
150
125
100
75
50
25
0
0
2
4
6
8
10
12
14
16

Figure 48. Contact resistance versus distance along center electrode

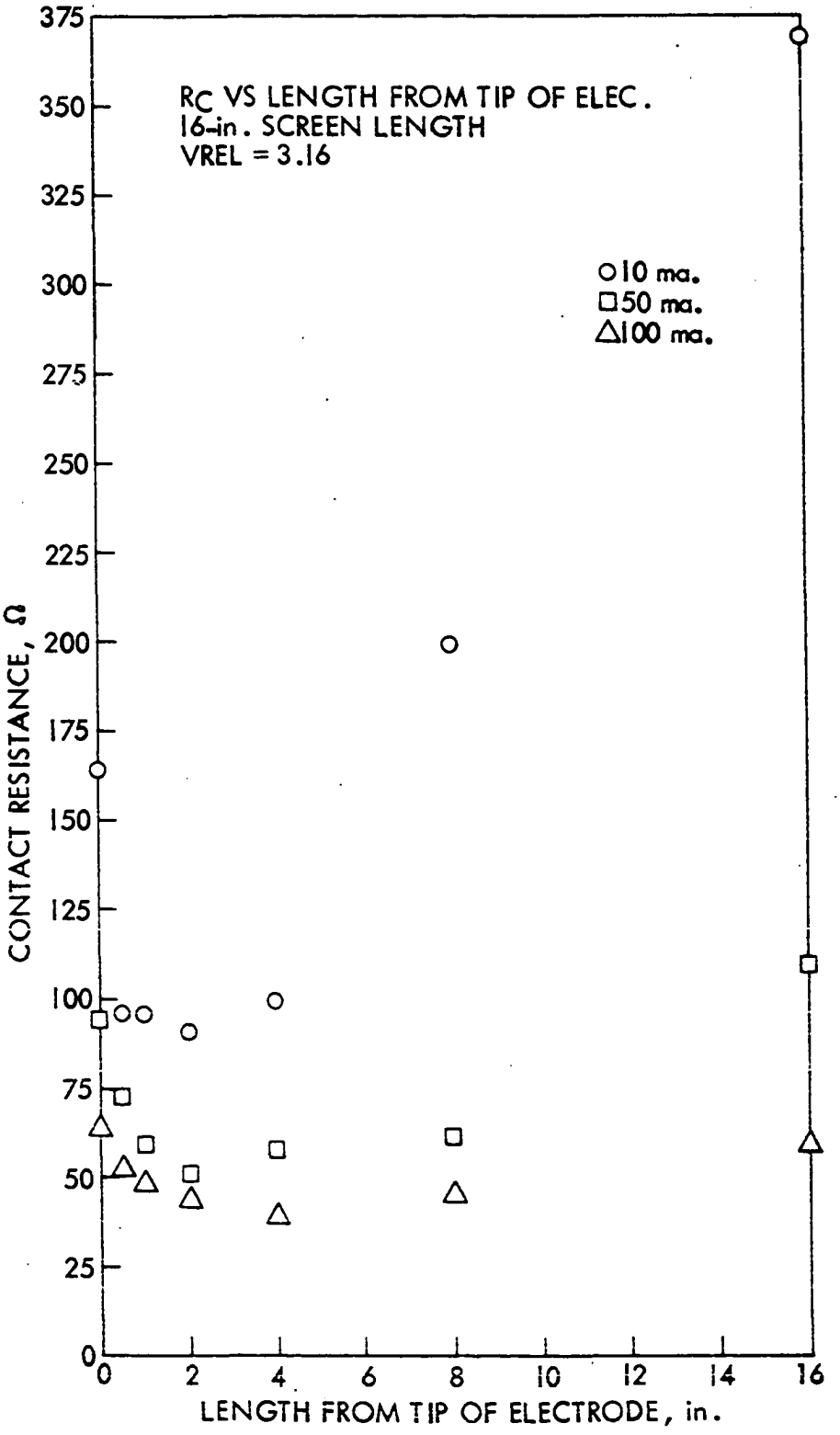
RC VS LENGTH FROM TIP OF ELEC.
16-in. SCREEN LENGTH
VREL = 3.16
○10 ma.
□50 ma.
△100 ma.
CONTACT RESISTANCE, Ω
LENGTH FROM TIP OF ELECTRODE, in.
375
350
325
300
275
250
225
200
175
150
125
100
75
50
25
0
0
2
4
6
8
10
12
14
16

Statistically designed parameter study

A statistically designed experiment was constructed to test the effect of several variables on contact resistance. In this experiment the effects of electrode shape, relative gas velocity, current density, and the longitudinal position of the uninsulated portion of the center electrode on contact resistance were measured. The experiment was carried out in a 6 in. diameter Plexiglas column with -48/+65 Tyler mesh calcined coke as the bed material. A fluidized bed depth of 16 in. was used. A 1 in. diameter carbon center electrode was used with a 16 in. long brass-screen outer electrode. Four electrode shapes (Figure 49), three levels of current density (10, 40, and 80 ma/sq. in.), and three levels of relative velocity (2, 3, and 4 times incipient fluidization velocity) were used in the experiment. In addition, an uninsulated area (0.785 sq. in.) was exposed at five positions for each electrode shape: the tip and then 1/2, 2, 4, and 10 in. above the tip of the electrode. The tip and the 1/2 and 2 in. exposed positions are shown as positions 1, 2, and 3, respectively in Figure 49.

The experiment was based upon a split plot type of statistical design. In this design the four variables were divided into two categories:

(1) those which involved a column set-up to change, and

(2) those which did not involve a set-up to change.

Electrode shape and the position of the uninsulated portion of the center electrode fell into category 1, while current

Figure 49. Electrode shapes and first three positions used in designed parameter study

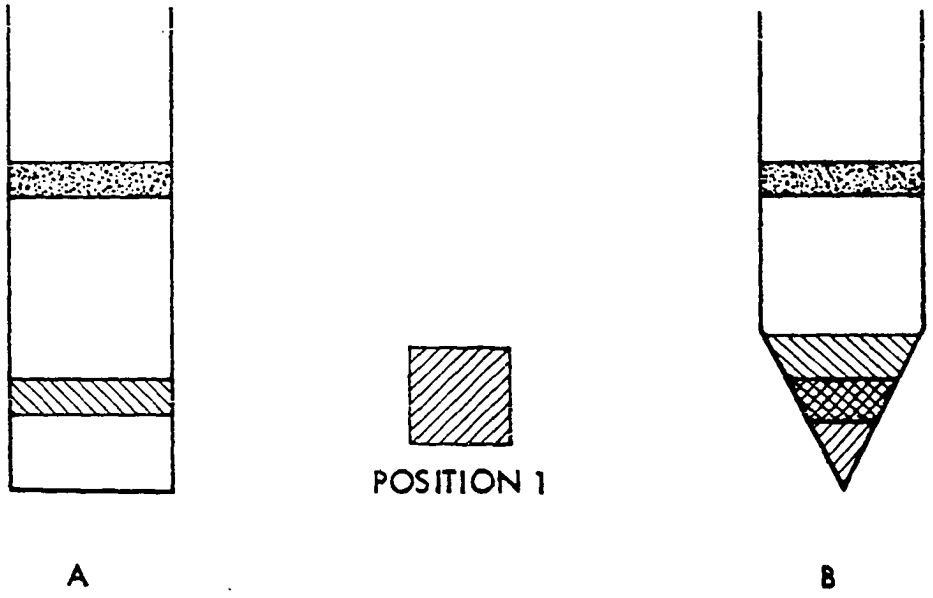
POSITION 1
A
B
POSITION 2
POSITION 3
C
D

density and relative velocity were in category 2. Therefore, the various combinations of current density and relative velocity were randomized for each set-up. The order of the set-ups was also randomized. Two replications were used in the experiment.

The total interelectrode resistance for each set-up was measured experimentally across the test cell. The bed resistance for each particular combination of shape, velocity, and position was then calculated using the field theory technique. The bed resistance was then subtracted from the interelectrode resistance giving the contact resistance. Again, the resistivity of the bed was assumed to be uniform throughout the bed.

The total variation among the contact resistances was partitioned according to the different sources by an analysis of variance technique. The analysis of variance was carried out using the Aardvark library computer program developed by the Iowa State University Computation Center. The computer output is shown in Table 5.

The four variables--shape, position, velocity, and current density--are designated by S, P, V, and D, respectively, in Table 5. The corresponding interactions between the four variables are shown by combining the letters corresponding to the variables. One asterisk by the F value in the table means that the effect of the parameter or interaction associated with it is significant at the 5% level (i.e., 95 times out of 100

Table 5. Analysis of variance for designed parameter study of contact resistance

Variation due to	Degrees of freedom	Mean square	Experimental F	Tabulated F (1%)	(5%)
Shape (S)	3	12,756.012	0.201	5.01	3.13
Position (P)	4	261,285.000	4.108*	4.50	2.90
SxP	12	10,431.598	0.164	3.30	2.31
Error A	19	63,609.734			
Velocity (V)	2	27,103.828	4.769**	4.73	3.05
Current density (D)	2	110,080.938	19.370**	4.73	3.05
SxV	6	10,356.165	1.822	2.97	2.15
PxV	8	131,456.125	23.131**	2.61	1.99
SxD	6	2,812.492	0.499	2.97	2.15
PxD	8	30,406.719	5.350**	2.61	1.99
VxD	4	26,750.141	4.707**	3.42	2.42
SxPxD	24	2,189.935	0.385	1.89	1.58
SxPxV	24	3,942.669	0.694	1.89	1.58
SxVxD	12	1,292.591	0.227	2.29	1.81
PxVxD	16	10,726.824	1.888*	2.10	1.70
SxPxVxD	48	1,202.780	0.212	1.65	1.42
Error B	180	5,683.035			

*Significant at 5% level.

**Significant at 1% level.

one can be confident that the effect or interaction is significant). Significance means that the variation in the data caused by the particular main effect or interaction is greater than that due to chance alone. Two asterisks designates that the effect or interaction is significant at the 1% level.

From Table 5, the following effects and interactions are significant at the 5% level: P, V, D, PV, PD, VD, and PVD. At the 1% level only V, D, PV, PD, and VD are significant. Thus, it would appear that contact resistance between the center electrode and the bed varies most strongly with relative velocity, current density, and the interactions of (1) position and velocity, (2) position and current density, and (3) velocity and current density. Electrode shape did not appear to be significant in this experiment. This experiment essentially confirmed the results of the previous section.

Contact resistivity

The contact resistance at the center electrode appears to be inversely proportional to the electrode area available for current flow. This can be seen from Figure 50. In this figure, contact resistance was calculated by the field theory method at a bed current of 10 ma. for configurations II, III and IV in Figure 20, and then plotted versus the reciprocal of the exposed electrode area. This lends support to the assumption that the contact resistance at the wall electrode is negligible compared to the contact resistance at the center

Figure 50. Contact resistance versus the reciprocal of exposed center electrode area at a bed current of 10 ma.

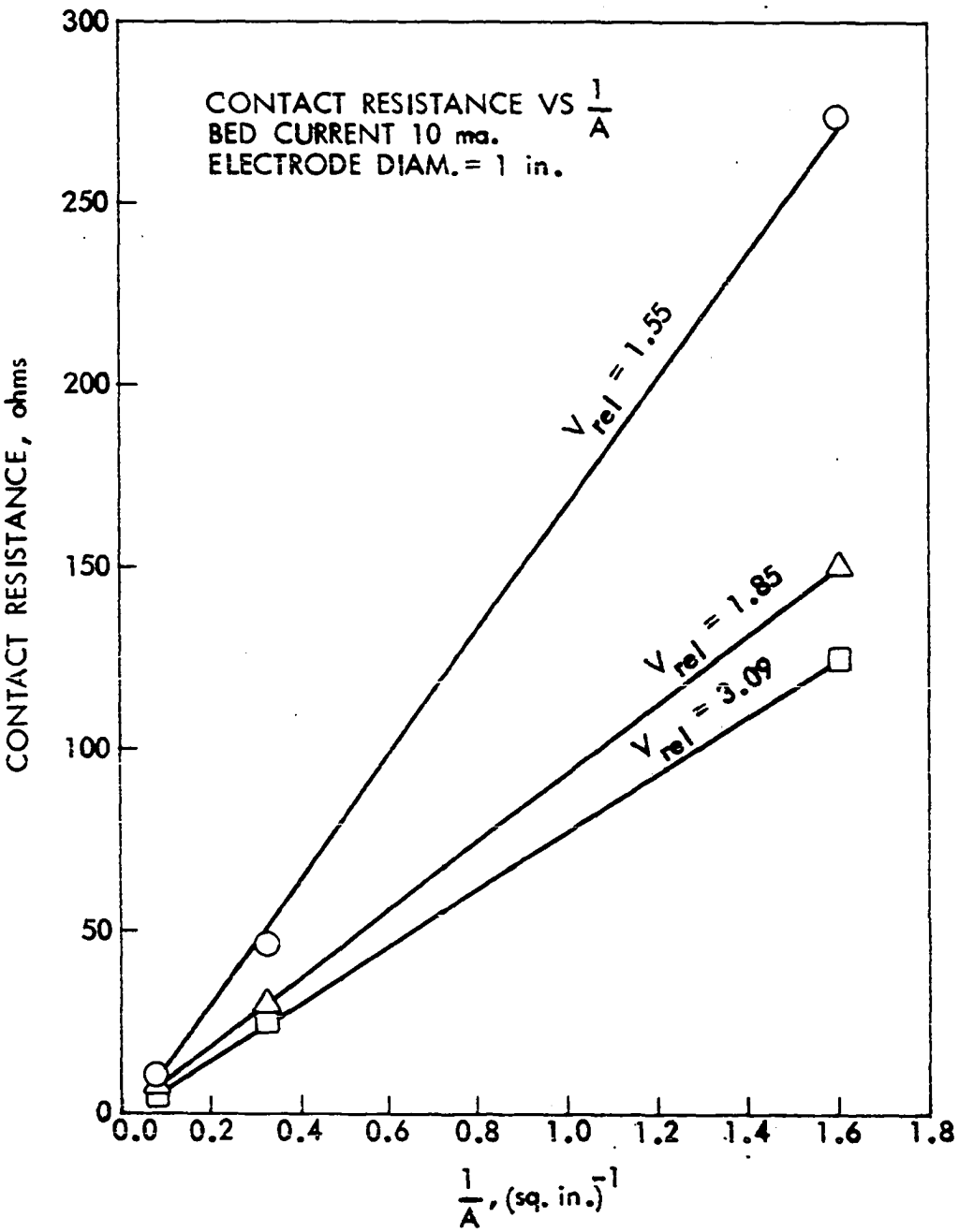
CONTACT RESISTANCE VS $\frac{1}{A}$
BED CURRENT 10 ma.
ELECTRODE DIAM. = 1 in.
$V_{rel} = 1.55$
$V_{rel} = 1.85$
$V_{rel} = 3.09$
CONTACT RESISTANCE, ohms
300
250
200
150
100
50
0
0.0
0.2
0.4
0.6
0.8
1.0
1.2
1.4
1.6
1.8
$\frac{1}{A}$, (sq. in.)$^{-1}$

electrode. This inverse dependence of contact resistance on area can be written mathematically as:

$$R_c = \frac{\rho_c}{A} \tag{43}$$

where R_c is the contact resistance at the center electrode, A is the area of the center electrode available for current flow, and ρ_c is a constant of proportionality which can be thought of as a pseudo-contact resistivity.

Knowing values of both contact resistance and area, values of contact resistivity could be calculated. Table 6 lists values of contact resistivity for varying electrode diameters and materials obtained at maximum bed current in the inter-electrode resistance versus current density runs. In general, contact resistivity increases as relative gas velocity decreases. For the case of the brass and steel electrodes having the same electrode area exposed, contact resistivity is nearly the same for both electrodes. This gives some indication that perhaps contact resistivity is not dependent upon electrode material. However, contact resistivity appears to change rapidly with area. The larger the area, the larger the contact resistivity.

Arcing Determination

An experiment was conducted to determine whether arcing or sparking could be visually observed near the tip of a small electrode inserted in a fluidized bed of calcined coke. In

Table 6. Contact resistivity values for different electrode diameters and materials calculated at maximum bed current

Electrode	Diameter, in.	Exposed area, sq. in.	Maximum current, ma.	V_{rel}	R_c, ohms	ρ_c, ohm-in.^{2}
Tungsten	1/25	0.0314	130	4	65	2.0
				3	60	1.9
				2	109	3.4
Brass	1/16	0.0491	100	4	85	4.2
				3	110	5.4
				2	149	7.3
Steel	1/16	0.0491	105	4	85	4.2
				3	100	4.9
				2	149	7.3
Carbon	1	0.785	120	4	50	39
				3	80	63
				2	94	74
Carbon	1	34.5	130	3.16	3.75	130
				1.91	5.6	194
				1.57	5.6	194

this experiment a small steel rod with a diameter of 1/16 in. was inserted through the wall of a 6 in. diameter Plexiglas fluidization column approximately 1/16 in. into the bed. The other electrode was a 1 in. diameter center carbon electrode of which only the bottom inch was uninsulated. It was thought that the small wall electrode size would concentrate the voltage gradient sufficiently so that arcing would occur near its tip. The shallow insertion into the bed would make it possible to visually detect arcing occurring at the electrode tip.

Direct current was passed between the two electrodes with the bed fluidized. No arcing was observed at the small electrode tip over a voltage range of 0 to 15 volts at relative velocities of 2 to 4. The DC voltage supply was then replaced with an AC variable transformer to provide a greater voltage range. The voltage applied across the electrodes was then varied from 0 to 80 volts at various relative gas velocities in the fluidized region. At lower voltages no arcing or sparking was observed, but with an applied voltage of 15 to 20 volts an intermittent sparking was observed near the tip of the wall electrode. At higher voltages the sparking became steady. Table 7 shows that the sparking voltage was slightly dependent upon relative gas velocity.

In the fluidized region the system generated radio noise at all voltage levels--even those below the sparking voltage. This noise was detected by holding a small radio near the column. Moving the radio near the column increased the sound and moving the radio away caused a corresponding decrease in sound. Noise level was also correlated with voltage changes.

In the fixed bed a somewhat different phenomenon was observed. A red glow appeared near the small electrode tip in the unfluidized bed at voltage levels producing sparking in the fluidized bed. However, no radio noise was associated with the glow. Also, the wall area adjacent to the small steel electrode became very hot if the glow was maintained for over

Table 7. Dependence of the onset of sparking on relative gas velocity and applied voltage

Volts	Relative gas velocity		
	2	3	4
5	None	None	None
10	None	None	None
15	None	Sparking	Sparking
20 or more	Sparking	Sparking	Sparking

a few seconds duration. Upon inspection of the Plexiglas column wall it was discovered that a hole had melted through the column wall around the wall electrode. Because of the heat associated with the glow and the absence of radio noise, it was surmised that the glow was the result of resistance heating of the bed near the outer wall electrode and was not related to the arcing phenomenon.

Region of Operation

An experiment was conducted to determine whether the electrofluid bed was operating in the Ohm's Law, intermediate, or arcing region in a high temperature electrofluid reactor. The reactor used for this purpose was a 4 in. inside diameter 446 stainless steel reactor used by Knowlton (29) and Ballain (1).

An electrical schematic of the experimental circuit used to analyze the region of operation is shown in Figure 14. A shunt was placed in the circuit between the Variac and the reactor. The wave form representative of the voltage drop across the shunt was then displayed on one beam of a dual beam oscilloscope. This waveform has the shape of the current waveform since:

$$V_{shunt} = R_{shunt} I .$$

The voltage waveform representative of the voltage drop across the bed was displayed on the second beam of the scope. By using the X-Y function switch of the scope, the current through the bed was plotted versus the voltage drop across the bed on the scope screen. Photographs of both types of scope displays were taken and a representative picture is shown in Figure 15.

The experiment was carried out at relatively constant temperature (1600°F) by using external heating in conjunction with the internal power. Voltage across the bed was varied from 25 to 150 volts. Bed current varied from 3 to 70 amps.

The shapes of the current and voltage waveforms did not change during the experiment. Also, the voltage versus current plot was essentially the same at all voltages. As can be seen in Figure 15, the voltage across the bed is the familiar sinusoidal AC waveform. The current waveform, however, appears to resemble a waveform intermediate between a sawtooth and a sinusoidal waveform.

The X-Y plot shows a loop type of configuration. Operation in the Ohm's Law region would have resulted in a straight line with a slope of 45°, and operation in the arcing region would have resulted in a horizontal straight line. Therefore, it was concluded that the region of operation was the intermediate region. This agrees with the results of Lee *et al.* (32).

ANALYSIS OF DIFFERENT ELECTRODE CONFIGURATIONS

Three different electrode configurations for commercial electrofluid reactors were analyzed using field theory. In each case Laplace's equation was solved numerically for values of the potential as a function of position, and then an interpolation scheme was used to determine lines of constant potential. The orthogonal solution of Laplace's equation was then solved and interpolated to obtain lines which bounded regions of constant current flow. The potential and flux lines were then superimposed, the superposition resulting in a field of curvilinear squares (Figures 51 and 52).

The lines for the first electrode configuration, which was concentric in nature, are shown in Figure 51. This configuration consisted of a 1 in. diameter center electrode immersed in a 16 in. deep bed to a depth of 10.75 in. The bed was contained in a 6 in. diameter column in which the outer wall served as the other electrode. Configuration 2, shown in Figure 52, also had the concentric electrode geometry, and differed from configuration 1 only in center electrode diameter (1.5 in.) and immersion (6.5 in.). Configuration 3 was entirely different in that the wall was not used as an electrode. Instead, two center electrodes 1-1/2 in. in diameter were used, one entering from the bottom (Figure 52). Again, a 6 in. diameter column was used with a bed height of 16 in. Both the top and bottom electrodes were immersed in the bed a distance of 4 in.

Figure 51. Constant potential and current flux lines for 1 in. diameter center electrode. Immersion = 10.75 in. (Config. 1)

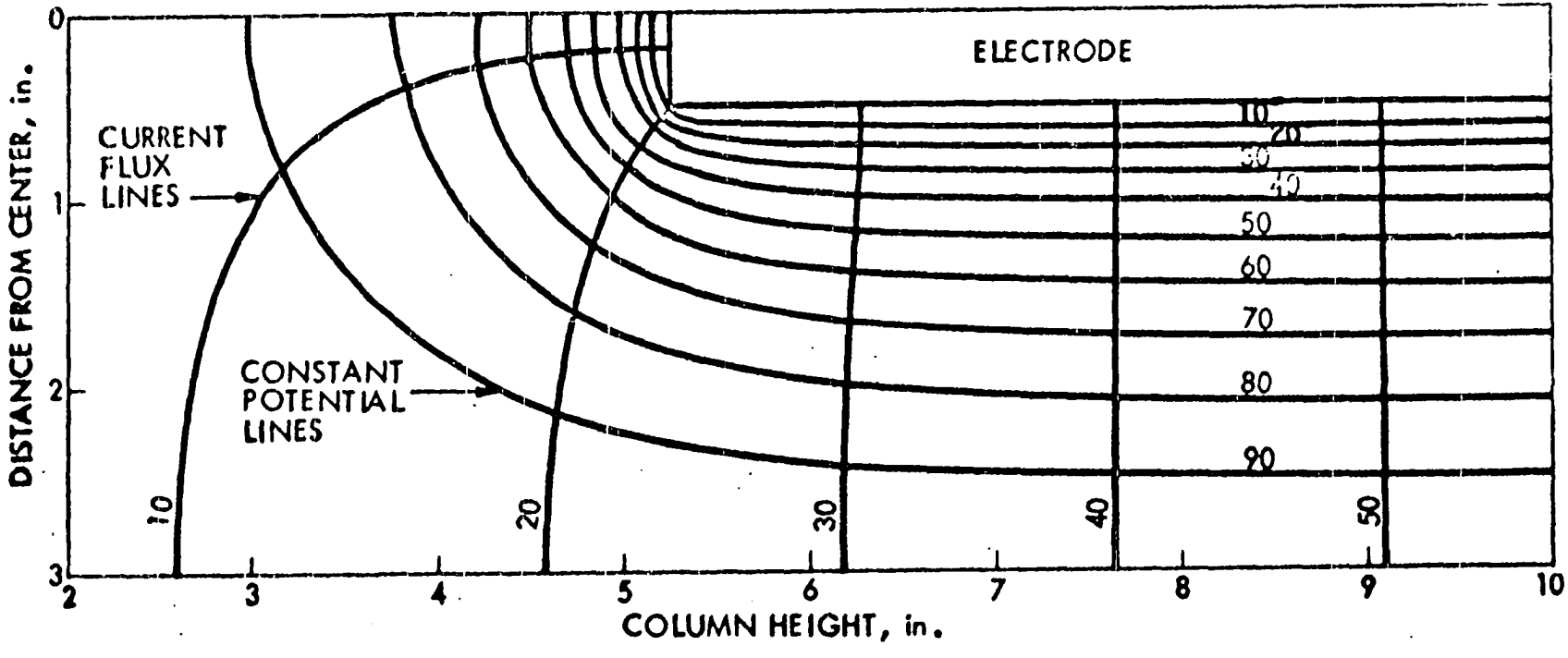
ELECTRODE
CURRENT FLUX LINES
CONSTANT POTENTIAL LINES
10
20
30
40
50
60
70
80
90
DISTANCE FROM CENTER, in.
COLUMN HEIGHT, in.
0
1
2
3
2
3
4
5
6
7
8
9
10

Figure 52. Constant potential and current flux lines for:

Config. 2. 1-1/2 in. diameter center electrode.
Immersion - 6.5 in.

Config. 3. end-to-end electrode configuration.
Electrode diameter = 1.5 in.
Immersion = 4 in.

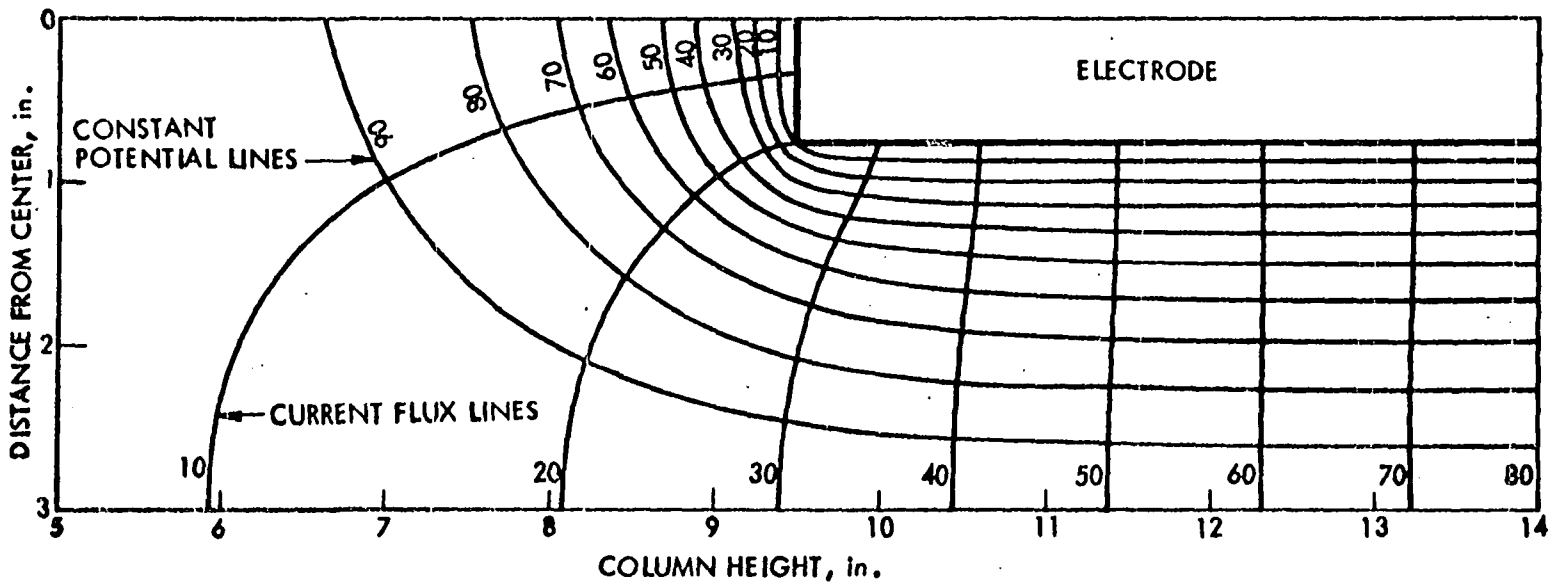
ELECTRODE
CONSTANT POTENTIAL LINES
CURRENT FLUX LINES
DISTANCE FROM CENTER, in.
COLUMN HEIGHT, in.
0
1
2
3
5
6
7
8
9
10
11
12
13
14
10
20
30
40
50
60
70
80

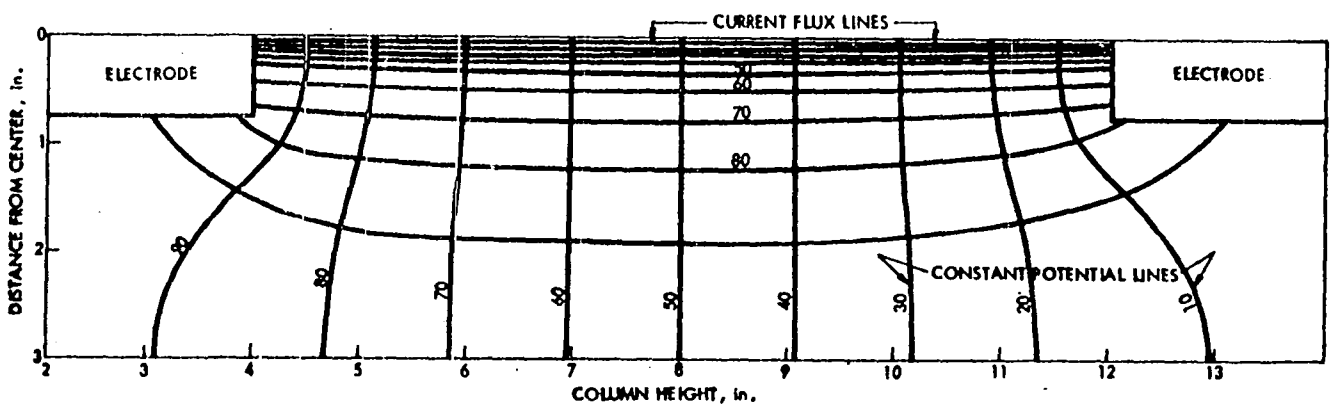
CURRENT FLUX LINES
ELECTRODE
ELECTRODE
CONSTANT POTENTIAL LINES
DISTANCE FROM CENTER, in.
COLUMN HEIGHT, in.
0
1
2
3
2
3
4
5
6
7
8
9
10
11
12
13
10
20
30
40
50
60
70
80

Bed Resistance

The bed resistance of each configuration was calculated by the field theory method. The calculated resistances for all three configurations are shown in Table 8 for a bed resistivity of 275 ohm-in. Of course, resistances for other bed resistivities can be obtained by multiplying the tabulated value of bed resistance by the ratio $\rho/275$ where ρ is the value of the other resistivity.

Table 8. Bed resistance for different electrode configurations based on a bed resistivity of 275 ohm-in.

Configuration	Bed resistance, ohms
1	6.3
2	6.5
3	43.2

The resistances of configurations 1 and 2 are about the same. Although the resistance of configuration 2 would be higher than configuration 1 because of its shallower center electrode immersion, this seems to be balanced by the effect of the larger electrode diameter used in configuration 2. The resistance of configuration 3 is much higher than the resistance of the other configurations apparently because of the greater separation between the electrodes.

Current Density

Data from the computer print-out on current flux, or an analysis of Figures 51 and 52 allowed the current density to be calculated at various points along the electrode. The current densities along the center electrodes for all three configurations are shown as a function of distance from the tip of the electrode in Figure 53. A total current flow of 30 amps was assumed in the calculation of the current density. Figure 53 shows that the current density at the tip in the end-to-end configuration is much higher than the tip current density of the two concentric configurations. In all cases the current density at the electrode tip was much greater than along the electrode length.

Bed Voltage Gradients

The field plots (Figures 51 and 52) also provide information about the relative magnitudes of the voltage gradients for the three electrode configurations. The plots of configurations 1 and 2 are, of course, very similar and show that the constant potential lines are grouped more closely near the center electrode than the wall. For example, at the bottom corner of the center electrodes of configurations 1 and 2 where the gradient appears to be the highest, 50% of the voltage drop occurs in about 20 to 25% of the total distance between the center and wall electrodes. This type of voltage gradient

Figure 53. Current density along electrode for end-to-end and concentric electrodes

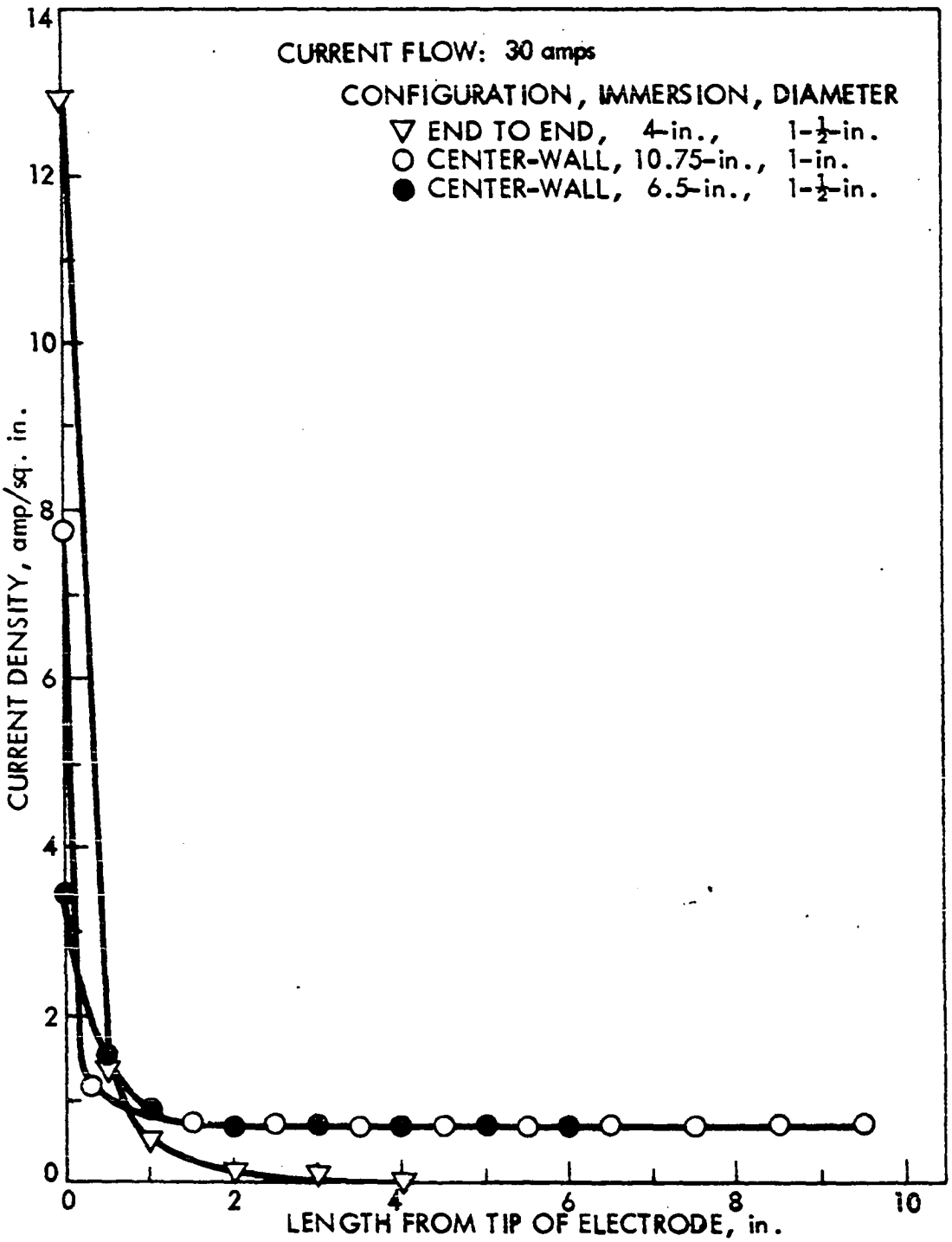
CURRENT FLOW: 30 amps
CONFIGURATION, IMMERSION, DIAMETER
▽ END TO END, 4-in., 1-½-in.
○ CENTER-WALL, 10.75-in., 1-in.
● CENTER-WALL, 6.5-in., 1-½-in.
CURRENT DENSITY, amp/sq. in.
LENGTH FROM TIP OF ELECTRODE, in.
0
2
4
6
8
10
12
14

contrasts with the gradient of configuration 3 where 50% of the voltage drop occurs in 50% of the distance between the two electrodes. Thus, the end-to-end electrode configuration appears to give lower voltage gradients throughout the bed than the concentric electric configuration. Assuming that arcing between the electrode and the bed occurs chiefly because of a high voltage gradient, arcing would occur more readily with the concentric electrode configuration than with the end-to-end configuration.

Heat Generation in the Bed

Again, by analyzing the field plots of the electrode configurations, it is possible to roughly calculate where most of the power would be dissipated in a high temperature electrofluid reactor bed. Since each curvilinear square has the same current flow through it and is bounded by equal voltage drops, the power dissipated in each square is the same. Therefore, the power dissipation (or equivalently the heat generation) is highest where the concentration of curvilinear squares is greatest. In configurations 1 and 2 this region of high power dissipation is near the tips of the center electrodes. For these configurations a rough calculation showed that about 15% of the total power dissipation in the bed occurs in 1% of the bed volume immediately surrounding the electrode tip. The high heat generation near the tip may partially explain why the tips

of several electrodes have melted in previous high temperature runs utilizing concentric electrode configurations (29).

In configuration 3, most of the heat generation appears to lie in a cylinder in the center of the bed extending from one electrode to the other. A rough calculation showed that 50% of the power is dissipated in this cylinder which constitutes less than 6% of the bed volume.

SUMMARIZING DISCUSSION

One of the primary contentions made in the investigation was that the interelectrode resistance is composed of several components, i.e.,

$$R_i = R_c + R_w + R_b \tag{44}$$

where R_i is the interelectrode resistance, R_c is the contact resistance between the center electrode and the bed, R_w is the contact resistance between the brass-screen electrode and the bed and R_b is the bed resistance. It was further assumed that contact resistance in general was inversely proportional to area. Because of this assumed area dependency, the contact resistance between the center electrode and the bed was taken to be much greater than the contact resistance between the brass-screen wall electrode and the bed because of the far greater area of the wall electrode. With this assumption Equation 44 was written:

$$R_i = R_c + R_b \quad . \tag{45}$$

Although the investigation did not prove any of the above assumptions conclusively, it did lend some support to them.

First, interelectrode resistance was found to decrease with increasing current density in all runs. However, bed resistivity (or equivalently, bed resistance) was not found to have a dependence upon current density. This suggested that

the interelectrode resistance was composed of two components---one varying with current density (contact resistance) and one not dependent upon current density (bed resistance).

Secondly, both the restricted bed and the Laplacian field theory models gave values for the bed resistance which were lower than values for the interelectrode resistance at all current densities. This result also indicated that interelectrode resistance was composed of bed and contact resistance components.

Contact resistance was found to be larger than bed resistance at all current densities and gas velocities used in the investigation. Although Glidden (9) did not find this to be the case in his room temperature work, Shine (43) reported that contact resistance was the greater component of interelectrode resistance in a high temperature, industrial scale electrofluid bed reactor. Furthermore he stated that the bed resistance component was usually negligible compared to the contact resistance. Although the results reported by Shine agree more with the results of this investigation than the findings of Glidden, it must be noted that the former's results were obtained using an end-to-end electrode configuration using multiple electrodes.

The assumption that contact resistance is inversely proportional to the electrode area available for current flow was not conclusively proven. The results in Figure 50 lend

extremely strong support to this assumption. However, the values of contact resistance in this figure were obtained for different electrode exposures near the tip of the electrode. At this point on the electrode contact resistance varies extremely rapidly with position (Figures 47 and 48). It would be more conclusive proof if contact resistance were shown to be inversely proportional to area using contact resistance values at a different electrode position where contact resistance does not vary as rapidly with position.

CONCLUSIONS AND RECOMMENDATIONS

1. In a fluidized bed of calcined coke particles in which current is passed between concentric electrodes, the interelectrode resistance of the bed appears to decrease with an increase in current density and with gas velocity. This decrease in interelectrode resistance does not appear to depend upon the composition of the center electrode.
2. Reversing the direction of direct current flow through a bed of conducting calcined coke particles did not appear to have an effect upon interelectrode resistance. It also appears that alternating current does not affect interelectrode resistance differently than direct current.
3. Over the current density range investigated, there appears to be no trend of bed volume resistivity with increasing bed current density in the fluidized or the unfluidized bed.
4. Column diameter affects bed resistivity. The larger the column diameter, the lower the bed resistivity at a particular velocity. This supports the data of Jones (24).
5. The Laplacian field model proposed for the fluid bed of calcined coke appears to accurately predict the voltage potential distribution throughout the bed with the exception of the bed area immediately under the electrode tip. This implies that the resistivity of a fluidized bed of calcined coke is homogeneous with respect to the

distribution of voltage potential throughout the bed.

6. Contact resistance appears to be the larger component of the interelectrode resistance components, and decreases with increasing current density.
7. Contact resistance is not homogeneously distributed over the center electrode surface, but varies along the length of the electrode. The contact resistance is high at the tip of the electrode, decreases to a minimum value at a point several inches above the tip and then increases again.
8. Contact resistance between the center electrode and the bed varies with current density, relative velocity, and the interactions of (1) relative velocity and current density, (2) longitudinal position of exposed center electrode area and relative velocity, and (3) longitudinal position of exposed center electrode area and current density. Contact resistance did not appear to vary significantly with electrode shape.
9. Current transfer by arcing can occur in a fluidized bed of conducting particles. The arcing region appears to be limited to an area near an electrode producing a high voltage gradient. Little dependence of arcing on gas velocity was noted.
10. An analysis of electrode configurations based on the use of the Laplacian field model showed that an end-to-end electrode configuration appears to have a more uniform

voltage distribution throughout the bed than a concentric electrode configuration. The end-to-end configuration tends to concentrate current flux to a greater extent than the concentric configuration. In an end-to-end configuration most of the heat generation is concentrated in the bed region directly between the two electrodes. In a concentric electrode configuration the heat generation is concentrated in the region immediately surrounding the center electrode tip.

11. In order to calculate the bed resistance for an industrial scale, high temperature, electrofluid bed reactor, it is necessary to know a value for bed resistivity obtained at the reactor operating conditions. Therefore, further investigation of bed resistivity should be made at elevated temperatures and still larger column diameters.
12. It is recommended that further investigation be made to determine more conclusively whether contact resistance is inversely proportional to electrode area. Electrode areas should be selected where contact resistance is not changing rapidly with electrode position.
13. It is recommended that an investigation be made to determine whether arcing is detrimental to the operation of an electrofluid bed.

NOMENCLATURE

A	area, sq. in.
a	shape factor
C	capacitance of system, microfarads
C_u	capacitance of a curvilinear square, microfarads
D	radius of test cell, in.
D_i	average diameter of particles in a particular size fraction, in.
D_p	average particle diameter of mixture, in.
d	density of bed particle, lb./cu. ft.
I	current, ma. or amps
l	length, in.
m	mass
N	total number of particles
n_i	number of particles between any two mesh sizes
n_1	length of wall electrode above uninsulated portion of center electrode, in.
n_2	length of wall electrode below uninsulated portion of center electrode, in.
R	resistance, ohms
R_b	bed resistance, ohms
R_c	center electrode contact resistance, ohms
R_i	interelectrode resistance, ohms
R_w	wall electrode contact resistance, ohms
r	radius variable

r_o radius of center electrode, in.

V voltage, volts

Z uninsulated electrode length, in.

z cylindrical coordinate variable

ε dielectric constant of bed material

Θ cylindrical coordinate variable

ρ volume resistivity of bed material, ohm-in.

ρ_C pseudo-contact resistivity, ohm-sq. in.

ρ_M volume resistivity of bed material at minimum point in ρ versus velocity curve, ohm-in.

σ_S volume resistivity of unfluidized bed, ohm-in.

σ_P standard deviation of particle size

ϕ potential function

LITERATURE CITED

1. Ballain, M. D. Electrical properties of an electrothermal fluidized bed. Unpublished M.S. thesis. Library, Iowa State University, Ames, Iowa. 1969.

2. Beeson, J. L. Continuous electrofluid reactor for coal char gasification. Unpublished M.S. thesis. Library, Iowa State University, Ames, Iowa. 1969.

3. Ciborowski, J. and Paderewski, M. Direct heating of a fluidized phase by electric current. International J. Heat Mass Transfer 9, No. 11: 1255-1267. 1966.

4. Ciborowski, J. and Paderewski, M. Electrical resistivity of a fluidized bed. Chem. Stosowana, Ser. B, 2, No. 4: 345-358. 1965. Original not available; abstracted in Chem. Abstracts 64: 10783b. 1966.

5. Ciborowski, J. and Paderewski, M. Heating of a fluidized bed by electric current. Chem. Stosowana, Ser. B, 1, No. 2: 209-218. 1964. Original not available; abstracted in Chem. Abstracts 63: 9483a. 1965.

6. Ciborowski, J. and Paderewski, M. Influence of temperature on the electrical conductivity of a fluidized bed. Chem. Stosowana, Ser. B, 3, No. 1: 27-37. 1966. Original not available; abstracted in Chem. Abstracts 65: 1800d. 1966.

7. Damn, F. C. Electrical resistivity of fluidized beds of conducting and non-conducting particles. Report of an investigation performed under the Undergraduate Research Participation Program of the National Science Foundation. Chemical Engineering Department, Iowa State University, Ames, Iowa. May 24, 1965.

8. Davidson, J. F. and Harrison, D. Fluidized particles. University Press, Cambridge, Mass. 1963.

9. Glidden, H. J., Jr. Electrode contact resistance in a fluidized bed. Unpublished M.S. thesis. Library, Iowa State University, Ames, Iowa. 1967.

10. Goldberger, W. M., Hanway, J. E., Jr. and Langston, B. G. The electrothermal fluidized bed. Chem. Eng. Prog. 61, No. 2: 63-67. 1965.

11. Goldschmidt, D. and Le Goff, P. Electrical methods for the study of a fluidised bed of conducting particles. Trans. Instn. Chem. Engrs. 45: 196-204. 1967.

12. Goldschmidt, D. and Le Goff, P. Resistance electrique des lit fluidises. I. Resistances moyennes de grains conducteurs fluidises par air: resultats preliminaries. Chem. Eng. Sci. 18: 805-806. 1963.

13. Goucher, F. S. The carbon microphone: an account of some researches bearing on its action. Franklin Institute Journal 17: 407-442. 1934.

14. Graham, W. Electrical conductivity of fluidized beds. National Research Laboratories (Division of Applied Chemistry, Ottawa, Canada) Progress Report C-60-58P. 1958.

15. Graham, W. and Harvey, E. A. The electrical resistance of fluidized beds of coke and graphite. Canadian J. of Chem. Eng. 43: 146-149. 1965.

16. Grisdale, R. O. The properties of carbon contacts. Journal of Applied Physics 24: 1288-1296. 1953.

17. Holm, R. Electric contacts. Springer-Verlag, Berlin. 1967.

18. Johnson, H. S. Reactions in a fluidized coke bed with self-resistive heating. Canadian J. of Chem. Eng. 39: 145-147. 1961.

19. Johnson, H. S. and Anderson, A. H. Process for the preparation of carbon disulphide and for the desulfurization of coke: assigned to Shawinigan Chemicals Limited, Montreal, Canada. U.S. Patent 3,009,781. November 21, 1961.

20. Johnson, H. S. and Anderson, A. H. Process for the preparation of carbon monoxide: assigned to Shawinigan Chemicals Limited, Montreal, Canada. U.S. Patent 2,921,840. January 19, 1960.

21. Johnson, H. S. and Anderson, A. H. Process for the preparation of hydrocyanic acid: assigned to Shawinigan Chemicals Limited, Montreal, Canada. U.S. Patent 2,948,584. November 1, 1960.

22. Johnson, H. S. and Anderson, A. H. Process for the preparation of titanium tetrachloride: assigned to Shawinigan Chemicals Limited, Montreal, Canada. U.S. Patent 2,948,587. August 9, 1960

23. Johnson, H. S. and Reid, J. Process for the preparation of carbon disulphide: assigned to Shawinigan Chemicals Limited, Montreal, Canada. U.S. Patent 3,034,863. May 15, 1962.

24. Jones, A. L. Electrical resistivity of carbon granules in a fluidized bed. Unpublished Ph.D. thesis. Library, Iowa State University, Ames, Iowa. 1966.

25. Kalinowski, B., Mucha, F. and Wlodarski, R. Generation of high temperatures in a furnace with a fluidized heating resistor. Przemysl Chem. 44, No. 5: 275-279. 1965. Original not available; abstracted in Chem. Abstracts 63: 9474b. 1965.

26. Kalinowski, B. and Wlodarski, R. A fluidized bed, heated directly by electric current, and its potential applications in chemical technology. Przemysl Chem. 44, No. 11: 601-605. 1965. Original not available; abstracted in Chem. Abstracts 64: 4623d. 1966.

27. Kennedy, K. J. Preparation of hydrocyanic acid: assigned to Shawinigan Chemicals Limited, Montreal, Canada. U.S. Patent 3,032,396. May 1, 1962.

28. Kennedy, K. J. and Shine, N. R. Production of hydrogen cyanide: assigned to Shawinigan Chemicals Limited, Quebec, Canada. U.S. Patent 3,097,921. July 16, 1963.

29. Knowlton, T. M. The carbon steam reaction in the electrofluid reactor. Unpublished M.S. thesis. Library, Iowa State University, Ames, Iowa. 1967.

30. Kossman, K. H. Process for heating beds of solid particles spouted with gas: assigned to Shawinigan Chemicals Limited, Montreal, Canada. U.S. Patent 2,968,683. January 17, 1961.

31. Lapidus, Leon. Digital computation for chemical engineers. McGraw-Hill Book Co., New York. 1962.

32. Lee, B. S., Pyrioch, E. J. and Schora, F. C., Jr. The electrical resistivity of a high-pressure fluidized bed. Progress Report. Institute of Gas Technology, Chicago, Illinois. 1968.

33. Leva, Max. Fluidization. McGraw-Hill Book Company, New York, New York. 1959.

34. Miles, C. D. and Stephens, F. M., Jr. Fluidised bed method of producing phosphorous: assigned to FMC Corporation, Princeton, New Jersey. U.S. Patent 3,118,734. January 21, 1964.

35. Moon, P. and Spencer, D. E. Field theory for engineers. D. Van Nostrand Co., New York, New York. 1961.

36. Othmer, D. F., editor. Fluidization. Reinhold Publishing Corp., New York, New York. 1956.

37. Paquet, J. L. and Foulkes, P. B. Calcination of fluid coke in an electrically heated fluidized bed. Can. J. Chem. Eng. 43, No. 4: 94-96. 1965.

38. Reed, A. K. and Goldberger, W. M. Electrical behavior in fluidized beds of conducting solids. Chem. Eng. Prog. 62, No. 67: 71-75. 1966.

39. Rice, C. W. An experimental method of obtaining the solution of electrostatic problems. AIEE Trans. 36, 905. 1917.

40. Schakel, L. L. Electrical resistivity of fluidized beds of conducting and non-conducting particles. Report of an investigation performed under the Undergraduate Research Participation Program of the National Science Foundation. Chemical Engineering Department, Iowa State University, Ames, Iowa. August 14, 1964.

41. Schenck, H. and Wenzel, W. Electrical heating process and apparatus. U.S. Patent 2,978,315. April, 1961.

42. Sevryukov, V. N. and Martyushin, I. G. The total electrical resistance of a fluidized bed of electrically conducting granular material. International Chem. Eng. 8, No. 2: 209-211. 1968.

43. Shine, N. B. Fluohmic process for HCN. Talk delivered at the Third Joint Meeting of the American Institute of Chemical Engineers, San Juan, Puerto Rico, May 17, 1970. Am. Chem. Engr., New York, N.Y. 1970.

44. Wickenden, L. and Okell, S. A. W. Process and apparatus for making decolorizing carbon. U.S. Patent 1,634,478. July 5, 1927.

45. Winkler, F. Production of water gas: assigned to I. G. Farbenindustrie. U.S. Patent 1,857,799. May 10, 1932.

46. Zenz, F. A. and Othmer, D. F. Fluidization and fluid-particle system. Reinhold Publishing Corp., New York, New York. 1960.

ACKNOWLEDGEMENTS

The author wishes to express his appreciation to the following people and organizations:

Dr. Thomas D. Wheelock who first suggested the project and supplied helpful guidance, advice, and assistance.

Dr. A. H. Pulsifer whose timely advice and assistance helped immeasureably.

Dr. David Robb for his expert advice concerning the electrical problems encountered in the investigation.

Dr. David V. Huntsberger for suggesting the statistical design used in the study, and for advice concerning the design.

The laboratory assistants for their time and assistance in gathering data.

The Office of Coal Research, under whose auspices the the investigation was carried out, for providing the impetus and financial support for the investigation.

The Iowa Engineering Research Institute which provided equipment and assisting personnel for the project.

Finally, the author wishes to express his appreciation to his wife for her support and understanding throughout the duration of the project.

APPENDIX A

Sample Computer Program

The computer program on the following pages solves Laplace's equation in cylindrical coordinates numerically to obtain the potential and flux distribution throughout the bed region. The center electrode for this case was a 1 in. diameter carbon rod with a 1/4 in. length exposed at its tip (configuration IV in Figure 20). The outer electrode was a brass-screen attached to the column wall and was 14 in. long. The top of the brass-screen electrode coincided with the top of the bed which was 16 in. deep. Both the potential and flux distributions were interpolated to obtain lines of constant potential and lines bounding regions of constant flux. This interpolation scheme is also included in the sample program.

```
      DIMENSION POT(67,15),PHI(67,15),DIFF(67,15),FLX(66,14),
     TAMP(66,14),COMP1(65,14),COMP2(65,14),COMP3(65,14),COMP4(65,14),
     TCOMP5(65,14),COMP6(65,14),COMP7(65,14),COMP8(65,14),COMP9(65,14),
     TXAMP1(13),XAMP2(13),XAMP3(13),XAMP4(13),XAMP5(13),XAMP6(13),XAMP7
     T(13),XAMP8(13),XAMP9(13),Y1(13),Y2(13),Y3(13),Y4(13),Y5(13),Y6(13)
     T,Y7(13),Y8(13),Y9(13),TEST1(66,15),TEST2(66,15),TEST3(66,15)
      DIMENSION TEST4(66,15),TEST5(66,15),TEST6(66,15),TEST7(66,15),
     TTEST8(66,15),TEST9(66,15),YPHI1(60),YPHI2(50),YPHI3(40),
     TYPHI4(30),YPHI5(30),YPHI6(25),YPHI7(20),YPHI8(15),YPHI9(10),
     TX1(60),X2(50),X3(40),X4(30),X5(30),X6(25),X7(20),X8(15),X9(10)
      EQUIVALENCE (COMP1,TEST1),(COMP2,TEST2),(COMP3,TEST3),(COMP5,TEST5
     T),(COMP6,TEST6),(COMP7,TEST7),(COMP8,TEST8),(COMP9,TEST9),(DIFF,
     TX1),(DIFF(1,2),X2),(DIFF(1,3),X3),(DIFF(1,4),X4),(DIFF(1,5),
     TX5),(DIFF(1,6),X6),(DIFF(1,7),X7),(DIFF(1,8),X8),(DIFF(1,9),X9),(
     TPOT,FLX,YPHI1),(POT(1,2),YPHI2),(POT(1,3),YPHI3),(POT(1,4),YPHI4),
     T(POT(1,5),YPHI5),(POT(1,6),YPHI6),(POT(1,7),YPHI7)
      EQUIVALENCE (POT(1,8),YPHI8),(POT(1,9),YPHI9),(COMP4,TEST4)
C     CALCULATION OF POTENTIAL DIXTRIBUTION
C       INPUT OF BOUNDARY VALUES
      DO 201 I=2,67
  201 POT(I,2)=0.
      DO 202 J=3,14
  202 POT(2,J)=0.
      DO 203 J=3,12
  203 POT(66,J)=0.
      DO 204 I=2,23
      S=I
  204 POT(I,14)=(S/23.)*15.
      POT(23,13)=15.0
      DO 500 I=23,66
  500 POT(I,12)=15.0
C  CALCULATION OF INTERIOR POINTS (INITIAL ESTIMATES)
      DO 3 I=23,65
      DO 3 J=2,10
      R=J
    3 POT(I,13-J)=POT(I,12)-((R-1.)/10.)*POT(I,12)
      DO 4 I=3,22
```

```
      DO 4 J=2,12
      R=J
    4 POT(I,15-J)=POT(I,14)-((R-1.)/12.)*POT(I,14)
C  BOUNDARY CONDITIONS BECAUSE OF DIFF. COND. ON BOUNDARY
      ITS=0
   21 DO 5 J=2,14
    5 POT(1,J)=POT(3,J)
      DO 506 I=2,9
  506 POT(I,1)=POT(I,3)
      DO 6 J=2,12
    6 POT(67,J)=POT(65,J)
      DO 8 I=1,23
    8 POT(I,15)=POT(1,13)
      POT(24,13)=POT(22,13)
      POT(24,14)=POT(22,14)
      DO 508 I=25,66
  508 POT(I,13)=POT(I,11)
C  ITERATION SCHEME
      ITS=ITS+1
      AL=0.4212
      PHI(1,2)=POT(1,2)
      DO 693 I=2,9
      PHI(I,1)=POT(I,1)
      F=1.
      G=(1.-1./(2.*(14.-F)))
      H=(1.+1./(2.*(14.-F)))
  693 PHI(I,2)=POT(I,2)+AL*(POT(I+1,2)+PHI(I-1,2)+G*POT(I,3)+
     TH*PHI(I,1)-4.*POT(I,2))
      DO 694 I=10,66
  694 PHI(I,2)=0.
      PHI(1,12)=POT(1,12)
      PHI(1,13)=POT(1,13)
      PHI(1,14)=POT(1,14)
      DO 10 J=3,11
      DO 10 I=2,66
      PHI(1,J)=POT(1,J)
      F=J
```

```
      G=(1.-1./(2.*(14.-F)))
      H=(1.+1./(2.*(14.-F)))
   10 PHI(I,J)=POT(I,J)+AL*(POT(I+1,J)+PHI(I-1,J)+G*POT(I,J+1)+
     TH*PHI(I,J-1)-4.*POT(I,J))
      DO 14 I=2,22
      G=0.75
      H=1.25
   14 PHI(I,12)=POT(I,12)+AL*(POT(I+1,12)+PHI(I-1,12)+G*POT(I,13)+
     TH*PHI(I,11)-4.*POT(I,12))
      PHI(23,12)=15.
      PHI(24,12)=15.
      DO 811 I=25,66
  811 PHI(I,12)=POT(I,12)+AL*(POT(I+1,12)+PHI(I-1,12)+G*POT(I,13)+
     TH*PHI(I,11)-4.*POT(I,12))
      DO 11 I=2,23
      G=.5
      H=1.50
   11 PHI(I,13)=POT(I,13)+AL*(POT(I+1,13)+PHI(I-1,13)+G*POT(I,14)+
     TH*PHI(I,12)-4.*POT(I,13))
      DO 509 I=2,23
  509 PHI(I,14)=POT(I,14)+AL*(POT(I+1,14)+PHI(I-1,14)+POT(I,15)+
     TPHI(I,13)-4.*POT(I,14))
C  COMPARISON OF POTS AND PHIS
      DO 15 J=2,12
      DO 15 I=2,66
      DIFF(I,J)=PHI(I,J)-POT(I,J)
      Q=ABS(DIFF(I,J))
      IF(Q-.0015)15,15,20
   15 CONTINUE
      DO 16 J=13,14
      DO 16 I=2,23
      DIFF(I,J)=PHI(I,J)-POT(I,J)
      Q=ABS(DIFF(I,J))
      IF(Q-.0015)16,16,20
   16 CONTINUE
      GO TO 22
   20 DO 41 J=2,12
```

```
      DO 41 I=2,66
   41 POT(I,J)=PHI(I,J)
      DO 42 J=13,14
      DO 42 I=2,23
   42 POT(I,J)=PHI(I,J)
      GO TO 21
   22 CONTINUE
      WRITE(3,26)((PHI(67-I,13-J),J=1,11),I=1,43)
   26 FORMAT('1'/('0',18XF6.3,2XF6.3,2XF6.3,2XF6.3,2XF6.3,2XF6.3,2XF6.3,
     T2XF6.3,2XF6.3,2XF6.3,2XF6.3))
      WRITE(3,25)((PHI(24-I,15-J),J=1,13),I=1,22)
   25 FORMAT('0',2XF6.3,2XF6.3,2XF6.3,2XF6.3,2XF6.3,2XF6.3,2XF6.3,2XF6.3
     T,2XF6.3,2XF6.3,2XF6.3,2XF6.3,2XF6.3)
      WRITE(3,27)ITS
   27 FORMAT('1',I4)
C     CALCULATION OF FLUX DISTRIBUTION
      DO 102 J=2,14
  102 FLX(1,J)=0.0
      DO 103 I=2,22
  103 FLX(I,14)=0.0
      DO 404 I=23,65
  404 FLX(I,12)=1.0
      FLX(22,12)=0.
      FLX(22,13)=0.0
      DO 105 J=2,11
  105 FLX(65,J)=1.0
      DO 106 I=2,64
      R=I-1
  106 FLX(I,2)=(R/64.)
C     CALCUTION OF INTERIOR POINTS, INITIAL ESTIMATE
      DO 107 I=2,22
      DO 107 J=3,13
      S=J-2
  107 FLX(I,J)=FLX(I,2)-(S/12.)*FLX(I,2)
      DO 109 I=22,64
      DO 109 J=3,11
      S=12-J
```

```
      IF(FLX(I,2)-FLX(I,12))80,80,81
   80 FLX(I,J)=FLX(I,12)-((S/10.)*(FLX(I,12)-FLX(I,2)))
      GO TO 109
   81 FLX(I,J)=FLX(I,12)+((S/10.)*(FLX(I,2)-FLX(I,12)))
  109 CONTINUE
C     CONDITIONS BECAUSE OF DIFFERENTIAL BOUNDARY CONDITIONS
      AL=0.4212
      ITS=0
  123 DO 111 I=10,64
  111 FLX(I,1)=FLX(I,3)
C     ITERATION SCHEME
      ITS=ITS+1
      DO 339 I=1,9
  339 AMP(I,2)=0.
      DO 340 J=3,11
      DO 340 I=2,9
      AMP(1,J)=0.
      F=J
      G=(1.-1./(2.*(14.-F)))
      H=(1.+1./(2.*(14.-F)))
  340 AMP(I,J)=FLX(I,J)+AL*(FLX(I+1,J)+AMP(I-1,J)+G*FLX(I,J+1)+
     TH*AMP(I,J-1)-4.*FLX(I,J))
      DO 112 J=2,11
      DO 112 I=10,64
      AMP(I,1)=FLX(I,1)
      AMP(65,J)=1.0
      F=J
      G=(1.-1./(2.*(14.-F)))
      H=(1.+1./(2.*(14.-F)))
  112 AMP(I,J)=FLX(I,J)+AL*(FLX(I+1,J)+AMP(I-1,J)+G*FLX(I,J+1)+
     TH*AMP(I,J-1)-4.*FLX(I,J))
      AMP(1,12)=0.
      AMP(1,13)=0.
      AMP(1,14)=0.
      DO 113 I=2,21
      G=0.75
      H=1.25
```

```
  113 AMP(I,12)=FLX(I,12)+AL*(FLX(I+1,12)+AMP(I-1,12)+G*FLX(I,13)+
     TH*AMP(I,11)-4.*FLX(I,12))
      AMP(22,12)=0.
      DO 115 I=23,65
  115 AMP(I,12)=1.0
      DO 116 I=2,21
      G=0.50
      H=1.50
  116 AMP(I,13)=FLX(I,13)+AL*(FLX(I+1,13)+AMP(I-1,13)+G*FLX(I,14)+
     TH*AMP(I,12)-4.*FLX(I,13))
      AMP(22,13)=0.
      DO 117 I=2,22
  117 AMP(I,14)=0.
C     COMPARISON OF FLXS AND AMPS
      DO 118 J=2,12
      DO 118 I=1,65
      DIFF(I,J)=AMP(I,J)-FLX(I,J)
      Q=ABS(DIFF(I,J))
      IF(Q-.0001)118,118,120
  118 CONTINUE
      DO 119 J=13,14
      DO 119 I=1,22
      DIFF(I,J)=AMP(I,J)-FLX(I,J)
      Q=ABS(DIFF(I,J))
      IF(Q-.0001)119,119,120
  119 CONTINUE
      GO TO 130
  120 DO 121 J=2,12
      DO 121 I=1,65
  121 FLX(I,J)=AMP(I,J)
      DO 122 J=13,14
      DO 122 I=1,22
  122 FLX(I,J)=AMP(I,J)
      GO TO 123
  130 CONTINUE
      WRITE(3,124)((AMP(66-I,13-J),J=1,11),I=1,43)
  124 FORMAT('1'/('0',18XF6.3,2XF6.3,2XF6.3,2XF6.3,2XF6.3,2XF6.3,2XF6.3,
```

```
     T2XF6.3,2XF6.3,2XF6.3,2XF6.3))
      WRITE(3,126)((AMP(23-I,15-J),J=1,13),I=1,22)
  126 FORMAT('0',2XF6.3,2XF6.3,2XF6.3,2XF6.3,2XF6.3,2XF6.3,2XF6.3,2XF6.3
     T,2XF6.3,2XF6.3,2XF6.3,2XF6.3,2XF6.3)
      WRITE(3,127)ITS
  127 FORMAT('1',I4)
C   INTERPOLATION SCHEME
      DO 131  J=2,12
      COMP1(1,J)=AMP(1,J)-.1
      COMP2(1,J)=AMP(1,J)-.2
      COMP3(1,J)=AMP(1,J)-.3
      COMP4(1,J)=AMP(1,J)-.4
      COMP5(1,J)=AMP(1,J)-.5
      COMP6(1,J)=AMP(1,J)-.6
      COMP7(1,J)=AMP(1,J)-.7
      COMP8(1,J)=AMP(1,J)-.8
  131 COMP9(1,J)=AMP(1,J)-.9
      L1=0
      L2=0
      L3=0
      L4=0
      L5=0
      L6=0
      L7=0
      L8=0
      L9=0
      DO 132 J=2,12
      DO 132 I=2,65
      R=I
      COMP1(I,J)=AMP(I,J)-.1
      IF(COMP1(I,J))132,133,133
  133 IF(COMP1(I-1,J))134,134,135
  134 DENOM=AMP(I,J)-AMP(I-1,J)
      XNUM=.1-AMP(I-1,J)
      PCTG=XNUM/DENOM
      L1=L1+1
      XAMP1(L1)=(R-2.)+PCTG
```

```
      Y1(L1)=J-2
  135 COMP2(I,J)=AMP(I,J)-.2
      IF(COMP2(I,J))132,136,136
  136 IF(COMP2(I-1,J))137,137,138
  137 DENOM=AMP(I,J)-AMP(I-1,J)
      XNUM=.2-AMP(I-1,J)
      PCTG=XNUM/DENOM
      L2=L2+1
      XAMP2(L2)=(R-2.)+PCTG
      Y2(L2)=J-2
  138 COMP3(I,J)=AMP(I,J)-.3
      IF(COMP3(I,J))132,139,139
  139 IF(COMP3(I-1,J))140,140,141
  140 DENOM=AMP(I,J)-AMP(I-1,J)
      XNUM=.3-AMP(I-1,J)
      PCTG=XNUM/DENOM
      L3=L3+1
      XAMP3(L3)=(R-2.)+PCTG
      Y3(L3)=J-2
  141 COMP4(I,J)=AMP(I,J)-.4
      IF(COMP4(I,J))132,142,142
  142 IF(COMP4(I-1,J))143,143,144
  143 DENOM=AMP(I,J)-AMP(I-1,J)
      XNUM=.4-AMP(I-1,J)
      PCTG=XNUM/DENOM
      L4=L4+1
      XAMP4(L4)=(R-2.)+PCTG
      Y4(L4)=J-2
  144 COMP5(I,J)=AMP(I,J)-.5
      IF(COMP5(I,J))132,145,145
  145 IF(COMP5(I-1,J))146,146,147
  146 DENOM=AMP(I,J)-AMP(I-1,J)
      XNUM=.5-AMP(I-1,J)
      PCTG=XNUM/DENOM
      L5=L5+1
      XAMP5(L5)=(R-2.)+PCTG
      Y5(L5)=J-2
```

```
147 COMP6(I,J)=AMP(I,J)-.6
    IF(COMP6(I,J))132,148,148
148 IF(COMP6(I-1,J))149,149,150
149 DENOM=AMP(I,J)-AMP(I-1,J)
    XNUM=.6-AMP(I-1,J)
    PCTG=XNUM/DENOM
    L6=L6+1
    XAMP6(L6)=(R-2.)+PCTG
    Y6(L6)=J-2
150 COMP7(I,J)=AMP(I,J)-.7
    IF(COMP7(I,J))132,151,151
151 IF(COMP7(I-1,J))152,152,153
152 DENOM=AMP(I,J)-AMP(I-1,J)
    XNUM=.7-AMP(I-1,J)
    PCTG=XNUM/DENOM
    L7=L7+1
    XAMP7(L7)=(R-2.)+PCTG
    Y7(L7)=J-2
153 COMP8(I,J)=AMP(I,J)-.8
    IF(COMP8(I,J))132,154,154
154 IF(COMP8(I-1,J))155,155,156
155 DENOM=AMP(I,J)-AMP(I-1,J)
    XNUM=.8-AMP(I-1,J)
    PCTG=XNUM/DENOM
    L8=L8+1
    XAMP8(L8)=(R-2.)+PCTG
    Y8(L8)=J-2
156 COMP9(I,J)=AMP(I,J)-.9
    IF(COMP9(I,J))132,157,157
157 IF(COMP9(I-1,J))158,158,132
158 DENOM=AMP(I,J)-AMP(I-1,J)
    XNUM=.9-AMP(I-1,J)
    PCTG=XNUM/DENOM
    L9=L9+1
    XAMP9(L9)=(R-2.)+PCTG
    Y9(L9)=J-2
132 CONTINUE
```

```
C  Y-INTERPOLATION FOR POTENTIAL
      DO 159 I=1,66
      PHI(1,2)=0.0
      TEST1(I,2)=PHI(I,2)-1.5
      TEST2(I,2)=PHI(I,2)-3.0
      TEST3(I,2)=PHI(I,2)-4.5
      TEST4(I,2)=PHI(I,2)-6.0
      TEST5(I,2)=PHI(I,2)-7.5
      TEST6(I,2)=PHI(I,2)-9.0
      TEST7(I,2)=PHI(I,2)-10.5
      TEST8(I,2)=PHI(I,2)-12.0
  159 TEST9(I,2)=PHI(I,2)-13.5
      K1=0
      K2=0
      K3=0
      K4=0
      K5=0
      K6=0
      K7=0
      K8=0
      K9=0
      DO 160 I=2,66
      DO 160 J=3,12
      A=J
      TEST1(I,J)=PHI(I,J)-1.5
      IF(TEST1(I,J))160,161,161
  161 IF(TEST1(I,J-1))162,162,163
  162 BTM=PHI(I,J)-PHI(I,J-1)
      TOP=1.5-PHI(I,J-1)
      PCT=TOP/BTM
      K1=K1+1
      YPHI1(K1)=(A-3.)+PCT
      X1(K1)=I-2
  163 TEST2(I,J)=PHI(I,J)-3.0
      IF(TEST2(I,J))160,164,164
  164 IF(TEST2(I,J-1))165,165,166
  165 BTM=PHI(I,J)-PHI(I,J-1)
```

```
      TOP=3.0-PHI(I,J-1)
      PCT=TOP/BTM
      K2=K2+1
      YPHI2(K2)=(A-3.)+PCT
      X2(K2)=I-2
  166 TEST3(I,J)=PHI(I,J)-4.5
      IF(TEST3(I,J))160,167,167
  167 IF(TEST3(I,J-1))168,168,169
  168 BTM=PHI(I,J)-PHI(I,J-1)
      TOP=4.5-PHI(I,J-1)
      PCT=TOP/BTM
      K3=K3+1
      YPHI3(K3)=(A-3.)+PCT
      X3(K3)=I-2
  169 TEST4(I,J)=PHI(I,J)-6.0
      IF(TEST4(I,J))160,170,170
  170 IF(TEST4(I,J-1))171,171,172
  171 BTM=PHI(I,J)-PHI(I,J-1)
      TOP=6.0-PHI(I,J-1)
      PCT=TOP/BTM
      K4=K4+1
      YPHI4(K4)=(A-3.)+PCT
      X4(K4)=I-2
  172 TEST5(I,J)=PHI(I,J)-7.5
      IF(TEST5(I,J))160,173,173
  173 IF(TEST5(I,J-1))174,174,175
  174 BTM=PHI(I,J)-PHI(I,J-1)
      TOP=7.5-PHI(I,J-1)
      PCT=TOP/BTM
      K5=K5+1
      YPHI5(K5)=(A-3.)+PCT
      X5(K5)=I-2
  175 TEST6(I,J)=PHI(I,J)-9.0
      IF(TEST6(I,J))160,176,176
  176 IF(TEST6(I,J-1))177,177,178
  177 BTM=PHI(I,J)-PHI(I,J-1)
      TOP=9.0-PHI(I,J-1)
```

```
      PCT=TOP/BTM
      K6=K6+1
      YPHI6(K6)=(A-3.)+PCT
      X6(K6)=I-2
  178 TEST7(I,J)=PHI(I,J)-10.5
      IF(TEST7(I,J))160,179,179
  179 IF(TEST7(I,J-1))180,180,181
  180 BTM=PHI(I,J)-PHI(I,J-1)
      TOP=10.5-PHI(I,J-1)
      PCT=TOP/BTM
      K7=K7+1
      YPHI7(K7)=(A-3.)+PCT
      X7(K7)=I-2
  181 TEST8(I,J)=PHI(I,J)-12.0
      IF(TEST8(I,J))160,182,182
  182 IF(TEST8(I,J-1))183,183,184
  183 BTM=PHI(I,J)-PHI(I,J-1)
      TOP=12.0-PHI(I,J-1)
      PCT=TOP/BTM
      K8=K8+1
      YPHI8(K8)=(A-3.)+PCT
      X8(K8)=I-2
  184 TEST9(I,J)=PHI(I,J)-13.5
      IF(TEST9(I,J))160,185,185
  185 IF(TEST9(I,J-1))186,186,160
  186 BTM=PHI(I,J)-PHI(I,J-1)
      TOP=13.5-PHI(I,J-1)
      PCT=TOP/BTM
      K9=K9+1
      YPHI9(K9)=(A-3.)+PCT
      X9(K9)=I-2
  160 CONTINUE
      DIMENSION XL(5),YL(5),GL(5),DL(5)
C   READ LABELS
      READ(1,666)XL,YL,GL,DL
  666 FORMAT(20A4)
      CALL GRAPH(L1,XAMP1,Y1,K,2,16.0,3.0,4.0,0.,4.0,0.,XL,YL,GL,DL)
```

```
CALL GRAPH(L2,XAMP2,Y2,K,2,0,0,0,0,0,0,0,0,0,0)
CALL GRAPH(L3,XAMP3,Y3,K,2,0,0,0,0,0,0,0,0,0,0)
CALL GRAPH(L4,XAMP4,Y4,K,2,0,0,0,0,0,0,0,0,0,0)
CALL GRAPH(L5,XAMP5,Y5,K,2,0,0,0,0,0,0,0,0,0,0)
CALL GRAPH(L6,XAMP6,Y6,K,2,0,0,0,0,0,0,0,0,0,0)
CALL GRAPH(L7,XAMP7,Y7,K,2,0,0,0,0,0,0,0,0,0,0)
CALL GRAPH(L8,XAMP8,Y8,K,2,0,0,0,0,0,0,0,0,0,0)
CALL GRAPH(L9,XAMP9,Y9,K,2,0,0,0,0,0,0,0,0,0,0)
CALL GRAPH(K1,X1,YPHI1,K,2,0,0,0,0,0,0,0,0,0,0)
CALL GRAPH(K2,X2,YPHI2,K,2,0,0,0,0,0,0,0,0,0,0)
CALL GRAPH(K3,X3,YPHI3,K,2,0,0,0,0,0,0,0,0,0,0)
CALL GRAPH(K4,X4,YPHI4,K,2,0,0,0,0,0,0,0,0,0,0)
CALL GRAPH(K5,X5,YPHI5,K,2,0,0,0,0,0,0,0,0,0,0)
CALL GRAPH(K6,X6,YPHI6,K,2,0,0,0,0,0,0,0,0,0,0)
CALL GRAPH(K7,X7,YPHI7,K,2,0,0,0,0,0,0,0,0,0,0)
CALL GRAPH(K8,X8,YPHI8,K,2,0,0,0,0,0,0,0,0,0,0)
CALL GRAPH(K9,X9,YPHI9,K,2,0,0,0,0,0,0,0,0,0,0)
STOP
END
```

APPENDIX B

Derivation of Resistance-Capacitance Relationship

Consider two electrodes immersed in a homogeneous conducting medium. If a voltage potential, V, is applied between the two electrodes producing a current, I, the resistance of the medium will be given by

$$R = \frac{V}{I} \quad . \tag{46}$$

The total current flowing through an equipotential surface, S, between the two electrodes is given by:

$$I = \iint_S J \cdot dS \tag{47}$$

where J is the current density. But

$$J = \frac{E}{\rho} \tag{48}$$

where E is the electric field intensity and ρ is the resistivity of the conducting medium. Substitution of Equation 48 into 47 results in:

$$I = \frac{1}{\rho} \iint_S E \cdot dS \quad . \tag{49}$$

The voltage potential between the two electrodes is given by

$$V = \int E \cdot dl. \tag{50}$$

Substitution of Equations 49 and 50 into 46 gives:

$$R = \rho \frac{\iint_S E \cdot dl}{\iint_S E \cdot dS} \quad . \tag{51}$$

Now consider the same electrode geometry described above but with a homogeneous dielectric between the two electrodes. The capacitance of this system, C, is given by the ratio of the absolute magnitude of the charge on either conductor, Q, to the voltage between the two conductors, V. Thus, capacitance is given by

$$C = \frac{Q}{V} \quad . \tag{52}$$

The charge on the capacitor is given by:

$$Q = \iint_S D \cdot dS \tag{53}$$

where D is the electric flux density. But

$$D = \varepsilon_r \varepsilon_o E \tag{54}$$

where ε_r is the dimensionless dielectric constant and ε_o is the permittivity of free space. The two constants are sometimes combined into one constant:

$$\varepsilon = \varepsilon_r \varepsilon_o \tag{55}$$

where ε is now called the dielectric constant. Thus, Equation 53 can now be written

$$Q = \varepsilon \iint_S E \cdot dS \quad . \tag{56}$$

The voltage between the two plates is given by

$$V = \int E \cdot dl \quad . \tag{57}$$

Since the geometry is the same for the two cases and the conducting medium and the dielectric were considered to be homogeneous, the electric field, E, should be the same for both cases. Thus, Equations 50 and 57 are identical and we can write the following equation:

$$R = \frac{V}{I} = \frac{Q}{CI} \quad . \tag{58}$$

Substituting Equations 47 and 53 into Equation 58 we have

$$R = \frac{\rho\varepsilon \iint_S E \cdot dS}{C \iint_S E \cdot dS} \quad . \tag{59}$$

Simplifying Equation 59 results in

$$R = \frac{\rho\varepsilon}{C} \quad . \tag{60}$$

Thus, knowing the resistivity of the conducting medium, the capacitance of a capacitor having the same geometry, and the dielectric constant of the dielectric in the capacitor, the resistance can be obtained for the geometry.

APPENDIX C

Run Conditions and Location of Data

The following tables list the location of data obtained from runs made during the investigation as well as the conditions used in the runs. The original data is contained in three bound research notebooks in the possession of Professor T. D. Wheelock, Chemical Engineering Department, Iowa State University, Ames, Iowa.

In order to facilitate the tabulation of run parameters and conditions, abbreviations and symbols were used in certain cases. Examples of these symbols and abbreviations and their explanations are listed below.

KEY

Under the heading "Electrode type" a two-unit symbol was used to denote first, the material of which the center electrode was made and second, the diameter of the electrode. Four different types of center electrode materials were used. The four materials and their abbreviations are:

Brass-B
Carbon-C
Steel-S
Tungsten-T.

Three different electrode diameters were used in the study--1, 1/16, and 1/25 in. Thus, the symbols C1 and T1/25 refer to a 1 in. diameter carbon electrode and a 1/25 in. diameter

tungsten electrode, respectively.

Under the table heading "Electrode configuration" a three-unit hyphenated symbol was used to describe the surface of the electrode. The first unit in the symbol refers to the electrode shape. Five electrode shapes were used. Four of the shapes are shown in Figure 51 and are designated as A, B, C, and D, respectively. The fifth shape is shown in Figure 27 and is designated as the letter E.

The second unit of the symbol refers to the exposed area of the center electrode that was electrically uninsulated. Instead of listing the areas themselves, a number referring to a particular area was used. The areas used and their corresponding numbers as well as other pertinent information are listed in the table below.

Table 9. Symbolic representation of exposed center electrode areas

Electrode diameter, in.	Longitudinal exposure, in.	Exposed area, sq. in.	Symbol
1	Tip	0.785	1
1	1/4	0.785	2
1	1	3.14	3
1	4	12.56	4
1	10.75	33.755	5
1	10.75+Tip	34.54	6
1/16	tip	0.00307	7
1/16	1/4	0.0491	8
1/25	tip	0.001256	9
1/25	1/4	0.0314	10

The third symbol used to complete the description of the electrode configuration refers to the position of the exposed area relative to the tip of the electrode. The distance of the exposed areas from the electrode tip and their corresponding symbols are listed in Table 10.

Table 10. Symbolic representation of longitudinal positions of exposed electrode areas

Distance of exposed area from tip, in.	Symbol
Tip[a]	T
0	1
1/2	2
1	3
2	4
4	5
7.75	6
8	7
10	8
16	9

[a]This refers to the exposed bottom tip area of electrode shapes A and D.

Table 11. Conditions and location of interelectrode resistance versus current density data obtained with direct current (negative ground) and the following conditions constant:

Column diameter: 6 in.
Bed material: Calcined coke
Particle size range: -48/+65 Tyler mesh
DC power supply voltage: 15 volts
Fluidizing gas: Nitrogen

Run no.	Bed height, in.	Screen length, in.	Elec. type	Elec. config-uration	Book	Page	V_{rel}
1N	21.5	15	C1	A-3-1	1	28	1.53
						29	2.47
						30	1.85
						31	1.25
						32	3.09
1ND	21.5	15	C1	A-3-1	1	36	1.23
						37	1.56
						38	1.85
						39	2.47
						40	3.09
2N	21.5	15	C1	A-3-1	1	44	0.24
						45	0.485
						46	0.734
						47	0.962
2ND	21.5	15	C1	A-3-1	1	51	0.24
						52	0.485
						53	0.73
						54	0.97
3N	21.5	15	C1	A-3-1	1	58	0.0
						59	00.0
4N	21.5	15	C1	A-3-1	1	63	0.24
						64	0.49
						65	0.74
						66	0.98
AND	21.5	15	C1	A-3-1	1	70	0.249
						71	0.485
						72	0.734
						73	0.965

Table 11 (Continued)

Run no.	Bed height, in.	Screen length, in.	Elec. type	Elec. config-uration	Book	Page	V_{rel}
5N	21.5	15	Cl	A-4-1	1	77	1.23
						78	1.55
						79	1.85
						80	2.47
						81	3.09
5ND	21.5	15	Cl	A-4-1	1	82	1.23
						83	1.55
						84	1.85
						85	2.47
						86	3.09
6N	21.5	15	Cl	A-4-1	1	91	0.00
						92	0.244
						93	0.485
						94	0.734
						95	0.965
6ND	21.5	15	Cl	A-4-1	1	96	0.00
						97	0.244
						98	0.485
						99	0.734
						100	0.965
7N	21.5	15	Cl	A-2-1	1	105	1.23
						106	1.55
						107	1.85
						108	2.47
						109	3.09
7ND	21.5	15	Cl	A-2-1	1	119	1.23
						120	1.55
						121	1.85
						122	2.47
						123	3.09
8N	21.5	15	Cl	A-2-1	1	110	0.00
						111	0.244
						112	0.485
						113	0.734
						114	0.963
8ND	21.5	15	Cl	A-2-1	1	124	0.00
						125	0.244

Table 11 (Continued)

Run no.	Bed height, in.	Screen length, in.	Elec. type	Elec. configuration	Book	Page	V_{rel}
						126	0.485
						127	0.734
						128	0.963
9N	21.5	15	C1	A-1-T	1	133	1.23
						134	1.55
						135	1.85
						136	2.47
						137	3.09
9ND	21.5	15	C1	A-1-T	1	147	1.23
						148	1.55
						149	1.85
						150	2.47
						151	3.09
10N	21.5	15	C1	A-1-T	1	138	0.00
						139	0.244
						140	0.485
						141	0.734
						142	0.963
10ND	21.5	15	C1	A-1-T	1	152	0.00
						153	0.244
						154	0.485
						155	0.734
						156	0.963
11N	16	16	C1	A-5-1	2	254	1.57
						255	1.91
						256	3.16
12N	16	16	C1	A-6-T	2	258	1.57
						259	1.91
						260	3.16
13N	16	16	S1/16	E-8-1	3	64	2.0
						65	3.0
						66	4.0
14N	16	16	T1/25	E-10-1	3	69	2.0
						70	3.0
						71	4.0

Table 11 (Continued)

Run	Bed height, in.	Screen length, in.	Elec. type	Elec. config-uration	Book	Page	V_{rel}
15N	16	16	B1/16	E-8-1	3	74	2.0
						75	3.0
						76	4.0
16N	16	16	S1/16	E-7-T	3	79	2.0
						80	3.0
						81	4.0
17N	16	16	B1/16	E-7-T	3	84	2.0
						85	3.0
						86	4.0
18N	16	16	T1/25	E-9-T	3	89	2.0
						90	3.0
						91	4.0

Table 12. Conditions and location of interelectrode resistance versus current density data obtained with direct current (positive ground) and the following conditions constant:

Column diameter: 6 in.
Bed material: Calcined coke
Particle size range: -48/+65 Tyler mesh
DC power supply voltage: 15 volts
Fluidizing gas: Nitrogen

Run	Bed height, in.	Screen length, in.	Elec. type	Elec. config-uration	Book	Page	V_{rel}
1P	16	16	C1	A-2-1	3	18	2.0
						19	3.0
						20	4.0
2P	16	16	C1	A-1-T	3	22	2.0
						23	3.0
						24	4.0
3P	16	16	C1	A-3-1	3	26	2.0
						27	3.0
						28	4.0

Table 13. Conditions and location of interelectrode resistance versus current density data obtained with alternating current and the following conditions constant:

Column diameter: 6 in.
Bed material: Calcined coke
Particle size range: -48/+65 Tyler mesh
AC power supply voltage: 15 volts
Fluidizing gas: Nitrogen

Run no.	Bed height, in.	Screen length, in.	Elec. type	Elec. config-uration	Book	Page	V_{rel}
1A	16	16	Cl	A-2-1	3	35	2.0
						36	3.0
						37	4.0
2A	16	16	Cl	A-3-1	3	39	2.0
						40	3.0
						41	4.0
3A	16	16	Cl	A-1-T	3	43	2.0
						44	3.0
						45	4.0
4A	16	16	Cl	A-6-T	3	47	2.0
						48	3.0

Table 14. Conditions and location of bed resistivity versus current density data with the following conditions constant:

Current type: Direct current (neg. ground)
Bed material: Calcined coke
Fluidizing gas: Nitrogen

Run no.	Bed height, in.	Part. size range	Column diameter, in.	Power supply volt., volts	Book	Page	V_{rel}
1B	19.5	-48/+65	4	15	1	171	0.00
						172	0.50
						173	0.80
2B	19.5	-48/+65	4	15	1	176	1.95
						177	1.28
						178	1.97
						179	2.60
2BD	19.5	-48/+65	4	15	1	188	1.32
						189	1.97
						190	1.97
						191	2.60
						192	2.60
						193	2.60
3B	19.5	-48/+65	4	25	1	198	1.32
						199	1.97
4B	21.5	-48/+65	6	15	2	8	0.184
						9	0.365
						10	0.00
						13	0.498
						14	0.872
4BD	21.5	-48/+65	6	15	2	17	0.845
						18	0.491
						19	0.244
						20	0.000
5B	21.5	-48/+65	6	15	2	23	1.57
						24	1.89
						25	3.16
5BD	21.5	-48/+65	6	15	2	28	1.57
						29	1.89
						30	3.16

Table 14 (Continued)

Run no.	Bed height, in.	Part. size range	Column diameter, in.	Power supply volt., volts	Book	Page	V_{rel}
6B	21.5	-48/+65	6	15	2	33	0.872
						34	0.491
						35	0.000
6BD	21.5	-48/+65	6	15	2	38	0.845
						39	0.491
						40	0.000
7B	21.5	-48/+65	6	15	2	43	1.54
						44	1.91
						45	3.16
7BD	21.5	-48/+65	6	15	2	48	1.57
						49	1.89
						50	3.16

Table 15. Conditions and location of bed resistivity versus velocity data with the following conditions constant:

Current type: Direct current (neg. ground)
Bed material: Calcined coke
Fluidizing gas: Nitrogen
Power supply voltage: 15 volts

Run no.	Particle size range	Column diameter, in.	Bed height, in.	Book	Page
RV1	-48/+65	4	Hi[a]	2	163
RV1D	-48/+65	4	Hi	2	166
RV2	-48/+65	4	Lo[b]	2	174
RV2D	-48/+65	4	Lo	2	177
RV3	-65/+100	4	Hi	2	185
RV3D	-65/+100	4	Hi	2	188
RV4	-65/+100	4	Lo	2	196
RV4D	-65/+100	4	Lo	2	199
RV5	-65/+100	6	Hi	2	206
RV5D	-65/+100	6	Hi	2	209
RV6	-65/+100	6	Lo	2	217
RV6D	-65/+100	6	Lo	2	220
RV7	-48/+65	6	Hi	2	227
RV7D	-48/+65	6	Hi	2	230
RV8	-48/+65	6	Lo	2	237
RV8D	-48/+65	6	Lo	2	240
RV8DD	-48/+65	6	Lo	3	52
RV8DDD	-48/+65	6	L0	3	54

Table 16. Conditions used and location of data for the statistically designed study of the effect of V_{rel}, current density, electrode shape, and exposed area position on contact resistance, the following conditions constant:

Column diameter: 6 in.
Bed material: Calcined coke
Particle size range: -48/+65 Tyler mesh
Current type: Direct current (neg. ground)
Bed height: 16 in.
Fluidizing gas: Nitrogen

Run no.	Elec. type	Elec. configuration	Book	Page
SP1	Cl	A-2-T	2	269
SP2	Cl	D-2-2	2	270
SP3	Cl	B-2-8	2	271
SP4	Cl	C-2-2	2	272
SP5	Cl	C-2-4	2	273
SP6	Cl	B-2-5	2	274
SP7	Cl	C-2-4	2	275
SP8	Cl	C-2-5	2	276
SP9	Cl	A-2-8	2	277
SP10	Cl	D-2-5	2	278
SP11	Cl	C-2-1	2	279
SP12	Cl	C-2-8	2	280
SP13	Cl	B-2-4	2	282
SP14	Cl	A-2-4	2	283
SP15	Cl	C-2-1	2	284
SP16	Cl	C-2-2	2	285
SP17	Cl	A-2-2	2	286

Table 16 (Continued)

Run no.	Elec. type	Elec. configuration	Book	Page
SP18	Cl	D-2-4	2	287
SP19	Cl	B-2-4	2	288
SP20	Cl	D-2-2	2	289
SP21	Cl	B-2-1	2	290
SP22	Cl	B-2-2	2	291
SP23	Cl	B-2-8	2	292
SP24	Cl	D-2-1	2	293
SP25	Cl	A-2-8	2	294
SP26	Cl	A-2-T	2	295
SP27	Cl	A-2-5	2	296
SP28	Cl	C-2-8	2	297
SP29	Cl	A-2-2	2	298
SP30	Cl	C-2-5	3	4
SP31	Cl	A-2-5	3	5
SP32	Cl	B-2-2	3	6
SP33	Cl	D-2-1	3	7
SP34	Cl	B-2-1	3	8
SP35	Cl	B-2-5	3	9
SP36	Cl	D-2-8	3	10
SP37	Cl	A-2-4	3	11
SP38	Cl	D-2-5	3	12
SP39	Cl	D-2-4	3	13
SP40	Cl	D-2-8	3	14

Table 17. Conditions used and the location of data for the visual determination of arcing investigation with the following conditions constant:

Column diameter: 6 in.
Bed material: Calcined coke
Particle size range: -48/+65 Tyler mesh
Bed height: 16 in.
Fluidizing gas: Nitrogen

Run no.	Current type	Book	Page	V_{rel}
A1	DC	3	95	2.0
			96	3.0
			97	4.0
A2	AC	3	102	2.0
			103	3.0
			104	4.0
A3	AC	3	105	1.0
			105	0.75
			105	0.00

Table 18. Conditions used and the location of data for the potential field verification investigation with the following conditions constant:

Column diameter: 6 in.
Bed material: Calcined coke
Bed height: 16 in.
Particle size range: -48/+65 Tyler mesh
Screen length: 14 in.
DC power supply voltage: 15 volts
Fluidizing gas: Nitrogen
$V_{rel} = 2.0$

Run no.	Elec. type	Elec. configuration	Book	Pages
PF1	Cl	A-6-T	3	108-113
PF2	Cl	A-2-1	3	114-119
PF3	Cl	A-2-2	3	120-124
PF3D	Cl	A-2-2	3	125-130
PF4	Cl	A-1-T	3	138-143
PF5	Cl	A-1-T	3	144-149
PF6	Cl	A-2-6	3	150-155
PF1D	Cl	A-6-T	3	132-137

Table 19. Conditions used and location of data for the contact resistance versus longitudinal electrode position study with the following conditions constant:

Column diameter: 6 in.
Bed material: Calcined coke
Bed height: 19 in.
Particle size range: -48/+65 Tyler mesh
Screen length: 16 in.
DC power supply voltage: 15 volts
Fluidizing gas: Nitrogen

Run no.	Elec. type	Elec. configuration	Book	Page	V_{rel}
CRP1	Cl	A-2-2	1	276	1.57
				277	1.91
				278	3.17
CRP2	Cl	A-2-3	1	280	1.57
				281	1.91
				282	3.17
CRP3	Cl	A-2-4	1	284	1.57
				285	1.89
				286	3.16
CRP4	Cl	A-2-5	1	288	1.59
				289	1.89
				290	3.16
CRP5	Cl	A-2-7	1	292	1.57
				293	1.89
				294	3.17
CRP6	Cl	A-2-9	1	296	1.57
				297	1.91
				298	3.17